

Supporting Information

Dielectric Constant Engineering of Nonfullerene Acceptors Enables a Record Fill Factor of 83.58% and a High Efficiency of 20.80% in Organic Solar Cells

Junwei Dong,^a Yinfeng Li,^a Chentong Liao,^b Xiaopeng Xu,*^a Liyang Yu,^a Ruipeng Li,^c and Qiang Peng*^a

^a School of Chemical Engineering and State Key Laboratory of Polymer Materials Engineering, Sichuan University, Chengdu 610065, P. R. China.

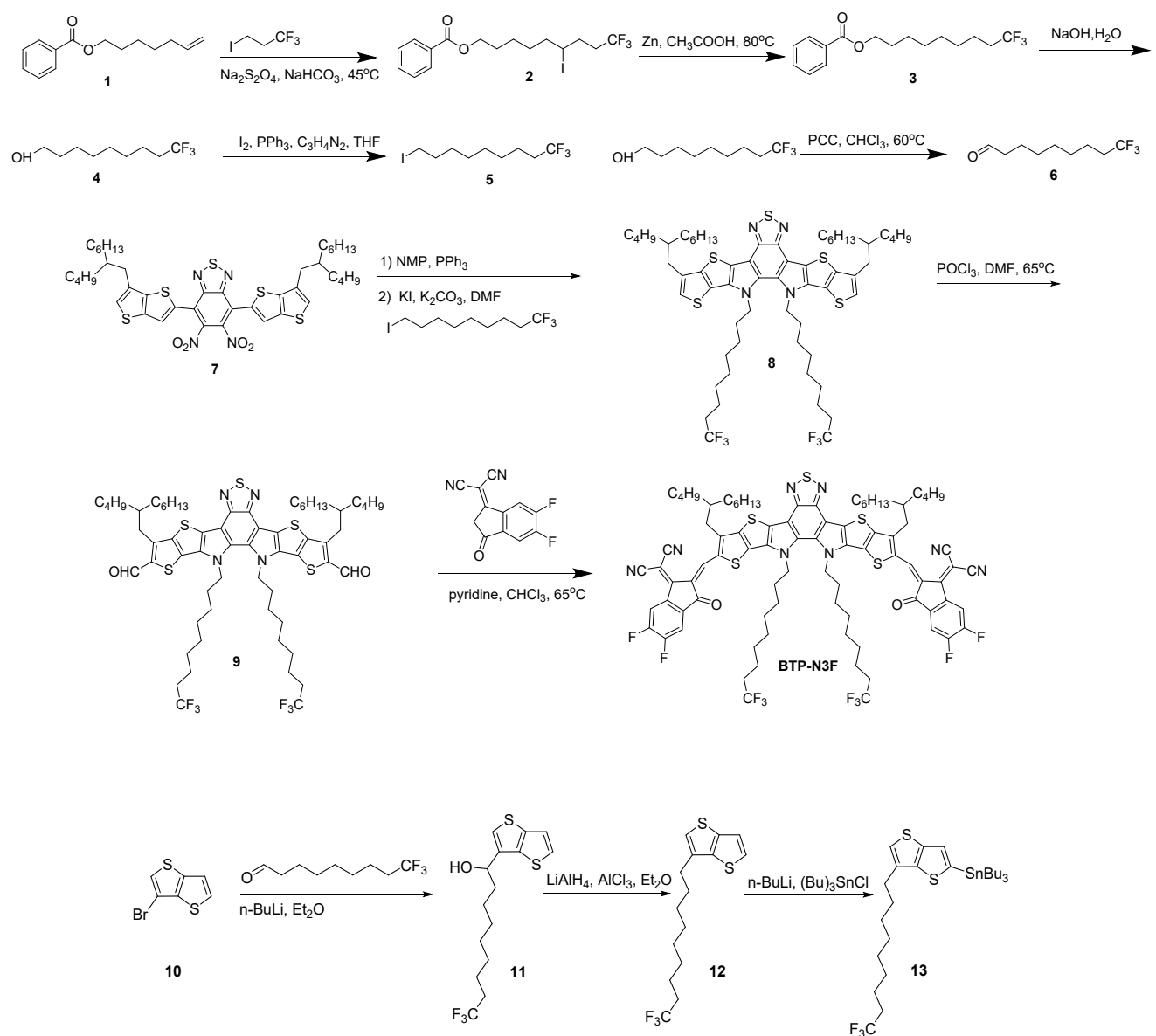
Email: xpxu@scu.edu.cn; qiangpeng@scu.edu.cn

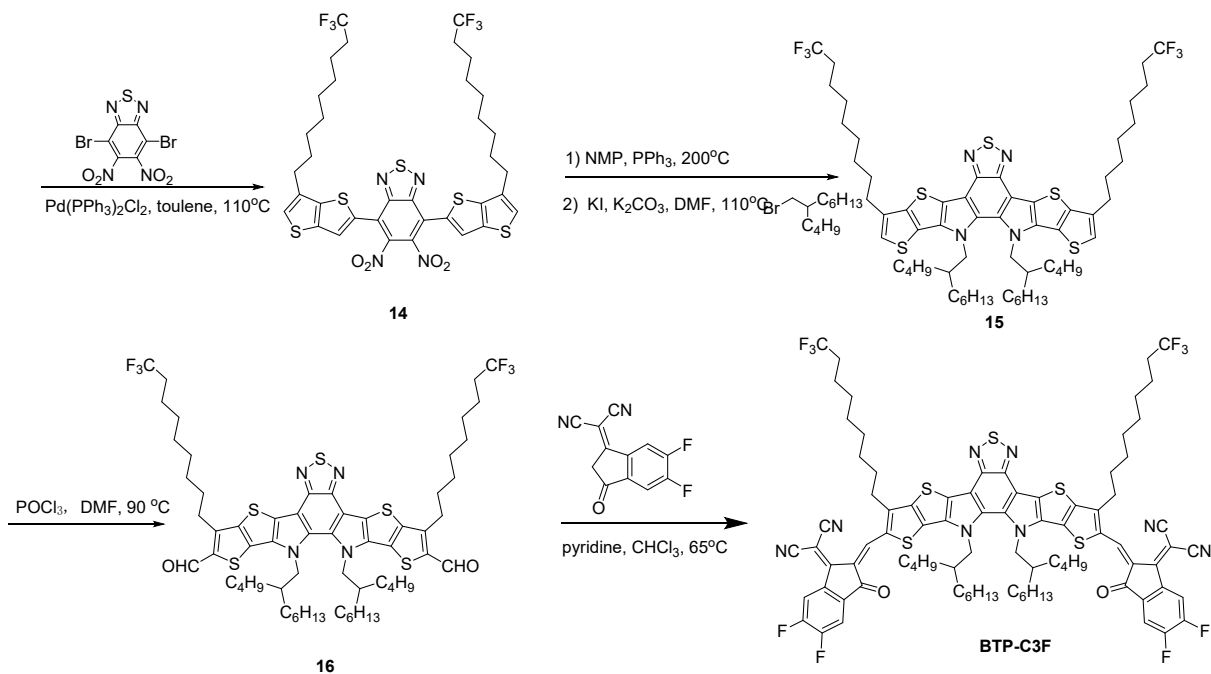
^b College of Materials and Chemistry & Chemical Engineering, Chengdu University of Technology, Chengdu 610059, P. R. China.

^c National Synchrotron Light Source II Brookhaven National Lab, Suffolk, Upton, NY 11973, USA

1. Materials and methods

Materials: D18-Cl and Y6 were purchased from eflexPV. 2-(5,6-Difluoro-3-oxo-2,3-dihydro-1H-inden-1-ylidene)malononitrile (IC-2F) was purchased from Derthon Optoelectronics Materials Science Technology Co., LTD. Compounds **1**, **7** and **10** were synthesized according to the previous reports.¹⁻³ 1,1,1-Trifluoro-2-iodoethane, 7-bromo-1-heptene and other chemicals were purchased from Aladdin Co., Adamas Co., Sigma-Aldrich Co. and Alfa Asear Chemical Co., and used without further purification. All solvents were freshly distilled prior to use.





Scheme S1. The synthetic routes of BTP-N3F and BTP-C3F.

Synthesis of compound 2: Sodium dithionite (16.95 g, 97.47 mmol, 5.0 eq.) and sodium bicarbonate (1.64 g, 19.51 mmol, 1.0 eq.) were suspended in a mixture of acetonitrile and water ($\text{CH}_3\text{CN}:\text{H}_2\text{O} = 25 \text{ mL}:25 \text{ mL}$, v/v). Commercially available 1,1,1-trifluoro-2-iodoethane (4.09 g, 19.51 mmol, 1.0 eq.) and compound 1 (12.75 g, 58.48 mmol, 3.0 eq.) were then added to the suspension. The resulting solution was allowed to warm to 45 °C under an atmospheric environment for 8.0 hours. Upon completion of the reaction, the solution was directly concentrated to remove the majority of the acetonitrile, and the resulting solution was extracted with petroleum ether. The combined organic layer was dried over anhydrous magnesium sulfate, filtered, and concentrated under reduced pressure to give the crude residue compound 2 (6.74 g, 81%).

Synthesis of compound 3: The crude residue 2 (6.74 g, 15.81 mmol, 1.0 eq.) was dissolved in aqueous acetic acid (20 mL), and zinc powder (3.47 g, 47.73 mmol, 3.0 eq.) was added. The resulting zinc suspension was vigorously refluxed for 8.0 hours. Upon cooling, the mixture was filtered and extracted with petroleum ether to separate the aqueous layer. The combined organic layer was washed

with 10% NaOH solution, separated, dried over anhydrous magnesium sulfate, filtered, and concentrated under reduced pressure to yield a crude residue. This residue was then purified by silica gel chromatography using petroleum ether and ethyl acetate (30:1, v/v) as eluents, resulting in the isolation of compound **3** as a colorless liquid (3.37 g, 71%). ¹H NMR (400 MHz, Chloroform-d) δ 8.03 (dd, *J* = 7.3, 1.6 Hz, 2H), 7.58 – 7.51 (m, 1H), 7.43 (ddd, *J* = 8.2, 6.7, 1.2 Hz, 2H), 4.31 (t, *J* = 6.7 Hz, 2H), 2.11 – 1.98 (m, 2H), 1.80 – 1.72 (m, 2H), 1.58 – 1.49 (m, 2H), 1.46 – 1.31 (m, 8H). ¹³C NMR (101 MHz, Chloroform-d) δ 132.83, 130.50, 129.53, 128.66, 128.33, 125.92, 65.01, 33.82, 33.54, 29.08, 29.00, 28.67, 28.60, 25.96, 21.84, 21.81. HRMS calcd for C₁₆H₁₂F₃O₂: 302.3372; found [M + H⁺]: 303.1570.

Synthesis of compound 4: Compound **3** (3.37 g, 11.65 mmol, 1 eq.) was added to a solution of sodium carbonate (2.01 g, 18.89 mmol, 1.5 eq.) in carbinol (60 mL) and reacted at room temperature for 8 hours. Following the reaction, the mixture was filtered, and the resulting residue was concentrated under reduced pressure. The residue was then purified by silica gel chromatography using petroleum ether and ethyl acetate (10:1, v/v) as eluents, yielding compound **4** as a colorless liquid (1.97 g, 85%). ¹H NMR (400 MHz, Chloroform-d) δ 3.59 (t, *J* = 6.6 Hz, 2H), 2.10 – 1.95 (m, 2H), 1.90 (s, 1H), 1.52 (dd, *J* = 13.9, 7.0 Hz, 4H), 1.30 (s, 8H). ¹³C NMR (101 MHz, Chloroform-d) δ 128.63, 125.88, 62.67, 33.76, 33.48, 32.58, 29.11, 28.57, 25.62, 21.79, 21.76. HRMS calcd for C₉H₁₇F₃O: 198.1231; found [M + H⁺]: 199.0768.

Synthesis of compound 5: Under nitrogen protection, compound **4** (1.3g, 6.6 mmol, 1.2 eq.), imidazole (0.56 g, 7.92 mmol, 1.44 eq.) and triphenyl phosphine (2.12 g, 7.92 mmol, 1.44 eq.) were dissolved in tetrahydrofuran (THF, 10 mL) at 0°C. Iodine (1.88 g, 5.48 mmol, 1 eq.) was then gradually added to the solution. The reaction mixture was brought to room temperature and stirred overnight. Upon completion, the reaction was quenched with ice water and extracted with

dichloromethane. The extract was concentrated, and the residue was purified by silica gel chromatography using petroleum ether as the eluent, yielding compound **5** as a colorless liquid (1.77 g, 87%). ¹H NMR (400 MHz, Chloroform-d) δ 3.17 (t, J = 7.0 Hz, 2H), 2.12 – 1.97 (m, 2H), 1.81 (p, J = 7.0 Hz, 2H), 1.58 – 1.49 (m, 2H), 1.45 – 1.27 (m, 8H). ¹³C NMR (101 MHz, Chloroform-d) δ 128.63, 125.89, 33.84, 33.56, 33.44, 30.37, 28.98, 28.58, 28.26, 21.82, 21.80, 7.13. HRMS calcd for C₉H₁₆F₃I: 308.1267; found: 308.1929.

Synthesis of compound 6: Under an ice bath, pyridinium chlorochromate (PCC, 3.72 g, 17.24 mmol, 1.5 eq.) was gradually added to a stirring solution of compound **4** (2.28 g, 11.48 mmol, 1 eq.) in trichloromethane (60 mL). The mixture was then stirred at 60 °C for an additional 4 hours. After the reaction was completed, the mixture was filtered, and the filtrate was concentrated. The resulting residue was purified by silica gel chromatography using petroleum ether and dichloromethane (2:1, v/v) as eluents, yielding compound **6** as a yellow liquid. ¹H NMR (400 MHz, Chloroform-d) δ 9.75 (d, J = 1.9 Hz, 1H), 2.42 (td, J = 7.3, 1.8 Hz, 2H), 2.08 – 2.00 (m, 2H), 1.62 (t, J = 7.0 Hz, 2H), 1.53 (t, J = 7.5 Hz, 2H), 1.32 (s, 6H). ¹³C NMR (101 MHz, Chloroform-d) δ 202.79, 43.83, 33.80, 33.52, 28.96, 28.86, 28.47, 21.91, 21.80. HRMS calcd for C₉H₁₅F₃O: 196.1075; found [M + H⁺]: 197.1150.

Synthesis of compound 8: Compound **7** (0.21 g, 0.24 mmol, 1 eq.) and triphenylphosphine (0.65 g, 2.4 mmol, 10 eq.) were dissolved in ultra-dry N-methylpyrrolidone (6 mL) under nitrogen protection and reacted at 220 °C for 9 hours. After cooling to room temperature, additional N-methylpyrrolidone (12 mL) was added, followed by Compound **5** (0.74 g, 2.4 mmol, 10 eq.), potassium carbonate (0.71 g, 4.8 mmol, 20 eq.), and potassium iodide (0.53 g, 3.0 mmol, 12.5 eq.). The mixture was reacted overnight under nitrogen protection at 90 °C. Upon completion, the reaction mixture was cooled to room temperature, diluted with methylene chloride, washed with ice water, and dried with anhydrous magnesium sulfate. The solution was then filtered and concentrated. The resulting residue was

purified by silica gel chromatography using petroleum ether and dichloromethane (4:1, v/v) as eluents to yield compound **8** as an orange-yellow oil (150 mg, 55%). ¹H NMR (400 MHz, Chloroform-d) δ 6.98 (s, 2H), 4.62 (t, J = 7.5 Hz, 4H), 2.73 (d, J = 7.1 Hz, 4H), 1.97 (d, J = 7.6 Hz, 2H), 1.95 – 1.88 (m, 4H), 1.85 (t, J = 7.5 Hz, 4H), 1.34 (d, J = 6.0 Hz, 20H), 1.28 – 1.23 (m, 20H), 1.12 (d, J = 4.2 Hz, 12H), 0.87 (d, J = 8.3 Hz, 12H). ¹³C NMR (101 MHz, Chloroform-d) δ 147.55, 142.54, 137.26, 136.19, 130.71, 128.56, 123.17, 122.70, 120.07, 111.87, 50.79, 37.42, 34.63, 33.69, 33.45, 33.36, 31.89, 30.60, 29.74, 28.82, 28.68, 28.42, 26.56, 26.28, 23.10, 22.69, 21.70, 14.12. HRMS calcd for C₆₀H₈₄F₆N₄S₅: 1134.5204; found: 1134.5193

Synthesis of compound 9: Compound **8** (150 mg, 0.15 mmol) was dissolved in 1,2-dichloroethane (7.5 mL) under nitrogen protection. N,N-dimethylformamide (7.5 mL) and phosphorus oxychloride (0.75 mL) were added to the solution at 0 °C, and the mixture was stirred for 1 hour before being heated to 90 °C and stirred overnight. After cooling to room temperature, the reaction mixture was poured into ice water and stirred for 4 hours. The mixture was then extracted with methylene chloride, dried over anhydrous magnesium sulfate, filtered, and concentrated. The resulting residue was purified by silica gel chromatography using petroleum ether and dichloromethane (1.5:1, v/v) as eluents, yielding compound **9** as an orange solid (110 mg, 72%). ¹H NMR (400 MHz, Chloroform-d) δ 10.08 (s, 2H), 4.63 (t, J = 7.6 Hz, 4H), 3.03 (d, J = 7.4 Hz, 4H), 2.01 (s, 2H), 1.99 – 1.91 (m, 4H), 1.89 (s, 4H), 1.46 – 1.29 (m, 20H), 1.29 – 1.18 (m, 32H), 0.89 – 0.83 (m, 12H). ¹³C NMR (101 MHz, Chloroform-d) δ 182.10, 147.40, 146.58, 143.47, 137.80, 136.81, 131.86, 129.09, 127.37, 112.65, 51.09, 39.26, 33.86, 33.80, 33.54, 33.20, 31.93, 31.08, 29.73, 29.02, 28.91, 28.87, 28.56, 26.66, 26.50, 23.11, 22.75, 21.85, 21.82, 14.21. HRMS calcd for C₆₂H₈₄F₆N₄O₂S₅: 1190.5102; found: 1190.5131.

Synthesis of compound BTP-N3F: Compound **9** (100 mg, 0.084 mmol, 1 eq.), IC-2F (78 mg, 0.336 mmol, 4 eq.), and pyridine (1 mL) were dissolved in chloroform (10 mL) under nitrogen protection,

and the reaction was conducted at 65 °C. After completion, the reaction mixture was poured into methanol, causing the solid to precipitate. The precipitate was collected by filtration. The residue was further purified by silica gel chromatography using petroleum ether and dichloromethane (2:1, v/v) as eluents, yielding compound **BTP-N3F** as a purple-black solid (100 mg, 74%). ¹H NMR (400 MHz, Chloroform-d) ¹H NMR (400 MHz, Chloroform-d) δ 8.80 (s, 2H), 8.43 (dd, *J* = 9.9, 6.5 Hz, 2H), 7.59 (t, *J* = 7.4 Hz, 2H), 4.71 (t, *J* = 8.1 Hz, 4H), 2.95 (d, *J* = 7.6 Hz, 4H), 2.04 (s, 4H), 2.02 – 1.96 (m, 4H), 1.95 (d, *J* = 5.2 Hz, 2H), 1.49 (d, *J* = 7.4 Hz, 4H), 1.41 (s, 12H), 1.32 (s, 12H), 1.21 (s, 24H), 0.83 (dt, *J* = 11.1, 6.8 Hz, 12H). ¹³C NMR (101 MHz, Chloroform-d) δ 186.10, 158.04, 153.54, 147.18, 145.36, 137.34, 133.69, 132.45, 130.53, 125.80, 119.89, 114.95, 114.47, 113.64, 69.14, 34.70, 33.80, 33.52, 33.28, 31.92, 31.50, 29.70, 29.16, 29.05, 28.95, 28.62, 26.83, 26.70, 23.07, 22.74, 21.88, 14.20, 14.17. MALDI-TOF-MS: m/z calcd for C₈₆H₈₈F₁₀N₈O₂S₅: 1614.5474; found: 1614.5456.

Synthesis of compound 11: Under a nitrogen atmosphere, n-butyl lithium (1.72 mL, 4.3 mmol, 1 eq.) was added to a stirring solution of compound **10** (0.95 g, 4.3 mmol, 1 eq.) in diethyl ether (25 mL) at -78 °C. After stirring for 1.5 hours at this temperature, the newly prepared compound **6** (1 g, 5.1 mmol, 1.2 eq.) was quickly added. The reaction mixture was allowed to warm to room temperature and stirred overnight. After completion, the solution was poured into water, extracted with methylene chloride, dried over anhydrous magnesium sulfate, and concentrated under reduced pressure. The resulting residue was purified by silica gel chromatography using petroleum ether and ethyl acetate (30:1, v/v) as eluents, yielding compound **11** as a grey-black oil (1 g, 69%). ¹H NMR (400 MHz, Chloroform-d) δ 7.36 (dd, *J* = 5.3, 1.6 Hz, 1H), 7.23 (d, *J* = 5.3 Hz, 1H), 7.13 (s, 1H), 4.79 (t, *J* = 6.7 Hz, 1H), 2.63 (s, 1H), 2.09 – 1.99 (m, 2H), 1.86 (d, *J* = 4.3 Hz, 2H), 1.53 (p, *J* = 7.7, 6.9 Hz, 2H), 1.29 (s, 8H). ¹³C NMR (101 MHz, Chloroform-d) δ 139.50, 137.82, 137.11, 127.54, 122.24, 119.51,

70.55, 36.56, 33.83, 33.55, 29.15, 29.08, 28.62, 25.50, 21.86. HRMS calcd for C₁₅H₁₉F₆F₃OS₂: 336.0829; found: 336.3263.

Synthesis of compound 12: Under nitrogen protection, aluminum trichloride (0.625 g, 4.69 mmol, 1.5 eq.) and lithium aluminum hydride (0.36 g, 9.37 mmol, 3.0 eq.) were slowly added to ether (50 mL) at 0 °C. The mixture was then heated to room temperature and stirred for an additional 3 hours. At 0 °C, compound **11** (1 g, 3.12 mmol) was dissolved in ether (10 mL) and added dropwise to the solution, which was stirred at room temperature overnight. After the reaction was complete, the solution was carefully poured into ice water, followed by the addition of concentrated hydrochloric acid. The mixture was then extracted with methylene chloride, dried over anhydrous magnesium sulfate, and filtered. The filtrate was concentrated under reduced pressure. The resulting residue was purified by silica gel chromatography using petroleum ether as the eluent, yielding compound **12** as a colorless oil (0.5 g, 50%). ¹H NMR (400 MHz, Chloroform-d) δ 7.35 (dd, J = 5.2, 1.6 Hz, 1H), 7.24 (d, J = 5.2 Hz, 1H), 6.98 (d, J = 1.3 Hz, 1H), 2.74 – 2.70 (m, 2H), 2.09 – 2.00 (m, 2H), 1.75 (t, J = 7.3 Hz, 2H), 1.55 – 1.48 (m, 2H), 1.33 (d, J = 7.6 Hz, 8H). ¹³C NMR (101 MHz, Chloroform-d) δ 139.92, 138.78, 134.77, 126.61, 121.82, 119.97, 33.88, 33.60, 31.54, 29.95, 29.24, 29.14, 28.70, 28.56, 21.89. HRMS calcd for C₁₅H₁₉F₆F₃S₂: 320.0880; found [M + H⁺]: 321.0952.

Synthesis of compound 13: Under nitrogen protection, *n*-butyllithium (1.5 mL, 3.57 mmol) was added to a solution of compound **12** (1 g, 3.24 mmol) dissolved in tetrahydrofuran (30 mL) at -78 °C, and the mixture was stirred for 1 hour. Tributyltin chloride (1 mL, 3.57 mmol) was then added, and the stirring continued for an additional hour. The solution was warmed to room temperature and stirred overnight. After the reaction was complete, it was quenched with a saturated sodium bicarbonate solution, followed by the addition of 2-3 mL of triethylamine. The mixture was then extracted with petroleum ether, dried over anhydrous magnesium sulfate, filtered, and concentrated

to obtain the unpurified product. The resulting crude product was then ready to proceed to the next step.

Synthesis of compound 14: Compound **13** (1 g, 1.67 mmol), tetrakis(triphenylphosphine) palladium(0) (50 mg), and 4,7-dibromo-5,6-dinitroso-benzene[c][1,2,5]thiadiazole (0.3 g, 0.76 mmol) were dissolved in toluene (12 mL) under nitrogen protection. The mixture was stirred at 110 °C for 2 hours and then allowed to cool to room temperature. The solvent was removed by rotary evaporation. The residue was purified by silica gel chromatography using petroleum ether and dichloromethane (5:1, v/v) as eluents, yielding compound **14** as a red solid (0.3 g, 61%). ¹H NMR (400 MHz, Chloroform-d) δ 7.71 (s, 2H), 7.17 (s, 2H), 2.77 (t, J = 7.7 Hz, 4H), 2.05 (ddd, J = 10.8, 8.0, 5.2 Hz, 4H), 1.78 (t, J = 7.4 Hz, 4H), 1.56 – 1.52 (m, 4H), 1.40 – 1.32 (m, 16H). ¹³C NMR (101 MHz, Chloroform-d) δ 151.79, 135.17, 125.27, 124.11, 123.54, 115.91, 34.74, 31.95, 31.63, 29.69, 29.10, 28.67, 22.72. ¹³C NMR (101 MHz, Chloroform-d) δ 151.79, 142.96, 135.17, 130.05, 125.27, 124.17, 124.11, 123.54, 115.91, 34.74, 34.29, 33.85, 31.63, 29.72, 29.66, 29.10, 22.72, 14.16. HRMS calcd for C₃₆H₃₆F₆N₄O₄S₅: 862.1244; found [M+H⁺]: 863.2081.

Synthesis of compound 15: Compound **14** (0.22 g, 0.24 mmol, 1 eq.) and triphenylphosphine (0.65 g, 2.4 mmol, 10 eq.) were dissolved in ultra-dry N-methylpyrrolidone (6 mL) under nitrogen protection and reacted at 220 °C for 9 hours. After cooling to room temperature, additional N-methylpyrrolidone (12 mL) was added, followed by 5-(bromomethyl)undecane (0.60 g, 2.4 mmol, 10 eq.), potassium carbonate (0.71 g, 4.8 mmol, 20 eq.), and potassium iodide (0.53 g, 3.0 mmol, 12.5 eq.). The mixture was then reacted overnight under nitrogen protection at 90 °C. Upon completion of the reaction, the mixture was cooled to room temperature, diluted with methylene chloride, washed with ice water, and dried over anhydrous magnesium sulfate. The solution was filtered and concentrated, and the resulting residue was purified by silica gel chromatography using petroleum

ether and dichloromethane (4:1, v/v) as eluents, yielding compound **15** as an orange-yellow oil (150 mg, 55%). ¹H NMR (400 MHz, Chloroform-d) δ 7.00 (s, 2H), 4.57 (d, *J* = 7.8 Hz, 4H), 2.81 (t, *J* = 7.6 Hz, 4H), 2.09 – 2.01 (m, 6H), 1.85 (t, *J* = 7.4 Hz, 4H), 1.35 (s, 20H), 0.92 (dt, *J* = 19.3, 7.2 Hz, 32H), 0.62 (dd, *J* = 13.3, 7.2 Hz, 12H). ¹³C NMR (101 MHz, Chloroform-d) δ 147.65, 142.04, 137.05, 136.68, 131.70, 125.92, 123.72, 122.78, 119.31, 111.51, 55.03, 38.66, 33.87, 33.59, 31.54, 30.29, 29.60, 29.36, 29.13, 28.78, 28.70, 28.01, 27.83, 25.31, 25.10, 22.74, 22.41, 21.83, 13.66. HRMS calcd for C₆₀H₈₄F₆N₄S₅: 1134.5204; found: 1134.5177.

Synthesis of compound 16: Compound **15** (150 mg, 0.15 mmol) was dissolved in 1,2-dichloroethane (7.5 mL) under nitrogen protection. N,N-dimethylformamide (7.5 mL) and phosphorus oxychloride (0.75 mL) were added to the solution at 0 °C, and the mixture was stirred for 1 hour before being heated to 90 °C and stirred overnight. After cooling to room temperature, the reaction mixture was poured into ice water and stirred for 4 hours. The mixture was then extracted with methylene chloride, dried over anhydrous magnesium sulfate, filtered, and concentrated. The resulting residue was purified by silica gel chromatography using petroleum ether and dichloromethane (1.5:1, v/v) as eluents, yielding compound **16** as an orange solid (110 mg, 72%). ¹H NMR (400 MHz, Chloroform-d) δ 10.13 (s, 2H), 4.61 (d, *J* = 7.8 Hz, 4H), 3.19 (t, *J* = 7.7 Hz, 4H), 2.10 – 1.99 (m, 6H), 1.92 (p, *J* = 7.7 Hz, 4H), 1.55 – 1.32 (m, 20H), 1.11 – 0.73 (m, 32H), 0.66 – 0.58 (m, 12H). ¹³C NMR (101 MHz, Chloroform-d) δ 181.72, 147.48, 146.62, 143.16, 137.06, 136.82, 132.97, 129.70, 128.63, 127.36, 125.88, 112.41, 55.29, 38.89, 33.84, 33.56, 31.49, 30.25, 29.52, 29.29, 29.11, 28.67, 28.11, 27.91, 27.74, 25.22, 25.02, 22.72, 22.41, 21.87, 13.92, 13.65. HRMS calcd for C₆₂H₈₄F₆N₄O₂S₅: 1190.5102; found: 1190.5139.

Synthesis of compound BTP-C3F: Compound **16** (100 mg, 0.084 mmol, 1 eq.), IC-2F (78 mg, 0.336 mmol, 4 eq.), and pyridine (1 mL) were dissolved in chloroform (10 mL) under nitrogen protection,

and the reaction was conducted at 65 °C. Once the reaction was completed, the solution was poured into methanol, causing the solid to precipitate. The precipitate was collected by filtration. The residue was further purified by silica gel chromatography using petroleum ether and dichloromethane (2:1, v/v) as eluents, resulting in the production of compound **BTP-C3F** as a purple-black solid (100 mg, 74%). ¹H NMR (400 MHz, Chloroform-d) δ 9.15 (d, *J* = 2.8 Hz, 2H), 8.56 (dd, *J* = 9.9, 6.5 Hz, 2H), 7.69 (t, *J* = 7.5 Hz, 2H), 4.75 (d, *J* = 7.6 Hz, 4H), 3.22 (t, *J* = 7.6 Hz, 4H), 2.14 – 2.01 (m, 6H), 1.88 (d, *J* = 8.1 Hz, 4H), 1.44 (d, *J* = 67.4 Hz, 20H), 1.23 – 0.82 (m, 32H), 0.70 – 0.62 (m, 12H). ¹³C NMR (101 MHz, Chloroform-d) δ 186.11, 158.87, 153.64, 147.50, 137.66, 135.99, 135.22, 134.51, 134.19, 133.28, 130.86, 114.98, 114.53, 113.56, 68.76, 55.70, 39.20, 33.85, 33.57, 31.57, 31.13, 30.39, 29.69, 29.38, 29.14, 29.03, 28.65, 28.07, 27.87, 25.41, 22.79, 22.45, 13.99, 13.74. MALDI-TOF-MS: m/z calcd for C₈₆H₈₈F₁₀N₈O₂S₅: 1614.5474; found: 1614.5456.

Methods: ¹H and ¹³C NMR spectra were recorded on a Bruker Avance-400 spectrometer with d-chloroform as solvent. The chemical shifts were reported as δ value (ppm) relative to an internal tetramethylsilane (TMS) standard. High resolution mass spectrum (HRMS) was recorded on Thermal Finnigan TSQ Quantum liquid chromatograph/mass spectrometer. Matrix assisted laser desorption ionization time of flight mass spectrometry (MALDI-TOF-MS) was recorded on a Bruker Solarix Fourier transform ion cyclotron resonance mass spectrometry (FT-ICR-MS) system. Molecular weights of the polymers were determined by Agilent GPC 50 GPC/SEC system at 25 °C (vs polystyrene standards) using tetrahydrofuran as the eluent. All molecular simulation calculations were carried out by density functional theory (DFT) at the B3LYP/6-31G(d) level, all the calculations were performed in the gas phase with Gaussian 09 program. Thermogravimetric analysis (TGA) was conducted on a TA Instrument Model SDT Q600. Differential scanning calorimetry (DSC) was conducted on a TA Differential Scanning Calorimeter DSC25 at a heating rate of 10 °C min⁻¹ and

under a N₂ flow rate of 90 mL min⁻¹. UV-vis-NIR spectra were obtained on a Shimadzu UV3600i spectrophotometer. LEIPS was tested by using PHI VersaProbe 4 (Scanning ESCA Microprobe). CV measurements were made on a CHI604E potentiostat/galvanostat electrochemical workstation at a scan rate of 50 mV s⁻¹ with the platinum wire as the counter electrode and the Ag/AgCl as a reference electrode, which was calibrated by the ferrocene/ferrocenium (Fc/Fc+) redox couple to be -4.382 eV. AFM and PiFM images were obtained by using a Bruker NanoIR3 atomic microscope. Droplet contact angle was measured on a Krüss DSA100 contact angle meter. GIWAXS measurements were performed at Complex Materials Scattering (CMS) beamline of the National Synchrotron Light Source II (NSLS-II), Brookhaven National Lab with a Pilatus 2M detector. Femtosecond transient absorption spectroscopy (fs-TAS) was conducted using a commercial Helios setup from Ultrafast Systems with a Ti: sapphire regenerative amplified laser system (Coherent Libra) delivered laser pulses at 780 nm (100fs, 1 kHz). An optical parametric amplifier (Vitara, Coherent) pumped by the regenerative amplifier was used to generate the pump beam at 780 nm (at wavelength resonant with the absorption of the NFAs). The probe beam was generated by focusing part of the fundamental femtosecond laser beam onto a sapphire plate or Yttrium aluminum garnet plate for visible (Vis) and near-IR (NIR) spectral windows, respectively. TAS results in this work are presented in the unit of ΔOD, negative features can reflect ground-state bleaching (GSB) or stimulated emission (SE), a positive signal is an excited-state absorption (ESA). During TA measurements, the samples were kept in nitrogen to avoid photodegradation. The pump fluence was kept at <5 μJ/cm² to minimize the exciton-exciton annihilation effect. The photoluminescence (PL) and transient photoluminescence (TRPL) measurements were conducted using a Fluorolog-3 spectrofluorometer with an excitation wavelength of 750 nm.

Impedance spectroscopy (IS) was performed in the range of 1 Hz to 1 MHz using a CHI604E

series electrochemical workstation under dark conditions and analyzed with the Zview measurement software. Devices with the architecture glass/ITO/PEDOT:PSS/dielectric layer/Ag were fabricated and tested inside a sealed, light-tight box to minimize photo-induced charges. A low AC excitation voltage (10 mV) and zero DC bias were used to prevent charge injection, enabling accurate determination of the dielectric constant in the high-frequency range, where only intrinsic electronic polarization contributes. The film thicknesses were measured by using a Bruker Inova atomic microscope. The dielectric constant (ε_r) was evaluated at the material's geometric capacitance, which corresponds to capacitance arising purely from electronic, atomic, and ionic polarization.⁴ Geometric capacitance was calculated using the film thickness (d) and device area (A) according to Equation (1).⁵

$$\varepsilon_r = \frac{C_g d}{\varepsilon_0 A} \quad (1)$$

2. Single-crystal analyses

Single crystal structure data were collected on Bruker D8 Venture with a rotating copper anode and a Pilatus 200K detector. CCDC 2384715 and 2384716 contain the supplementary crystallographic data for BTP-N3F and BTP-C3F, respectively, which can be obtained free of charge from the Cambridge Crystallographic Data Centre via <http://www.ccdc.cam.ac.uk/structures>. Check CIF reports of single crystals of BTP-N3F and BTP-C3F were summarized in Supplementary Table S1.

3. Device fabrication and measurements

Device fabrication: The patterned indium tin oxide (ITO, sheet resistance = 15 Ω square⁻¹) glass substrates were sequentially ultrasonicated with detergent, deionized water, acetone, and isopropanol. Then, the ITO glasses were treated with UV-ozone for 30 min. The hole transporting layer Nb₂O₅/2PACz was prepared according to our previous report.⁶ The D18-Cl (8.5 mg mL⁻¹ in

chlorobenzene) solution was spin-coated on the ITO/Nb₂O₅/2PACz substrate to form the underlying donor layer, and the NFA solutions (8.5 mg mL⁻¹ without or with PPFS) were spin-coated on the top of the donor layer to form the photoactive layers with thickness around 100 nm. The above substrates were then baked at 100 °C for 10 min on a hot plate. 2,9-dimethyl-4,7-diphenyl-1,10-phenanthroline (BCP, 6 nm) and argentum electrode (Ag, 100 nm) were thermally deposited under high vacuum (~10⁻⁵ Pa) in an evaporation chamber. The device area was exactly fixed at 4.00 mm².

Fabrication of electron-only and hole-only devices: Electron-only and hole-only devices designed for space-charge-limited current (SCLC) measurements, were fabricated using similar methods with device architectures of ITO/ZnO/active layer/PNDIT-F3N/Ag and ITO/Nb₂O₅/2PACz/active layer/Au, respectively. The ZnO layer was fabricated using a sol-gel method, Ag and Au electrodes were deposited by thermal evaporation in vacuum. All device fabrications were performed in an argon gas filled glove box. The mobility was determined by fitting the dark current to the Mott-Gurney law, described by equation (2):

$$J = \frac{9}{8} \varepsilon_0 \varepsilon_r \mu \frac{V^2}{d^3} \quad (2)$$

where J is the current density, ε_r is the relative dielectric constant of the transport medium, ε_0 is the vacuum permittivity, μ is the electron or hole mobility, V is the effective voltage, and d is the thickness of the active layer. The SCLC region was identified with a slope of 2±0.1 in the log-log plot. Mobility values for electrons and holes were estimated by fitting the data to the Mott-Gurney law in this region.

Device measurements:

I-V characterization was performed using a computer-controlled Keithley 2400 Source Meter under AM1.5G illumination (100 mW cm⁻²) provided by a solar simulator (XES-70S1, SAN-EI), calibrated with a standard Si solar cell (AK-200, Konica Minolta, Inc.). External quantum efficiency (EQE)

spectra were obtained using an EQ-R solar quantum efficiency test system (Enlitech Co., Ltd., Taiwan, China). For these measurements, a metal mask with a 4 mm² aperture was precisely aligned with the device area. TPV and TPC measurements were performed using the all-in-one characterization platform Paios (Fluxim AG, Switzerland). For storage stability tests, devices were stored in a glove box, and their performance was evaluated at regular intervals. Thermal stability tests were conducted by placing the devices on a heating table set to 85 °C, with periodic performance assessments.

Dielectric constant-dependent mobility models:

Three prominent theoretical frameworks demonstrate how the ϵ_r significantly influences charge carrier mobility in organic semiconductors:

Marcus charge transfer theory⁷

The charge carrier mobility is proportional to the hopping rate ν and the square of the hopping distance d :

$$\mu \propto \nu \cdot d^2$$

Where, the hopping rate ν is derived from Marcus theory as:

$$\nu = A \cdot \exp\left(-\frac{\Delta G^\ddagger}{k_B T}\right)$$

Where, A is the pre-exponential factor, related to electronic coupling between adjacent sites, T is the absolute temperature, and k is Boltzmann's constant, ΔG^\ddagger is the activation free energy, given by:

$$\Delta G^\ddagger = \frac{\lambda}{4} \left(1 + \frac{\Delta E}{\lambda}\right)^2$$

Here, ΔE is the energy difference between initial and final states, λ is the reorganization energy, a measure of the interaction between the charge carrier and the molecular or environmental

polarization, composed of two components:

$$\lambda = \lambda_{internal} + \lambda_{external}$$

Where, $\lambda_{internal}$ arises from intramolecular vibrations and geometric rearrangements, and is typically independent of the dielectric constant; $\lambda_{external}$ stems from the interaction between the localized charge and the polarization of the surrounding medium. Its dependence on the dielectric constant is expressed as:

$$\lambda_{external} \propto \frac{1}{\epsilon_r}$$

When the static dielectric constant increases, the external reorganization energy ($\lambda_{external}$) decreases. This leads to a reduction in the activation energy ΔG^\ddagger , enhancing the hopping rate k and thereby increasing the mobility μ .

Poole-Frenkel Theory⁸⁻¹⁰

$$\mu(E) = \mu_0 \times \exp\left(\frac{\beta_{PF}\sqrt{E}}{kT}\right)$$

$$\beta_{PF} = \sqrt{\frac{q^3}{\pi\epsilon_0\epsilon_r}}$$

Where, E represents the applied electric field, μ_0 is the zero-field mobility, derived from Poole-Frenkel theory as:

$$\mu_0 = RT^2 \exp\left(-\frac{\Phi_t}{kT}\right)$$

Where, R is the Richardson constant, and the Coulomb trap barrier height Φ_t from Poole-Frenkel theory as:

$$\Phi_t = \frac{q^2}{4\pi\epsilon_0\epsilon_r|r|} + \frac{q^2}{4\pi\epsilon_0\epsilon_r|r-s|} + qEr\cos\theta$$

Where, r is radius of trap and s is the distance between the two trap centers. The increase in ϵ_r

reduces the trap barrier height and thus improves zero-field mobility, thereby increasing mobility.

Bässler Gaussian Disorder Model¹¹

$$\mu \propto \exp\left(-\left(\frac{2\sigma}{kT}\right)^2\right)$$

Where, the energetic disorder parameter σ from Bässler Gaussian Disorder Model as:

$$\sigma^2 = \sigma_d^2 + \sigma_p^2 + \sigma_{vdw}^2$$

Where, the dipolar disorder σ_d from Bässler Gaussian Disorder Model as:

$$\sigma_d^2 = 0.74c^{0.5} \frac{p}{\xi^2 \epsilon_r \epsilon_0}$$

Where, p is the molecular dipole moment, ξ^2 is the intermolecular separation and c is the fraction of sites occupied by randomly oriented dipoles with dipole moment. Materials with higher ϵ_r effectively screen the electric fields generated by molecular dipoles and quadrupoles, reducing energetic disorder (σ) and consequently enhancing charge carrier mobility through more uniform energy landscapes.

4. Supplementary figures

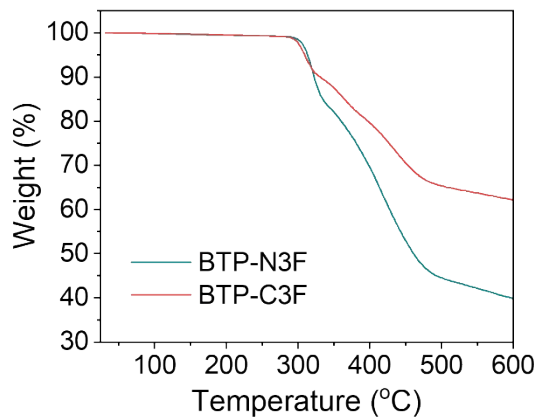


Fig. S1 TGA curves of the NFAs. The samples were tested at heating a rate of 10 °C min⁻¹ and under a N₂ flow rate of 90 mL min⁻¹.

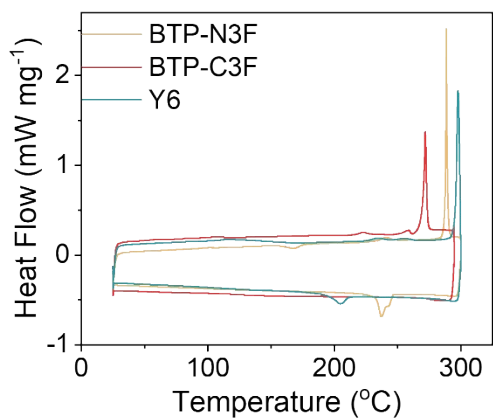


Fig. S2 DSC curves of the NFAs. The samples were tested at heating/cooling rate of $10\text{ }^{\circ}\text{C min}^{-1}$ and under a N_2 flow rate of 90 mL min^{-1} .

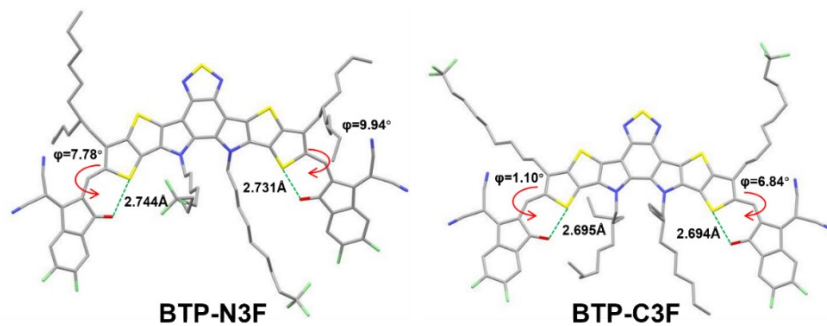


Fig. S3 The monomolecular crystallographic structures of BTP-N3F and BTP-C3F. The intramolecular $\text{S}\cdots\text{O}$ distances, the D-A dihedral angles (ϕ) were illustrated.

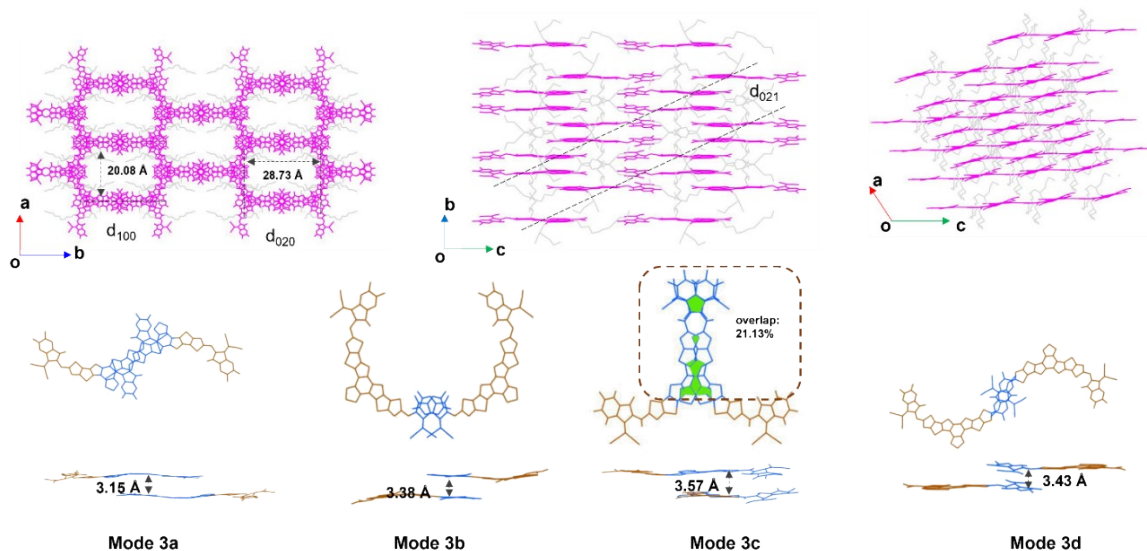


Fig. S4 Molecular stacking diagrams with various intermolecular packing modes of Y6.

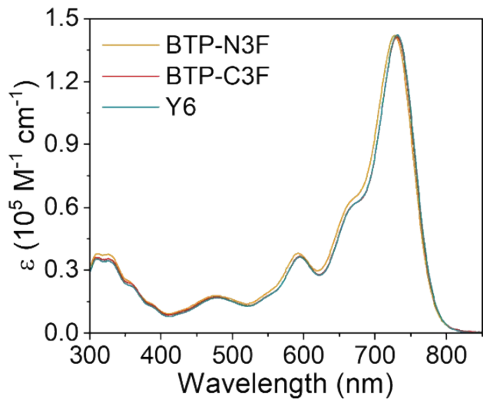


Fig. S5 Molar extinction coefficient profiles of the NFAs in chloroform solutions.

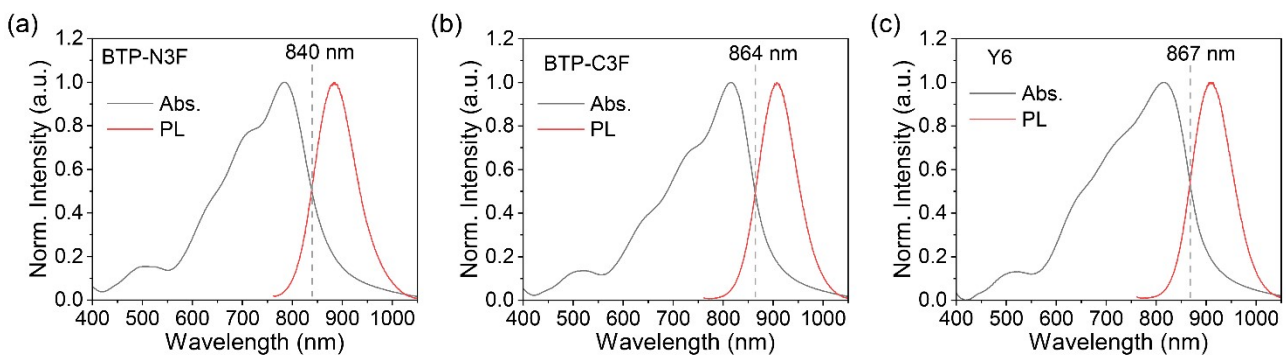


Fig. S6 Normalized UV-vis-NIR absorption and photoluminescence (PL) spectra of the NFAs, with their intersections used to estimate the bandgaps.

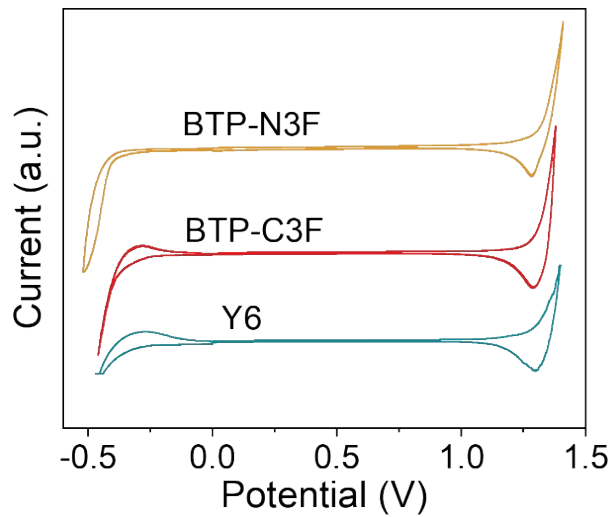


Fig. S7 CV curves of the NFAs.

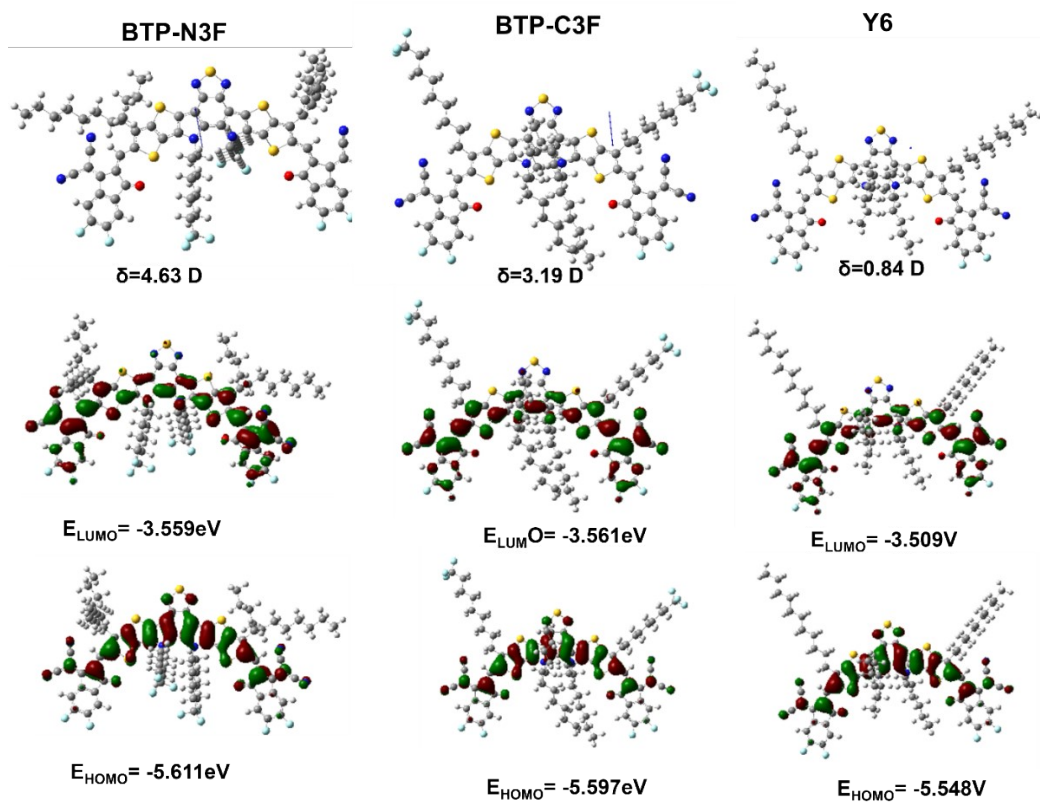


Fig. S8 Optimized molecular geometries and frontier orbitals of the NFAs.

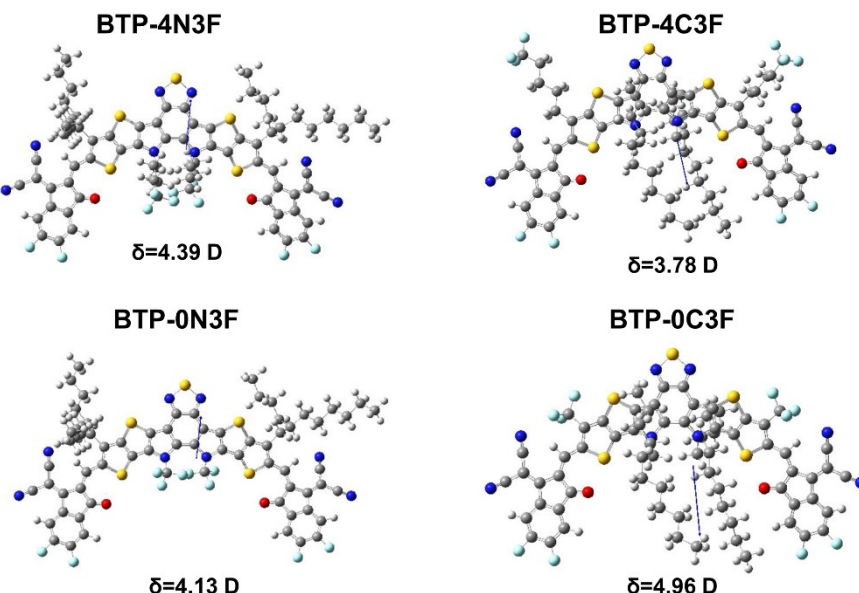


Fig. S9 Optimized molecular geometries and dipole moments of the NFAs with trifluoromethyl sidechains.

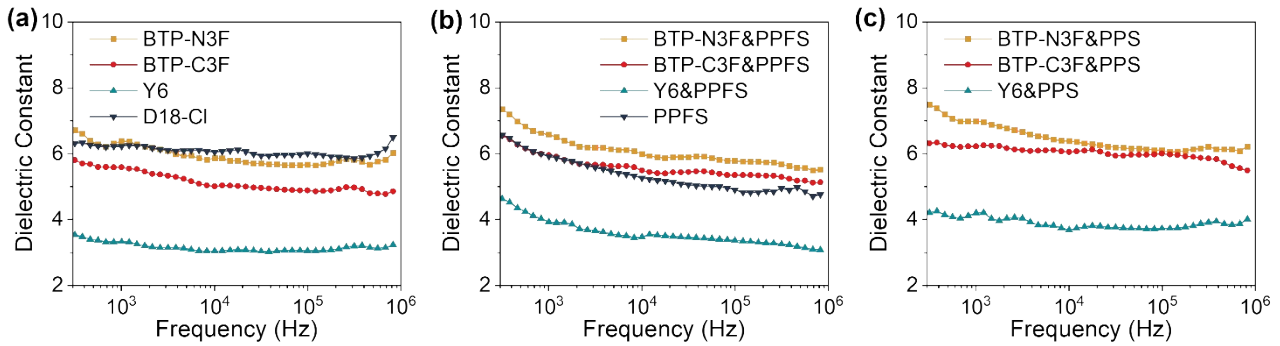


Fig. S10 Frequency-dependent ϵ_r of the donor and acceptor materials. (f) Frequency-dependent ϵ_r of the NFAs with PPFS additive. (f) Frequency-dependent ϵ_r of the D18-Cl/NFA films with PPFS additive.

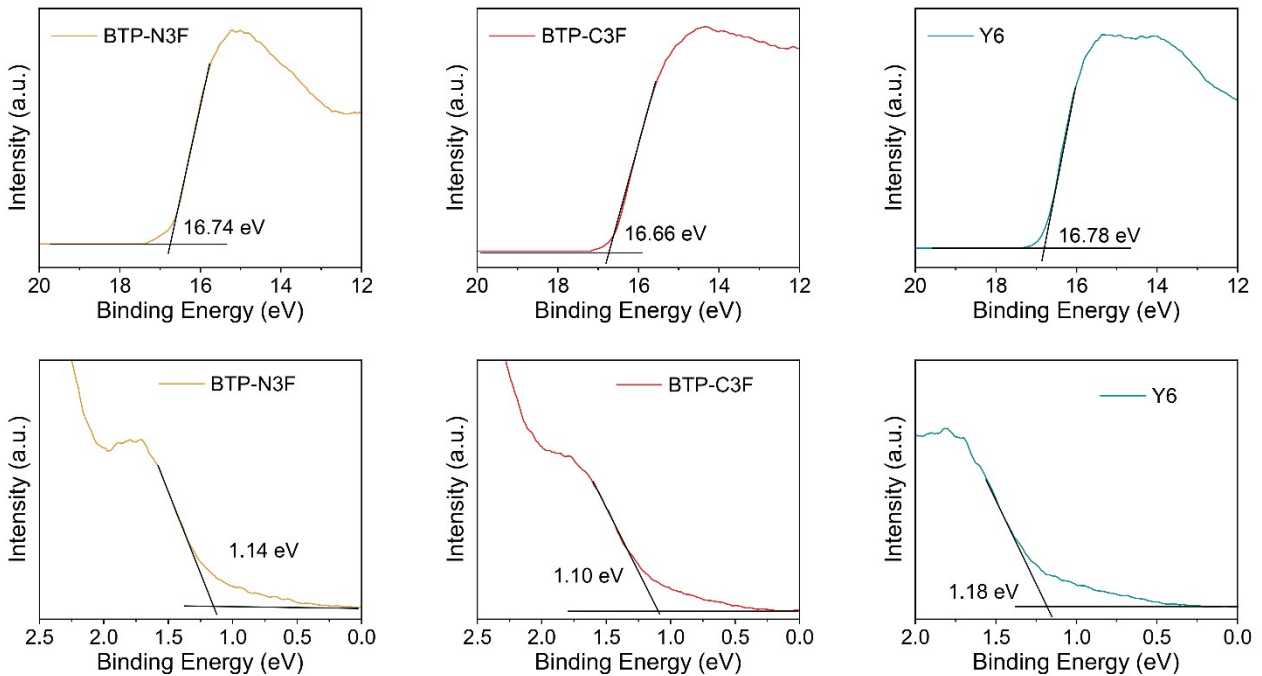


Fig. S11 UPS curves of BTP-N3F, BTP-C3F and Y6 films.

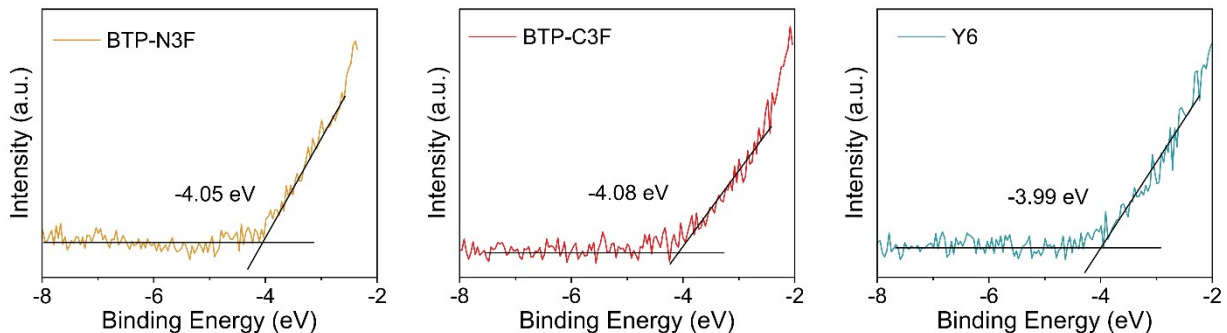


Fig. S12 LEIPS curves of BTP-N3F, BTP-C3F and Y6 films.

Molecular Weight Averages

Sample name	Data file	Peak #	RT (min)	M _p (g/mol)	M _n (g/mol)	M _w (g/mol)	M _z (g/mol)	M _{z+1} (g/mol)	PD
8706-F1	2025-02-26 18-51-42+08-00-04.dx	1	7.730	28954	17138	28816	41856	54439	1.681410

Molecular Weight Distribution Plots

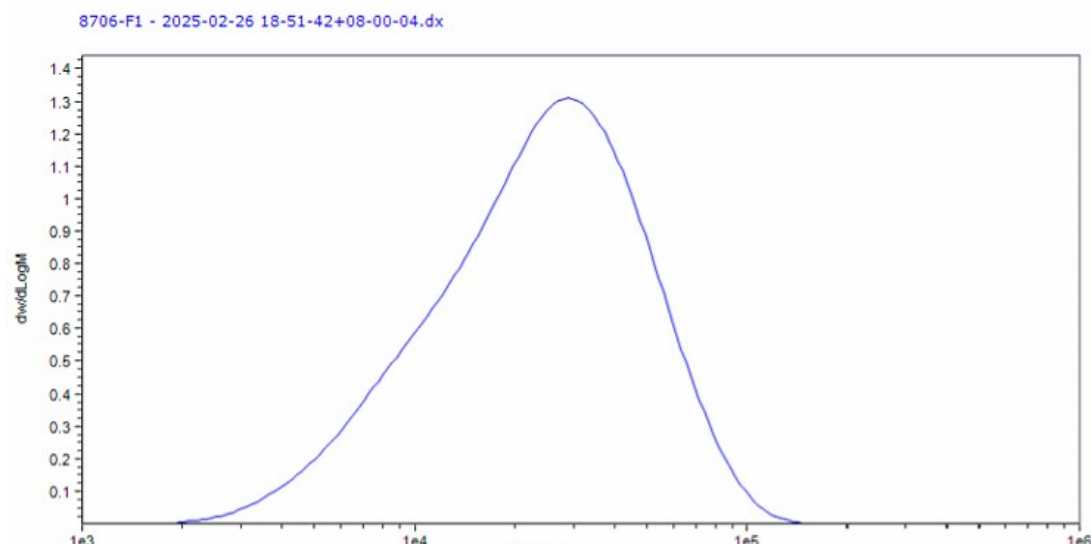


Fig. S13 Molecular weights of PPFS determined by gel permeation chromatography (GPC).

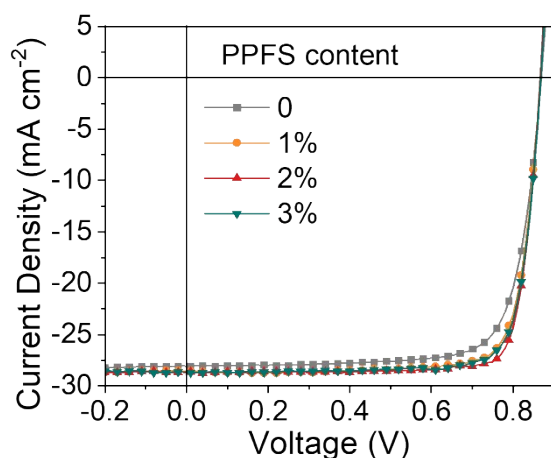


Fig. S14 $J-V$ curves of D18-Cl/BTP-C3F-based OSCs with varying PPFS additive concentrations.

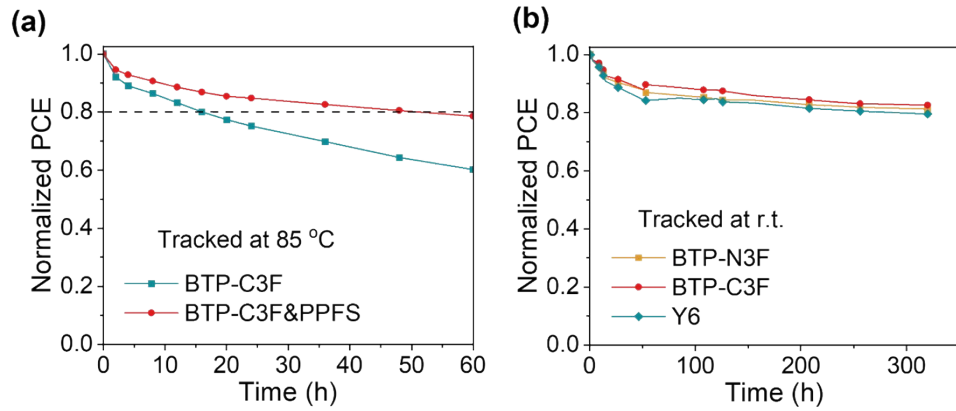


Fig. S15 (a) Thermal stability of unencapsulated D18-Cl/BTP-C3F-based devices with or without the PPFS additive, tested at 85 °C in glove box. (b) Storage stability of unencapsulated OSCs with the PPFS additive in room temperature (r.t.) glove box.

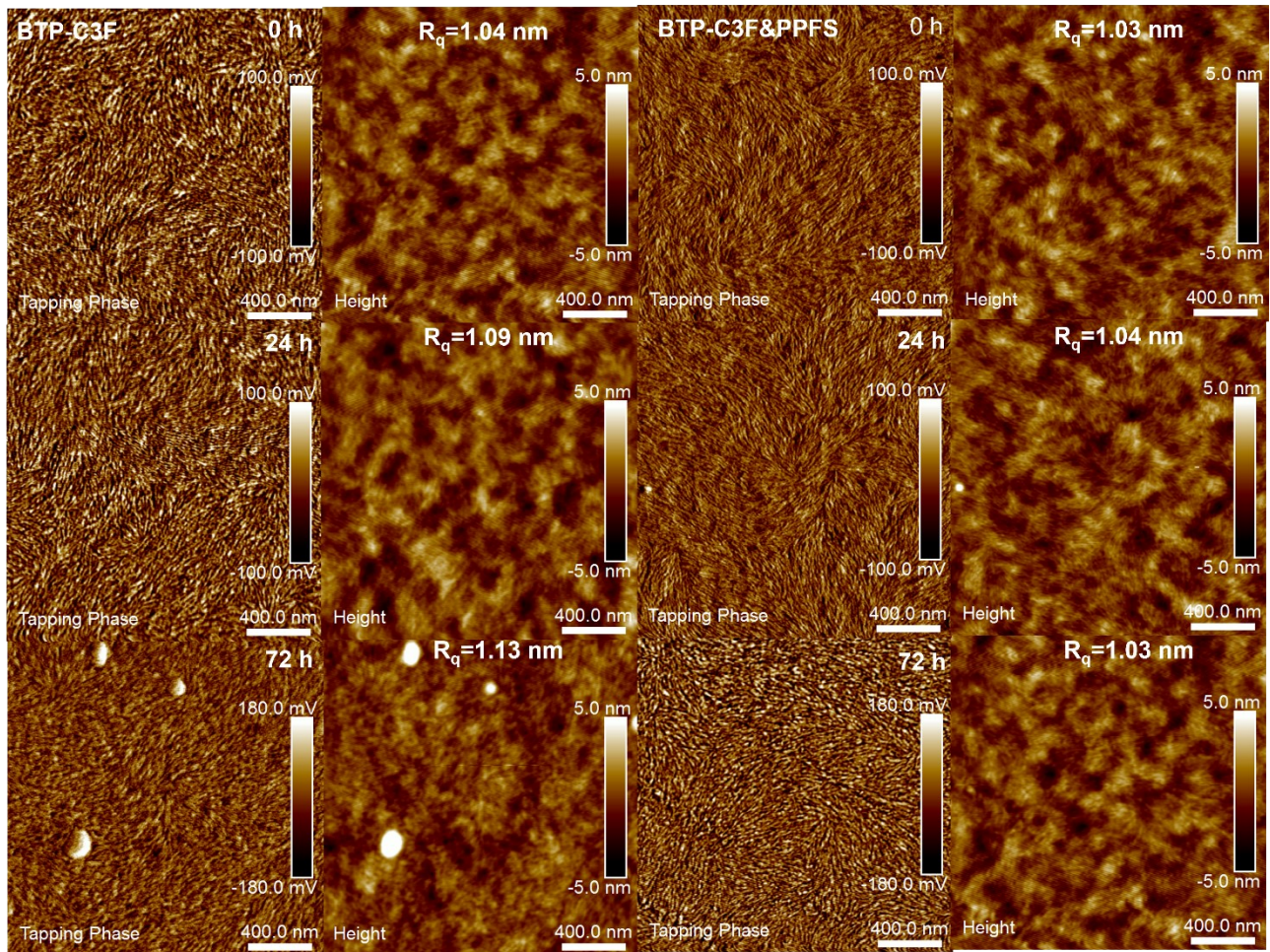


Fig. S16 AFM images of the D18-Cl/BTP-C3F films with and without PPFS additive were heated at 85 °C for different times.

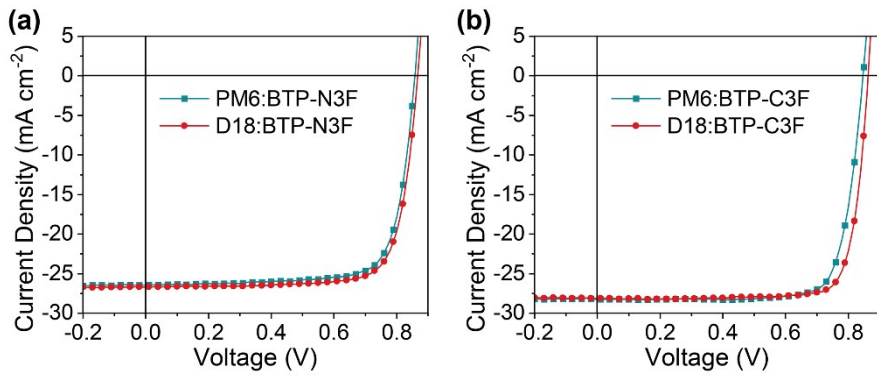


Fig. S17 J - V curves of the OSCs with various donor and acceptor materials.

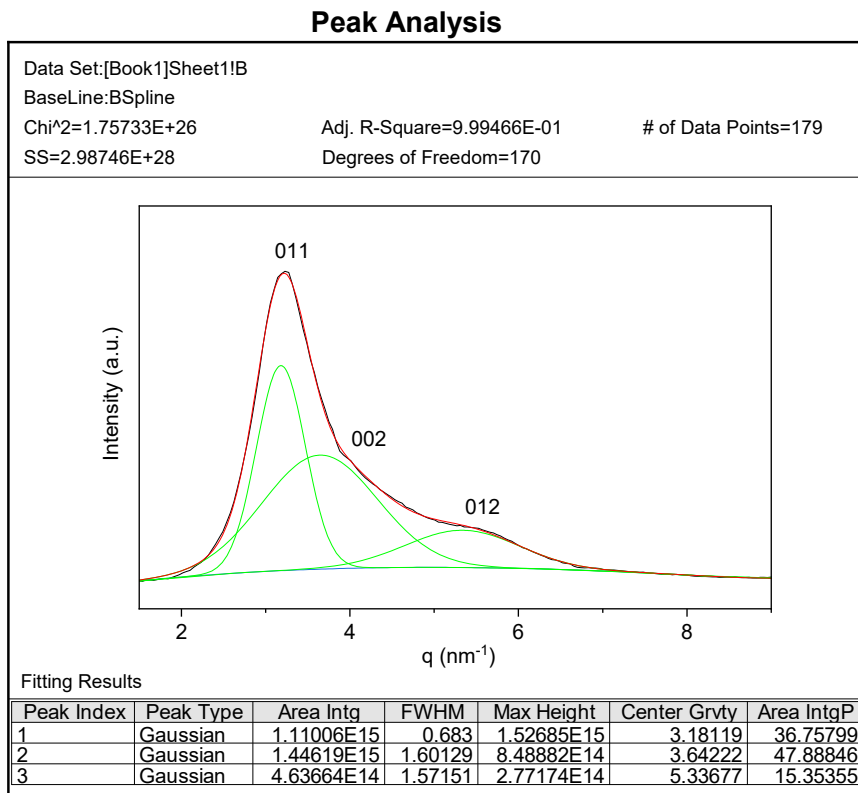


Fig. S18 In-plane X-ray diffraction peak fitting analysis of BTP-N3F.

Peak Analysis

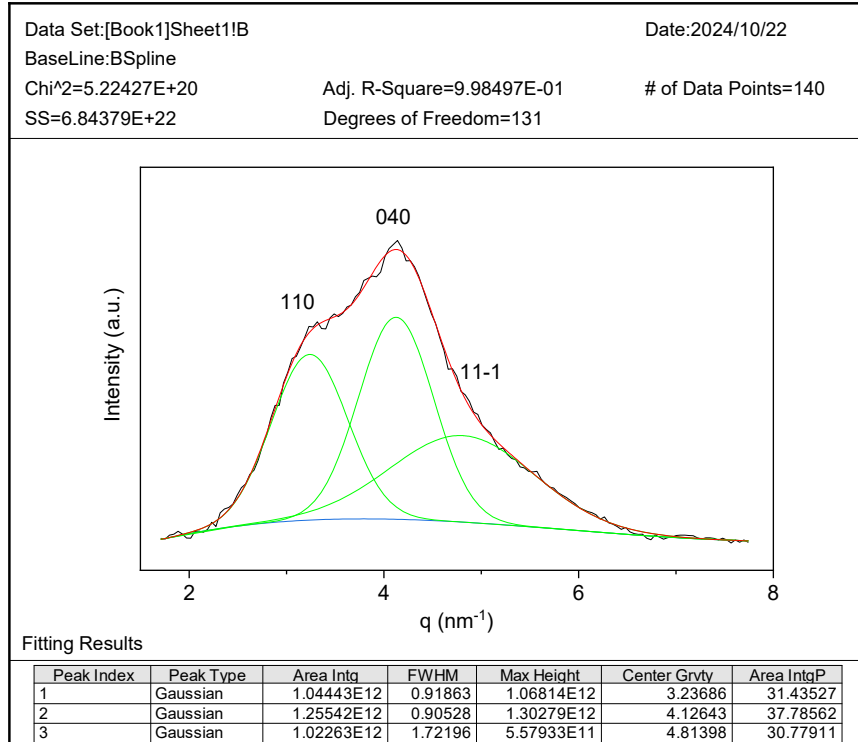


Fig. S19 In-plane X-ray diffraction peak fitting analysis of BTP-C3F.

Peak Analysis

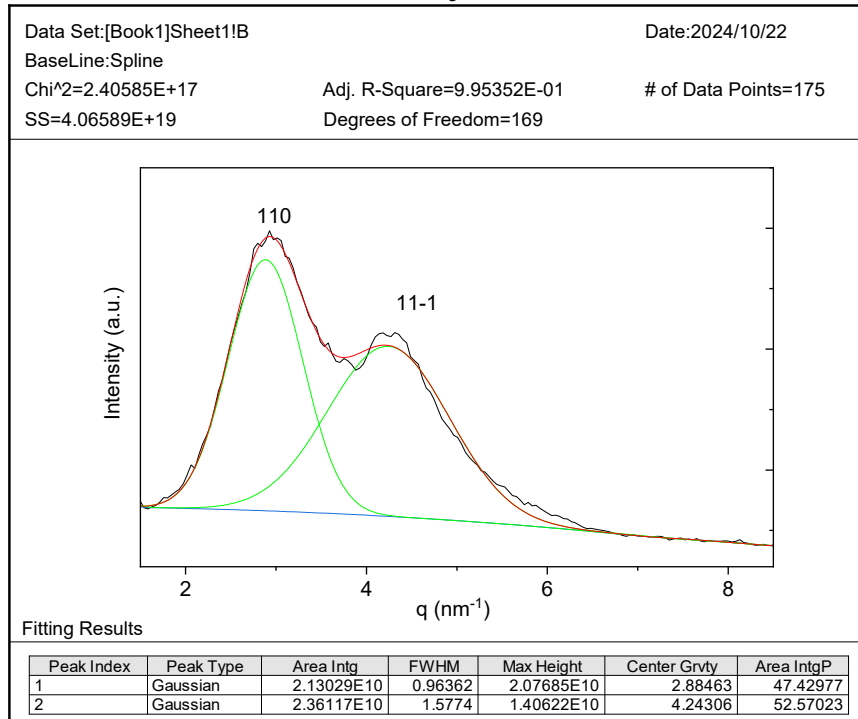


Fig. S20 In-plane X-ray diffraction peak fitting analysis of Y6.

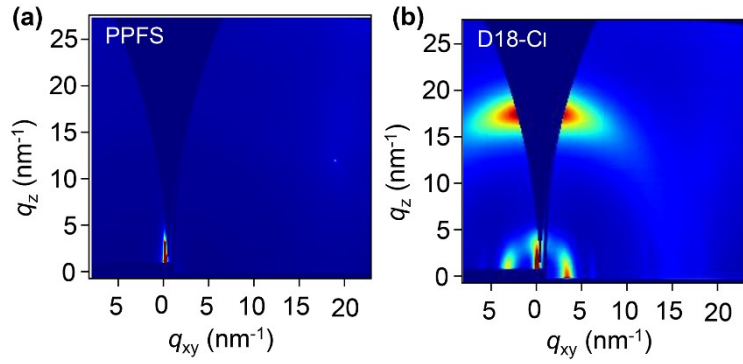


Fig. S21 GIWAXS patterns of the PPFS additive and D18-Cl donor.

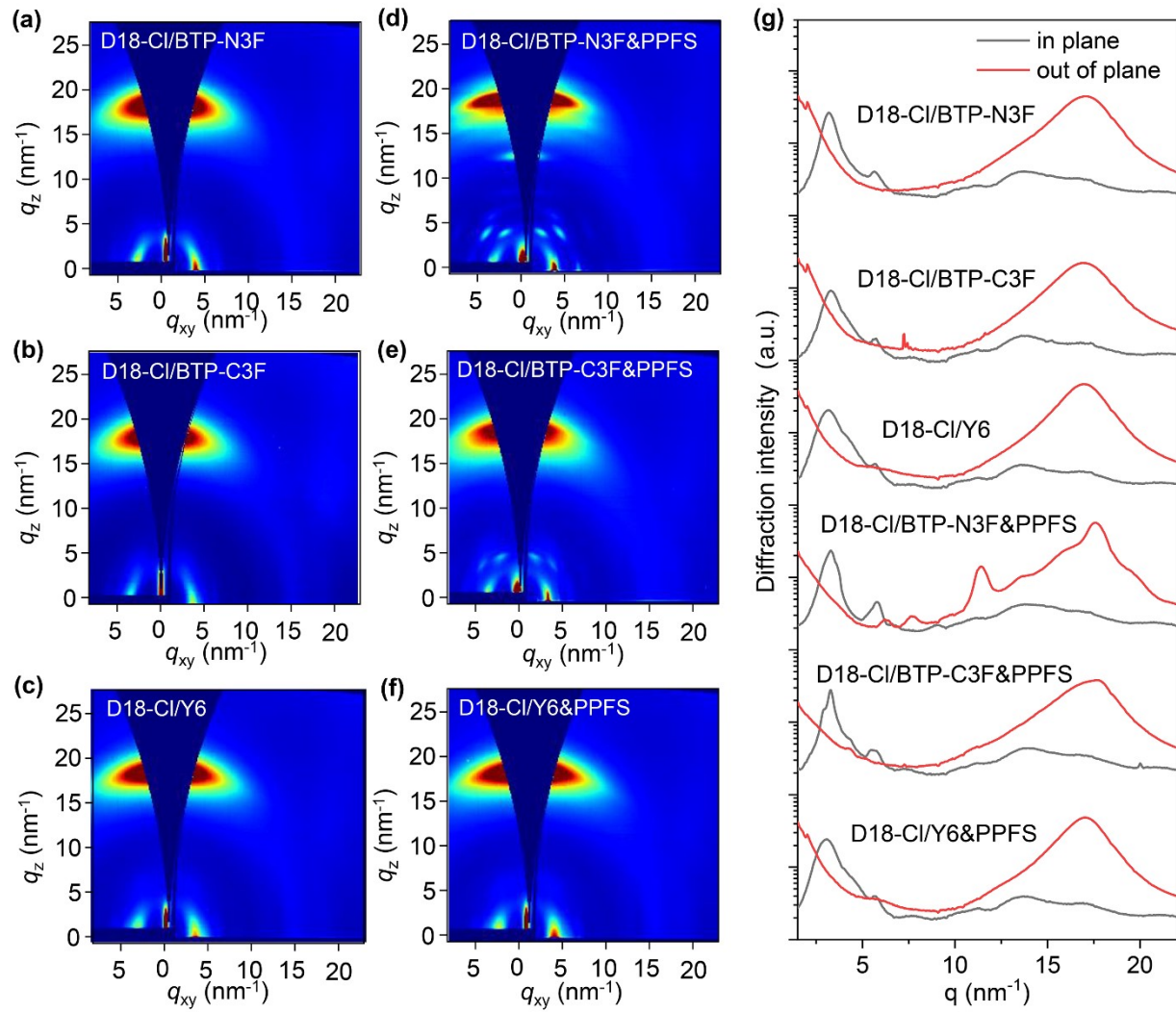


Fig. S22 GIWAXS patterns of D18-Cl/BTP-N3F (a), D18-Cl/BTP-N3F with PPFS (d), D18-Cl/BTP-C3F (b), D18-Cl/BTP-C3F with PPFS (e), D18-Cl/Y6 (c) and D18-Cl/Y6 with PPFS (f). (g) The corresponding in-plane and out-of-plane diffraction line-cuts.

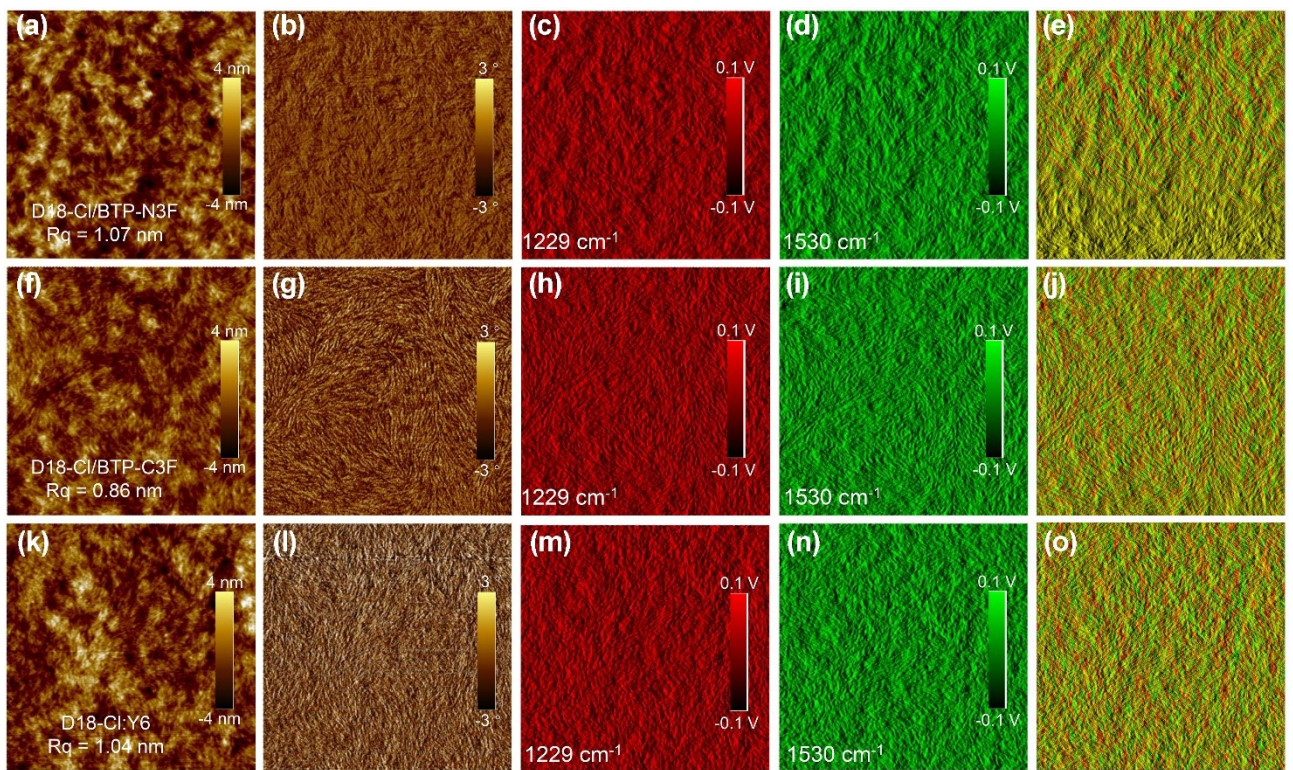


Fig. S23 AFM and PiFM images of the D18-Cl/NFA films without PPFS additive. Top row: D18-Cl/BTP-N3F; Middle row: D18-Cl/BTP-C3F; Bottom row: D18-Cl/Y6. PiFM images at the wave numbers of 1229 and 1530 cm^{-1} were denoted to the D18-Cl donor and the NFAs, respectively. Image size: $2 \times 2 \mu\text{m}^2$.

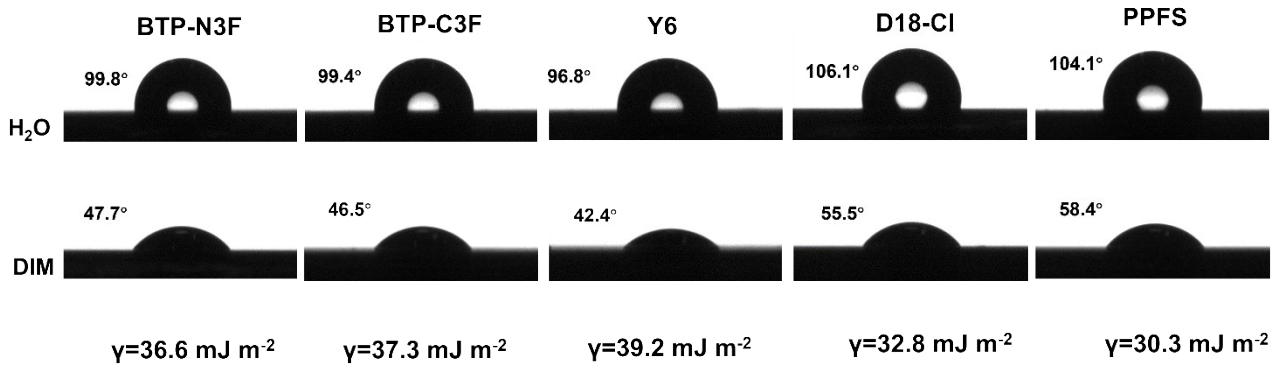


Fig. S24 Water (H_2O) and diiodomethane (DIM) droplets contact angles of the materials.

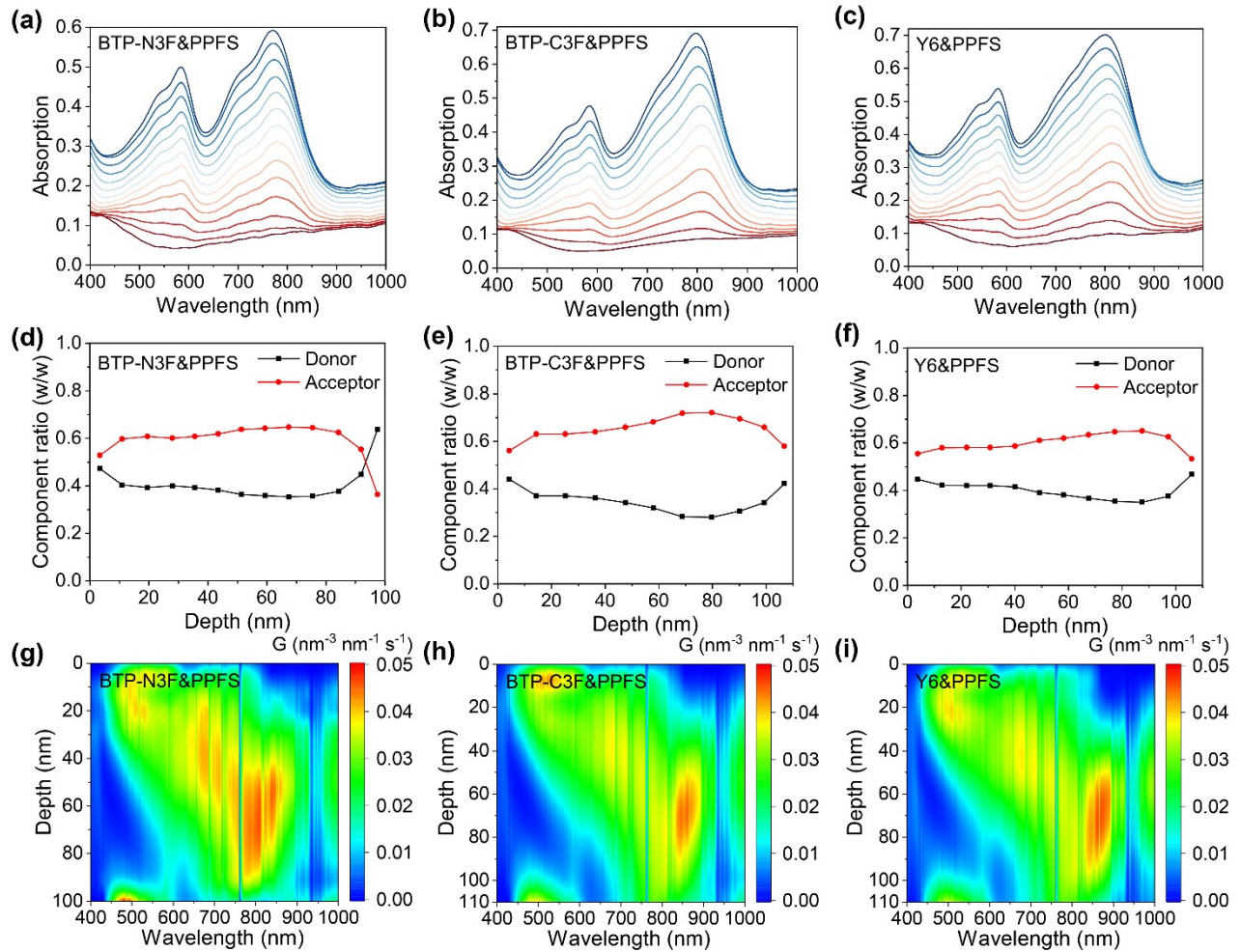


Fig. S25 (a-c) Film-depth-dependent profiling light absorption spectra of the active layer films based on different acceptors modified with PPFS additive. (d-f) Film-depth-dependent component distribution profiles. (g-i) The calculated exciton generation contour maps of the active layer films based on different acceptors modified with PPFS additive.

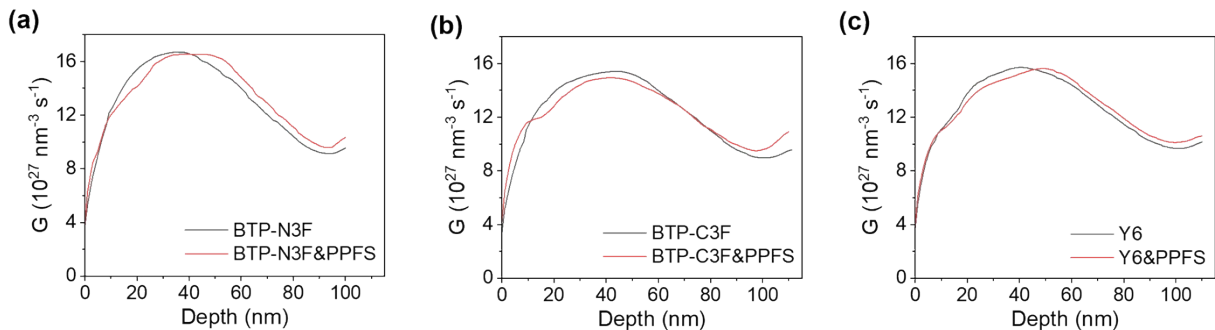


Fig. S26 Film-depth-dependent exciton generation rate (G) of the active layers with and without adding PPFS additive.

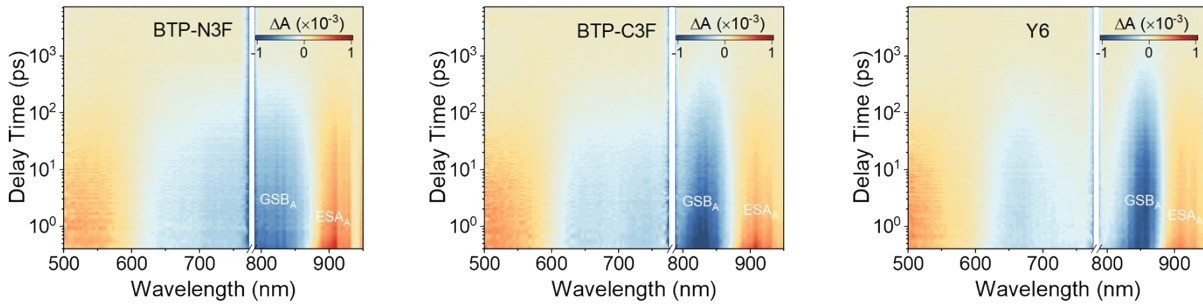


Fig. S27 Color plots the fs-TA spectra of the NFA films.

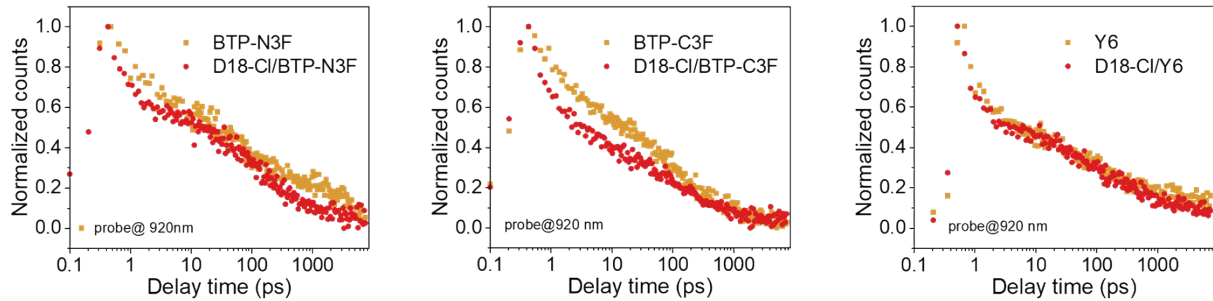


Fig. S28 TA kinetics of the NFA and D18-Cl/NFA films.

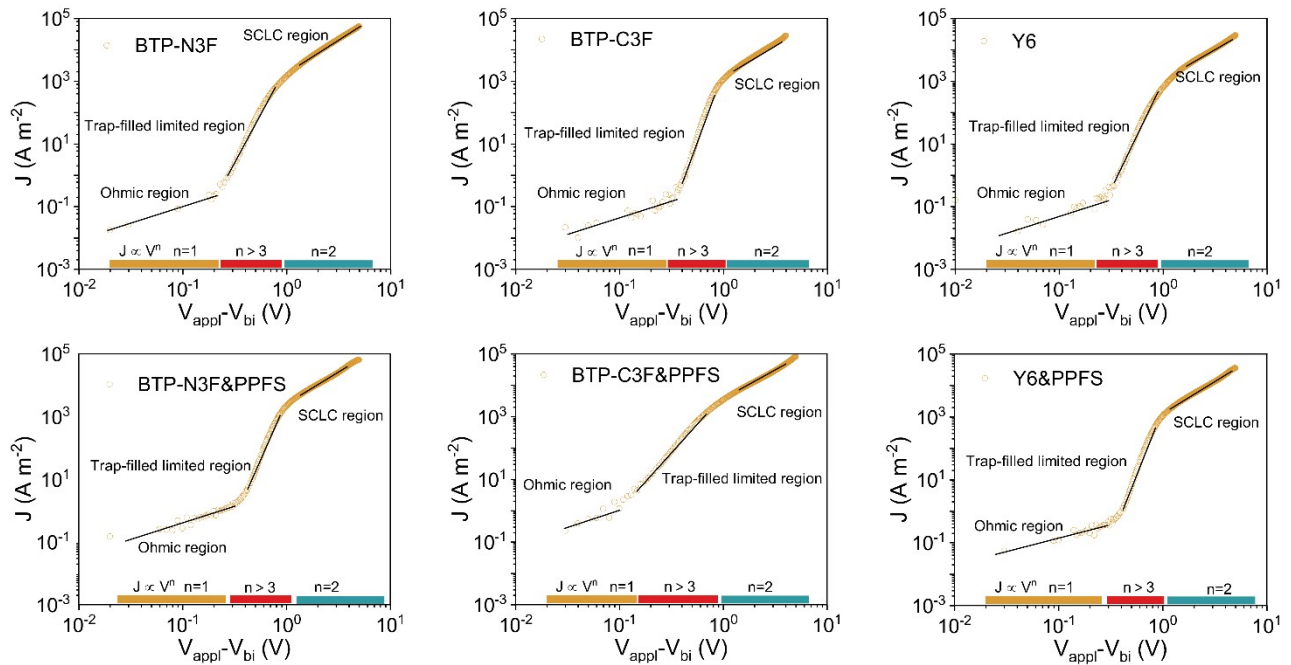


Fig. S29 SCLC measurements of electron-only devices under the same active layer conditions as the optimal devices. The solid lines represent the fitting results based on the Mott-Gurney law.

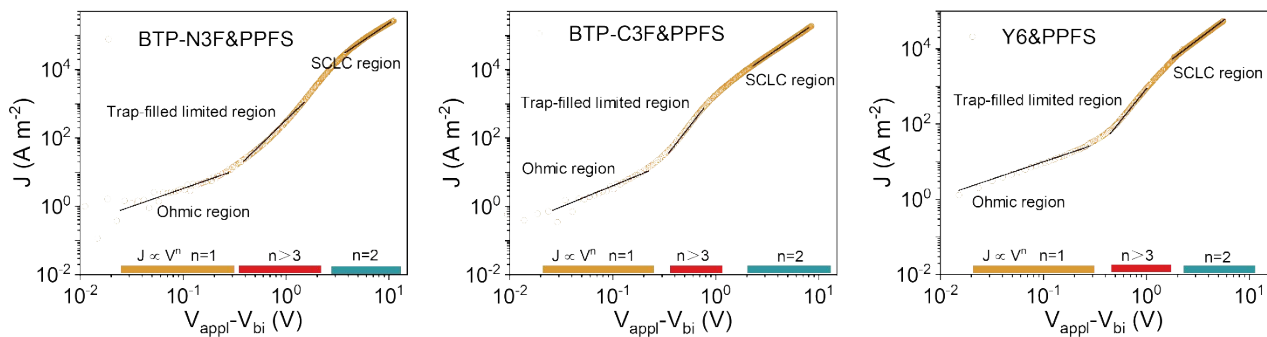


Fig. S30 SCLC measurements of hole-only devices under the same active layer conditions as the optimal devices.

The solid lines represent the fitting results based on the Mott-Gurney law.

5. Supplementary Tables

Table S1 CIF reports for single crystals of the NFAs.

Compound	BTP-N3F	BTP-C3F
CCDC number	2384715	2384716
Temperature (K)	193	193
C-C bond precision (Å)	0.0188	0.0211
Wavelength (Å)	1.34139	1.34139
<i>a</i> (Å)	23.814(4)	31.297(4)
<i>b</i> (Å)	58.590(11)	19.609(2)
<i>c</i> (Å)	14.026(3)	32.373(6)
α (°)	90	90
β (°)	110.855(6)	111.572(4)
γ (°)	90	90
Volume	18288 (6)	18475(4)
Crystal system	Monoclinic	Monoclinic
Space group	C12/c1	C12/c1
Formula	$C_{86}H_{88}F_{10}N_8O_2S_5$	$C_{86}H_{88}F_{10}N_8O_2S_5$
Molecular Weight	1615.94	1615.94
D_x (g cm $^{-3}$)	1.174	1.162
Z	8	8

μ (mm ⁻¹)	1.132	1.121
F (000)	6768.0	6768.0
h, k, l_{\max}	28, 69, 16	36, 23, 38
Data completeness	0.998	0.975
Theta (max)	52.982	52.095
R (reflections)	0.1641(6019)	0.1789(4975)
wR ₂ (reflections)	0.3925(16137)	0.4299(15362)
S	1.121	1.273
Npar	1248	978

Table S2 Photovoltaic parameters of the OSCs based on D18/BTP-C3F with various amounts of PPFS in the acceptor layer.

PPFS content	V_{oc} (V)	J_{sc} (mA cm ⁻²)	FF (%)	PCE (%)
0	0.869	28.08	77.07	18.80
1 wt%	0.867	28.59	80.90	20.05
2 wt%	0.867	28.71	83.58	20.80
3 wt%	0.868	28.69	81.22	20.22

Table S3 Summary of the photovoltaic parameters with efficiencies over 19%.

Active layer	Additive	V_{oc} (V)	J_{sc} (mA cm ⁻²)	FF (%)	PCE (%)	Reference
PM6:L8-BO	BDT	0.893	26.59	80.03	19.01	¹²
D18: D18-Cl:L8-BO	DIO	0.915	26.22	79.75	19.13	¹³
D18-Cl/BTP-4F-P2EH	CN	0.923	27.9	80.8	20.8	¹⁴
PM6:L8-BO:BTP-eC9	BBDC	0.89	27.16	79.0	19.10	¹⁵
D18:L8-BO	D1-Cl	0.914	26.48	79.7	19.29	¹⁶
D18:BTP-eC9	D1-Cl	0.872	28.08	79.3	19.39	¹⁶
PM6:L8-BO:BTP-eC9	Th-ClSi	0.886	27.22	79.5	19.17	¹⁷

PM6:BTP-eC9	IPA	0.862	28.26	79.42	19.35	¹⁸
PM6:BTP-eC9	w/o	0.851	28.38	78.95	19.07	¹⁹
D18:BTP-eC9-4F	CNB	0.874	28.22	77.01	19.00	²⁰
D18:BTP-eC9-4F	DCNB	0.880	28.45	77.60	19.43	²⁰
D18:2BO	w/o	0.951	25.32	78.96	19.01	²¹
DL1/Y6	w/o	0.869	27.82	78.94	19.10	²²
D18:AQx-18:L8-BO	w/o	0.928	25.9	79.2	19.1	²³
D18:BTP-eC9-4F:2TT	w/o	0.88	27.29	79.67	19.39	²⁴
PM6:Dimer-2CF	CN	0.900	26.39	80.03	19.02	²⁵
PM6:BO-4Cl/PM6:L8-BO	DIM	0.902	26.98	79.41	19.32	²⁶
PBDB-TF:AA-2:BO-4I	DIO	0.917	26.0	81.0	19.3	²⁷
D18-Cl:L8-BO	DIO	0.914	26.76	78.9	19.30	²⁸
D18-Cl:PM6:L8-BO	M1	0.924	26.95	79.1	19.70	²⁹
HW-D18:L8-BO	DIB	0.916	26.04	80.55	19.2	³⁰
MIX-D18:L8-BO	DIB	0.920	26.75	81.00	20.0	³⁰
D18:D18-Cl:CH8F	w/o	0.909	26.81	26.81	19.28	³¹
PM6:PY-DT:L8-BO	SF-2	0.961	26.50	74.5	19.02	³²
PM1:BTP-PC6:BTP-F5	CN	0.876	27.4	79.8	19.2	³³
PM6:L8-BO	DIB	0.922	26.83	78.62	19.44	⁶
PM6:BTP-eC9	DIB	0.879	27.76	78.63	19.18	⁶
D18:BTP-eC9	DIB	0.886	28.48	79.79	20.12	⁶
PM6:L8-PhMe	CN	0.901	26.86	79.67	19.27	³⁴
PM6:D-TPh	2-MN	0.946	25.59	78.7	19.05	³⁵
D18:AQx-2F	w/o	0.937	26.1	80.4	19.7	³⁶
PM6:CH22	w/o	0.884	26.74	80.62	19.06	³⁷
PM6:BTP-eC9:o- BTP-eC9	DIB	0.860	28.75	80.41	19.88	³⁸
PM6:L8-ThCl/L8-BO:L8-ThC	w/o	0.895	26.8	81.1	19.4	³⁹
D18:L8-BO	w/o	0.901	27.2	78.7	19.3	³⁹
D18:L8-BO:L8-ThCl	w/o	0.904	27.4	78.4	19.5	³⁹
D18:L8-ThCl/L8-BO:L8-ThCl	w/o	0.910	27.5	80.3	20.1	³⁹

PM6 + 1%L8-B0/L8-BO + 1% PM6	w/o	0.883	26.8	81.8	19.4	⁴⁰
D18:N3:QX-a	w/o	0.862	27.86	80.5	19.33	⁴¹
PM6:L8-BO	DCBB	0.89	27.5	80.1	19.7	⁴²
D18:L8-BO	DCBB	0.91	27.2	79.8	19.6	⁴²
D18:20%PM6:L8-BO	DCBB	0.90	26.9	79.3	19.3	⁴²
D18:20%PM6:L8-BO	DCBB	0.90	27.5	80.4	19.9	⁴²
PiNT:BTP-eC9	CN	0.88	27.8	77.6	19.1	⁴³
PM6:BTP-eC9:Qx-5Cl	DIO	0.862	29.04	79.24	19.83	⁴⁴
PM6:BTP-eC9(TA)	DIO	0.858	28.73	78.0	19.22	⁴⁵
PM6:D18-2F:BTP-eC9(TA)	DIO	0.863	28.97	79.4	19.84	⁴⁵
PM6:D18-Cl:CH-Tz:L8-BO	w/o	0.859	27.72	80.12	19.09	⁴⁶
PM6:CH22	CN	0.887	26.78	80.34	19.09	⁴⁷
PM6:L8-BO with 1% B6Cl	DCBB	0.895	27.4	80.6	19.8	¹²
D18:L8-BO	DCBB	0.908	26.6	80.0	19.3	¹²
D18:L8-BO with 0.5% B6Cl	DCBB	0.919	27.2	80.7	20.2	¹²
PM6:L8-BO	DIO	0.904	26.57	79.55	19.11	⁴⁸
D18:PM6:L8-BO	DIM	0.908	27.21	79.52	19.66	⁴⁸
PM6:L8BO:3BTT6F	DIB	0.898	26.64	80.51	19.26	⁴⁹
PM6:BTP-eC9 BTP-2FC1O	DIO	0.863	27.96	80.15	19.34	⁵⁰
D18:N3:DP-BTP	DIB	0.87	27.95	78.50	19.07	⁵¹
D18:PM6:Z9	DIB	0.896	26.5	80.1	19.0	⁵²
D18:DT-C8	w/o	0.869	27.85	79.6	19.27	⁵³
D18:DT-C8Cl	w/o	0.851	28.17	80.9	19.40	⁵³
PM6:BTP-eC9	DIO	0.856	29.20	78.8	19.70	⁵⁴
PDTP-BDD+20%D18/L8-BO	DIB	0.905	26.90	79.53	19.36	⁵⁵
PM6:L8-BO	PMMA _L	0.89	27.4	79.80	19.23	⁵⁶
M6:Y6	DBrDIB	0.87	27.2	80.4	19.1	⁵⁷
D18:L8-BO	CBB	0.901	26.51	80.98	19.38	⁵⁸
D18:L8-BO	CIB	0.895	26.50	81.37	19.26	⁵⁸

PM6/BTP-eC9	P-Cl	0.853	27.81	80.50	19.10	⁵⁹
D18:BTP-3FBr:IDIC	w/o	0.931	26.50	78.31	19.32	⁶⁰
D18:BTP-Cy-4F:BTP-eC9	w/o	0.925	26.06	80.31	19.36	⁶¹
PM6-BNBP-4:L8-BO	DIM	0.909	26.65	78.97	19.13	⁶²
PNB-3:L8-BO	DIM	0.907	26.59	78.86	19.02	⁶³
PBTz-F:PM6:L8-BO	DIB	0.905	27.24	79.26	19.54	⁶⁴
D18-Cl:BTP-eC9/PM6:L8-BO	DIB	0.898	27.02	80.81	19.61	⁶⁵
PM6:D18:L8-BO	w/o	0.90	27.17	79.71	19.49	⁶⁶
PBD-10:PBTz-F:L8-BO	DIM	0.897	27.27	79.49	19.45	⁶⁷
PBD-10:L8-BO	DIM	0.904	26.46	79.58	19.04	⁶⁷
PM6:L8-BO-X	TCB	0.891	28.12	79.46	19.91	⁶⁸
PM6:DQx-Ph/L8-BO	1-CN	0.919	26.8	80.8	19.9	⁶⁹
D18-Cl:N3	BBT	0.875	27.63	80.8	19.53	⁷⁰
PM6:PBTz-F:L8-BO	SIB	0.907	27.10	80.06	19.68	⁷¹
D18:BTP-Th	DIB	0.891	26.77	79.71	19.02	⁷²
SA1:PFDTQ:PY-IT	w/o	0.927	26.85	77.67	19.33	⁷³
PM6:D18/L8-BO:SeDZ-3TR	w/o	0.908	26.82	79.62	19.38	⁷⁴
PM6:D18:L8-BO	DIM	0.912	27.27	78.82	19.60	⁷⁵
PM6:PY-NFT	ODT	0.940	25.94	78.4	19.12	⁷⁶
PM6:L8-BO	PyMCS	0.904	27.25	79.10	19.52	⁷⁷
PM6:GMA-SSeS	w/o	0.917	27.38	77.12	19.37	⁷⁸
D18:N3-BO:F-BTA3	w/o	0.924	26.77	81.85	20.25	⁷⁹
D18:BTP-TTS:IDIC	DIO	0.879	27.55	79.30	19.22	⁸⁰
PM6:BTP-eC9	w/o	0.864	28.69	79.30	19.66	⁸¹
PM6+AO1010/L8-BO	AO1010	0.896	26.81	79.22	19.03	⁸²
BO:BTP-ThMeCl	DIO	0.87	26.7	82.2	19.1	⁸³
PM6:D18:L8-BO	w/o	0.896	29.7	81.9	19.6	⁸⁴
TQ10: <i>m</i> -BTP-PhC6	1-CN	0.844	27.20	81.8	19.67	⁸⁵
D18:L8-BO	w/o	0.895	26.42	81.31	19.09	⁸⁶
D18:Z8:L8-BO	w/o	0.92	27.2	80.8	20.2	⁸⁷

D18:L8-BO:DM-F	DIB	0.92	26.98	81.0	20.09	88
PBDB-TF:L8-BO:BTP-eC9	w/o	0.88	28.4	80.86	20.17	89
PM6:L8-BO	DBCL	0.882	26.56	81.2	19.02	90
PM6:L8-BO-X:Tri-V	1-MN	0.892	27.45	81.1	19.86	91
PM6:D18-Cl:L8-BO	CIB	0.881	26.7	81.1	19.1	92
PBDB-TF:eC9	DIO	0.856	27.8	80.9	19.3	93
PBQx-TF:eC9-2Cl:F-BTA3	w/o	0.879	26.7	80.9	19.0	94
PM6:L8-BO	w/o	0.898	26.17	80.87	19.01	95
PB2:HLG:BTP-eC9	DIO	0.883	27.3	80.8	19.5	96
PM6:PM6-PA:L8-BO	DIO	0.88	27.0	80.8	19.3	97
PM6:L8-BO:TQT	w/o	0.888	26.75	80.7	19.15	98
D18:L8-BO	w/o	0.91	26.48	80.65	19.65	99
PM6:DY-P2EH:BTP-ec9	1-CN&DIO	0.871	27.19	80.61	19.09	100
PTQ10:BTP-FTh:IDIC	CN	0.870	27.17	80.6	19.05	101
PM6:L8-BO	FA-C12	0.88	26.68	80.5	19.02	102
PM6: L8-BO: BTP-ec9	DIO	0.872	28.12	80.43	19.71	103
PM6:BTP-eC9	TCB	0.861	27.88	80.39	19.33	104
D18-Cl:L8-BO-X	w/o	0.893	26.78	79.6	19.04	105
D18:2BTh-2F-C2	DIB	0.913	26.71	77.98	19.02	106
PM6:PY-IT	DIB	0.945	26.37	76.48	19.06	107
PBQx-TF:eC9-2Cl	DCBB	0.879	27.2	80.4	19.2	108
PM6:L8-BO:Qx-p-N4F	CN	0.887	27.83	78.91	19.48	109
PM6:BTP-eC9:C60-Y	DBCL	0.858	28.75	77.88	19.22	110
PM6:PY-DT	4-BDBTP	0.951	25.85	78.5	19.30	111
PTQ11:PEH-F	CN	0.936	26.53	79.45	19.73	112
PM6:BTP-eC9	CB-NH ₂	0.87	28.09	79.73	19.48	113
PM6:D18:L8-BO	2Br	0.903	26.93	80.24	19.51	114
PM6:3QY	CN	0.951	26.36	76.86	19.27	115
D18:1wt.% Py7/Py7:1wt.% D18	DIO	0.885	27.72	79.9	19.60	116
D18:Y-SeSe	w/o	0.895	27.86	78.16	19.49	117

D18/L8-BO	0.05% T-2OOD	0.906	27.7	81.2	20.1	¹¹⁸
PM6:L8-BO	DBrTz	0.887	27.4	79.9	19.4	¹¹⁹
PM6:CH8-4:L8-BO-D	CN	0.906	27.70	79.6	20.0	¹²⁰
PM6:BTP-eC9	DIB	0.87	28.85	78.37	19.67	¹²¹
D18:AQx-22	w/o	0.970	25.8	78.0	19.5	¹²²
PM6:L8-BO:L-DBDD	w/o	0.899	27.03	80.29	19.51	¹²³
PM6:G-1	ODCB	0.938	26.2	79.7	19.6	¹²⁴
D18:L8-BO:PY-C11	HBT-2	0.910	27.41	80.23	20.01	¹²⁵
D18-Cl:L8-BO	TTz-Pt	0.929	26.61	79.4	19.63	¹²⁶
PM6:BTA-E3	DIO	0.852	28.99	80.63	19.92	¹²⁷
D18-Cl:N3:AT-β2O	DPE	0.876	29.16	81.49	20.82%	¹²⁸
PB3:FTCC-Br:BTP-Cy	DIO	0.896	27.79	81.3	20.2	¹²⁹
PM6:L8-BO-C ₄ :L8-BO-C ₄ -Br	2,5-dibromo-3-chlorothiophene	0.894	27.96	81.7	20.42	¹³⁰
PM6/L8-BO/BTA3-16F	DIB	0.896	27.31	80.99	19.82	¹³¹
PM6:BTP-eC9-4F:DM-F	TZ-3Cl	0.902	28.01	79.83	20.2	¹³²
D18:Six-IC	w/o	0.92	27.0	78.5	19.4	¹³³
PM6:4Y-BO	CN	0.944	26.59	78.63	19.75	¹³⁴
D18 (PY-IT diluted)/L8-BO:C ₅ -16	w/o	0.914	27.7	82.8	21.0	¹³⁵
D18/L8-BO	DIB	0.914	27.34	80.34	20.08	¹³⁶
PM6:BTP-BO-TBO	1-CN	0.913	26.67	81.17	19.76	¹³⁷
PM6:L8-BO	1,5-BM	0.91	27.5	82	20.5	¹³⁸
PM6:P(BTzE-BDT):BTP-eC9	w/o	0.870	28.3	81.2	20.0	¹³⁹
D18:AQx-2F:eC9	w/o	0.937	27.2	80.8	20.6	¹⁴⁰
D18/HE-2	DIB	0.938	26.7	82.1	20.6	¹⁴¹

Table S4. Photovoltaic parameters of the OSCs with various donors and the new acceptors

Devices	V_{oc} (V)	J_{sc} (mA cm ⁻²)	FF (%)	PCE (%)

PM6/BTP-N3F	0.858	26.45	77.22	17.52
D18/BTP-N3F	0.867	26.69	77.89	18.02
PM6/BTP-C3F	0.847	28.21	79.73	19.06
D18/BTP-C3F	0.864	28.11	81.97	19.91

Table S5 Ordered molecular structure parameters of the NFA films without and with PPFS additive.

Film	Lamellar stacking			π - π stacking		
	q/d	FWHM	CCL	q/d	FWHM	CCL
	(nm ⁻¹)/(nm)	(nm ⁻¹)	(nm)	(nm ⁻¹)/(nm)	(nm ⁻¹)	(nm)
BTP-N3F	3.18/1.97	0.683	12.4			
	3.64/1.73	1.60	5.28	17.3/0.363	2.40	3.53
	5.34/1.177	1.57	5.38			
BTP-C3F	3.24/1.94	0.92	9.17			
	4.13/1.52	0.91	9.28	17.2/0.365	2.93	2.90
	5.58/1.126	1.72	4.91			
Y6	2.08/3.02	0.96	8.79			
	1.41/4.46	1.58	5.34	17.20.365	2.29	3.70
BTP-N3F&PPFS	/	/	/	16.9/0.372	1.57	5.40
BTP-C3F&PPFS	/	/	/	17.5/0.359	2.70	3.14
Y6&PPFS	2.75/2.28	0.864	9.77			
	4.29/1.46	1.14	7.40	17.2/0.365	2.15	3.95

Table S6 Information about surface energies of PPFS, Y6, BTP-N3F, BTP-C3F and D18-Cl films amd the Flory–Huggins interaction parameter (χ) between PPFS and the photoacitve materials.

Materials	θ_{water} (°)	θ_{DIM} (°)	γ_d (mJ m ⁻²)	γ_p (mJ m ⁻²)	γ (mJ m ⁻²)	χ
PPFS	104.1	58.4	0.1	30.2	30.3	/
Y6	96.8	42.4	0.2	39.1	39.3	0.584

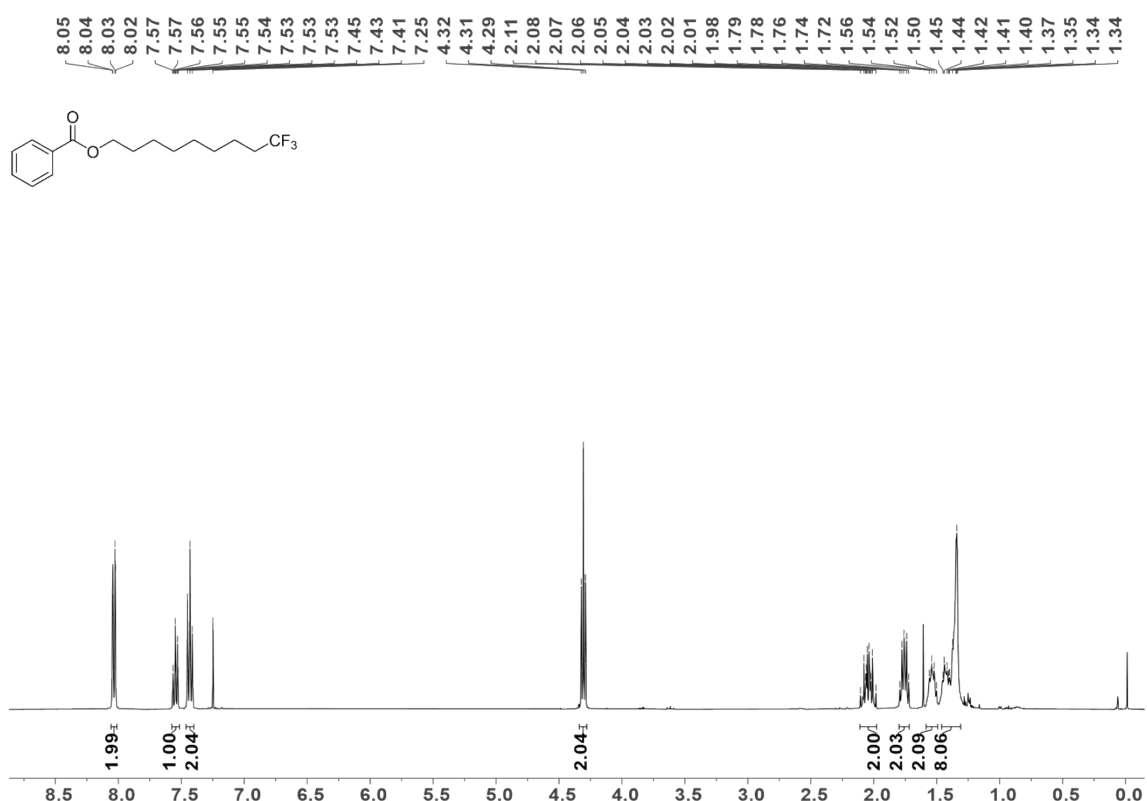
BTP-N3F	99.8	47.7	0.1	36.5	36.6	0.297
BTP-C3F	99.4	46.5	0.1	37.2	37.3	0.363
D18-Cl	106.1	55.5	/	32.8	32.8	0.049

Table S7 Electron mobilities of the different NFA-based photoactive layers without and with PPFS additive.

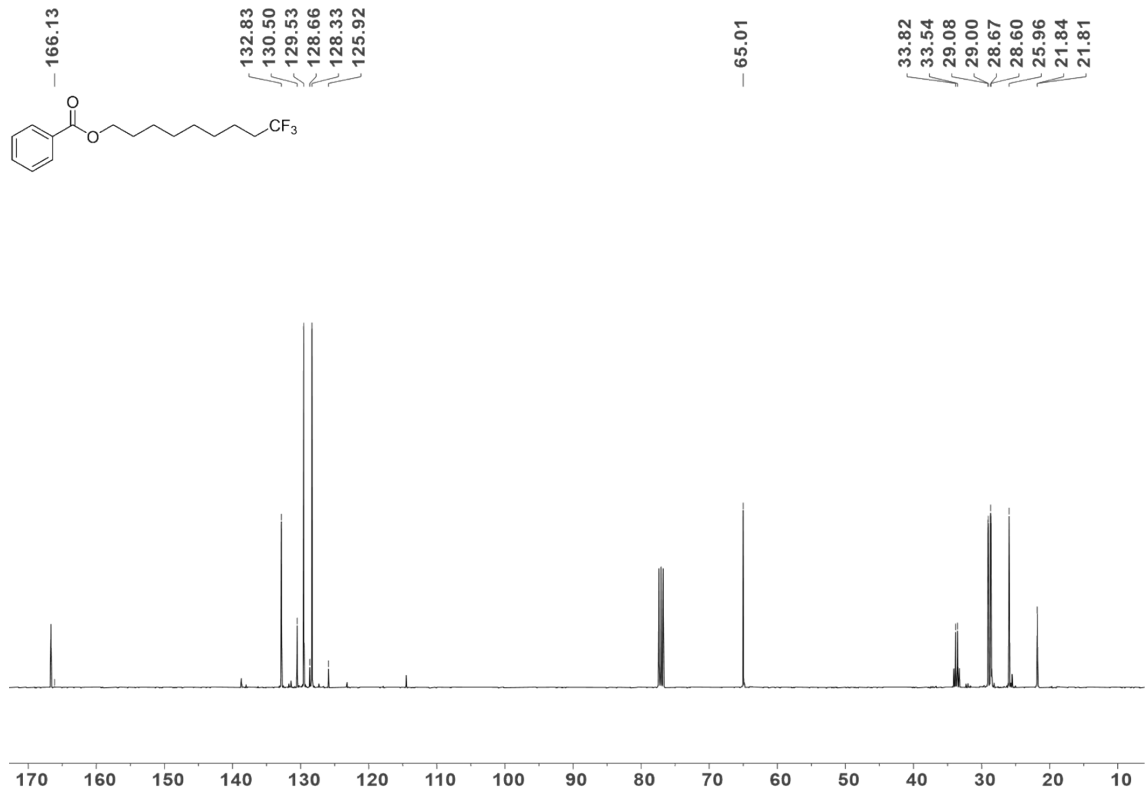
NFA	Film thickness	w/o PPFS	With PPFS
BTP-N3F	124 nm	$5.84 \times 10^{-4} \text{ cm}^2 \text{V}^{-1} \text{s}^{-1}$	$8.96 \times 10^{-4} \text{ cm}^2 \text{V}^{-1} \text{s}^{-1}$
BTP-C3F	122 nm	$7.13 \times 10^{-4} \text{ cm}^2 \text{V}^{-1} \text{s}^{-1}$	$1.15 \times 10^{-3} \text{ cm}^2 \text{V}^{-1} \text{s}^{-1}$
Y6	120 nm	$5.02 \times 10^{-4} \text{ cm}^2 \text{V}^{-1} \text{s}^{-1}$	$7.64 \times 10^{-4} \text{ cm}^2 \text{V}^{-1} \text{s}^{-1}$

Table S8 Hole mobilities of the different NFA-based photoactive layers with PPFS additive and their Langevin recombination rates.

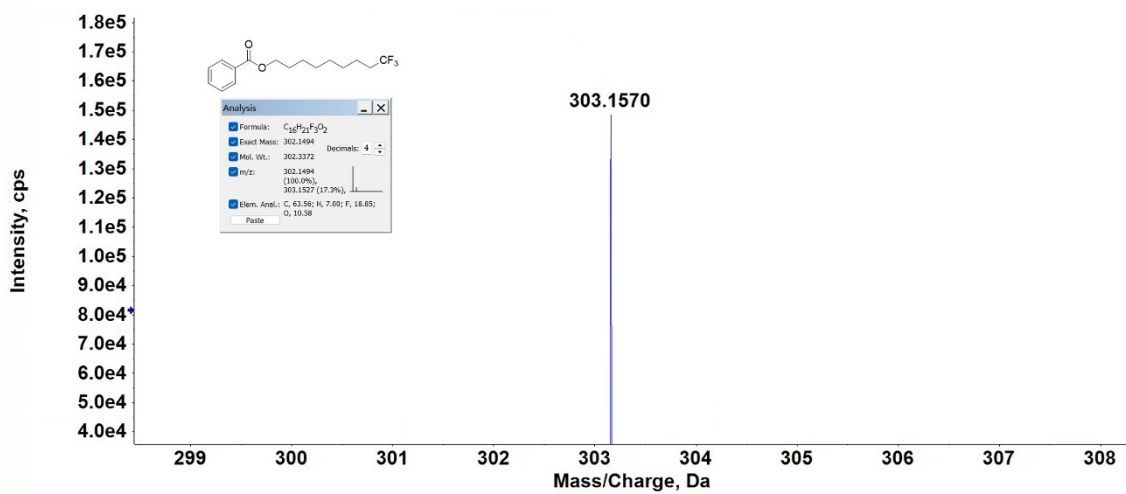
NFA	ϵ_r	Hole mobility	k_L
BTP-N3F	6.08	$9.83 \times 10^{-4} \text{ cm}^2 \text{V}^{-1} \text{s}^{-1}$	$5.6 \times 10^{-12} \text{ cm}^3 \text{s}^{-1}$
BTP-C3F	5.98	$1.01 \times 10^{-3} \text{ cm}^2 \text{V}^{-1} \text{s}^{-1}$	$6.5 \times 10^{-12} \text{ cm}^3 \text{s}^{-1}$
Y6	3.73	$9.51 \times 10^{-4} \text{ cm}^2 \text{V}^{-1} \text{s}^{-1}$	$8.3 \times 10^{-12} \text{ cm}^3 \text{s}^{-1}$



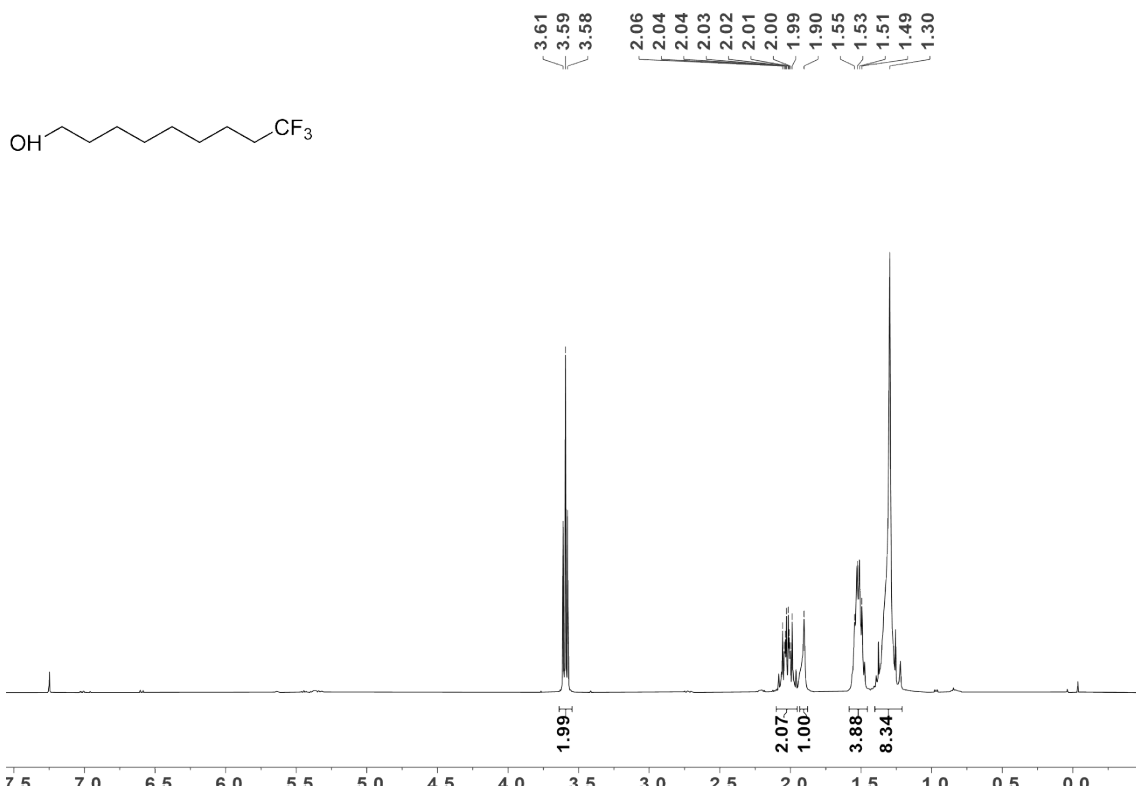
¹H NMR spectrum of Compound 3



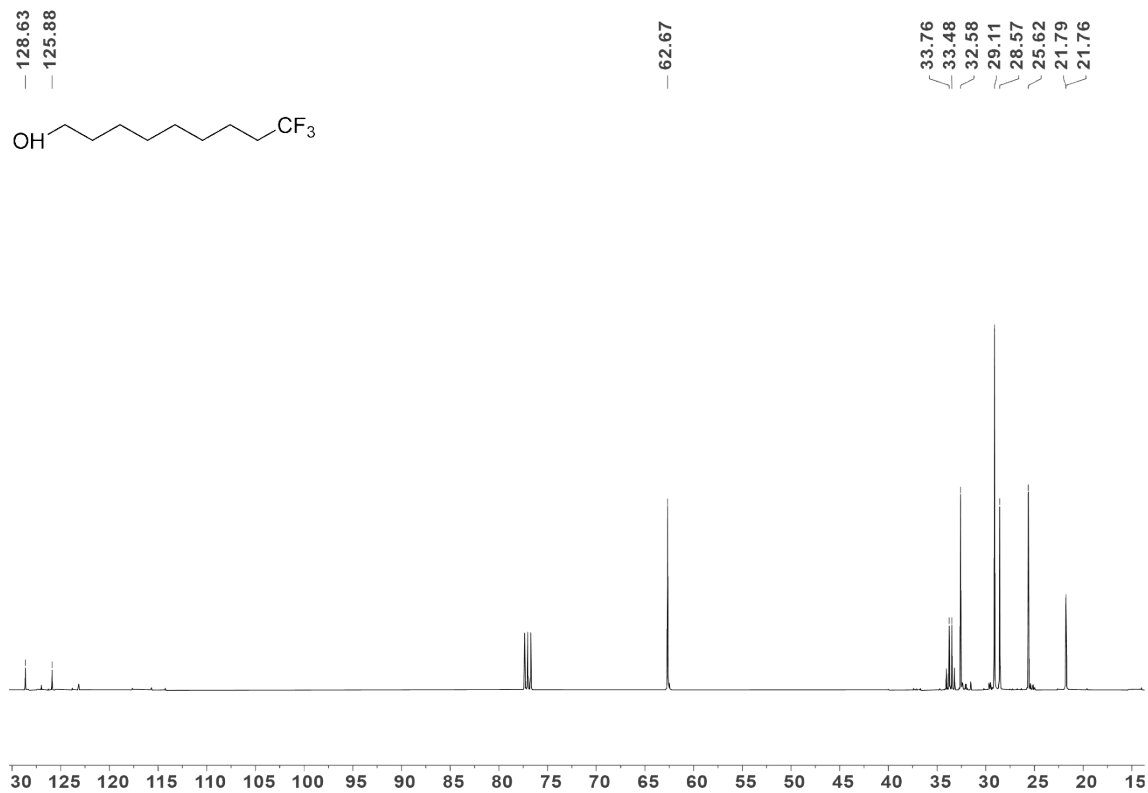
¹³C NMR spectrum of Compound 3



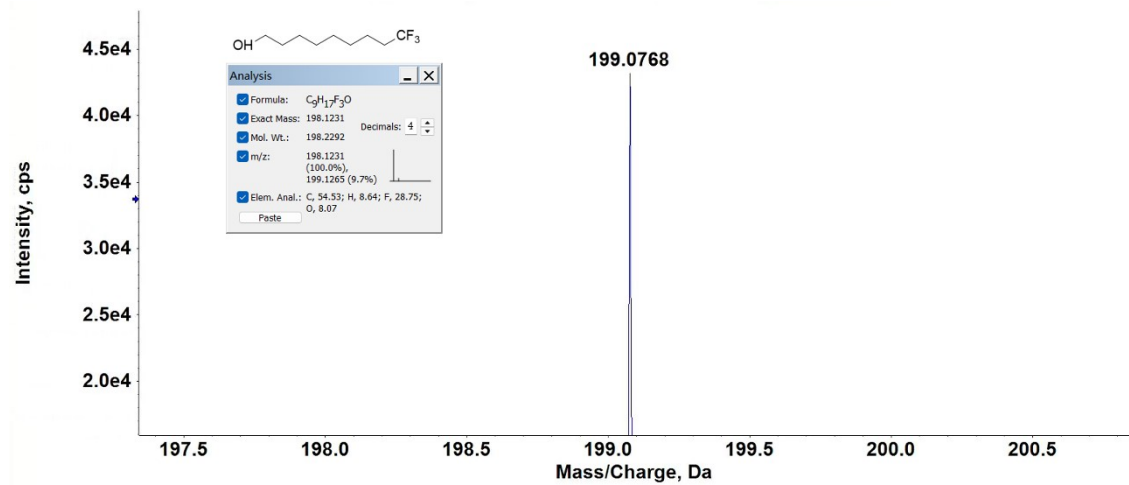
HRMS spectrum of **Compound 3**



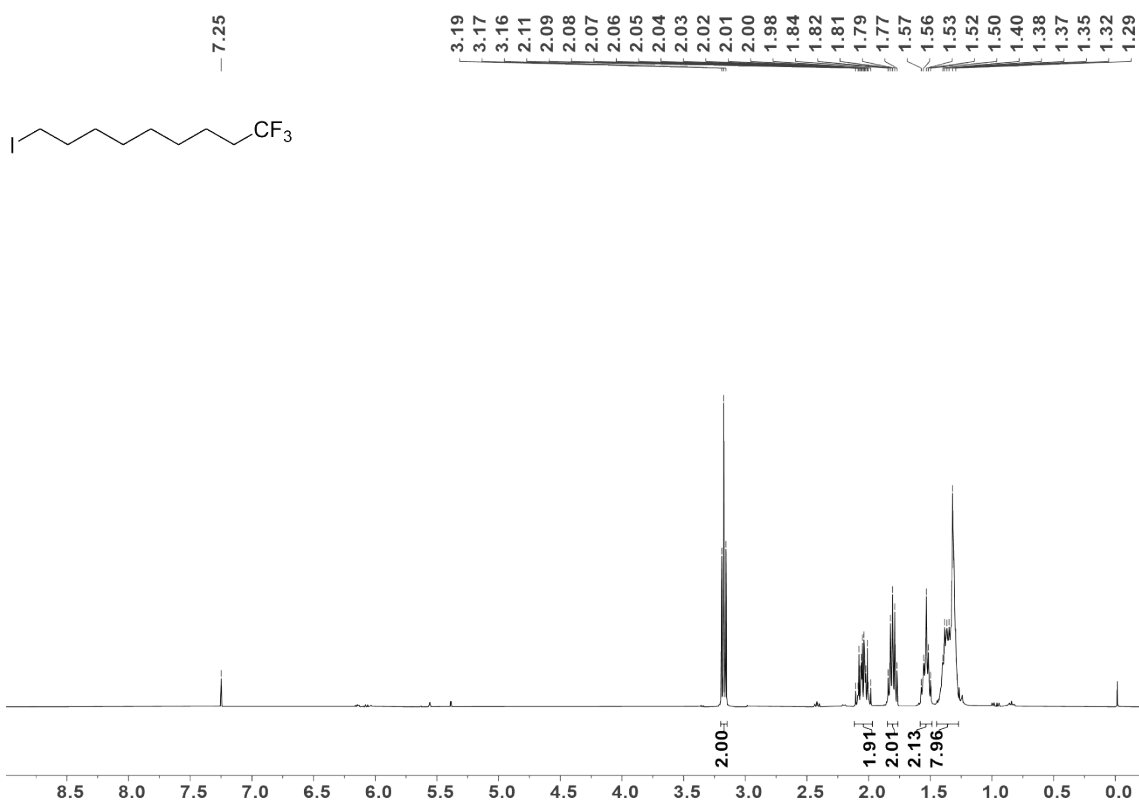
¹H NMR spectrum of **Compound 4**



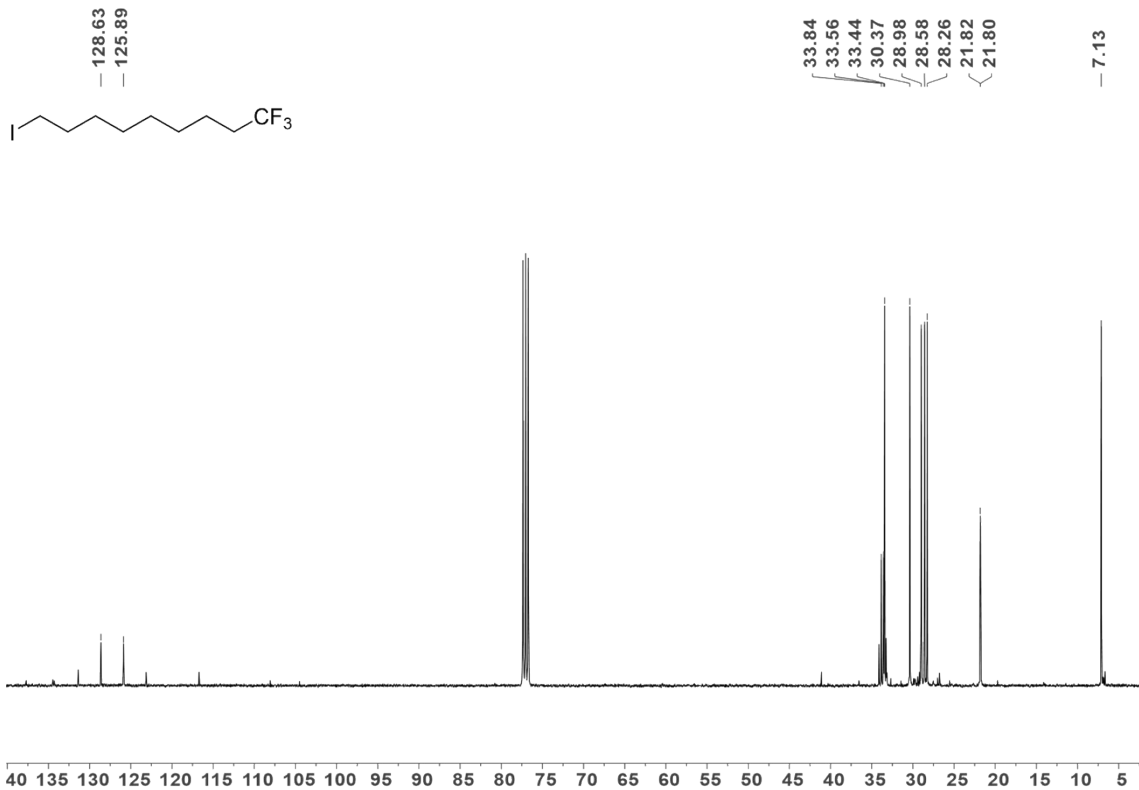
¹³C NMR spectrum of Compound 4



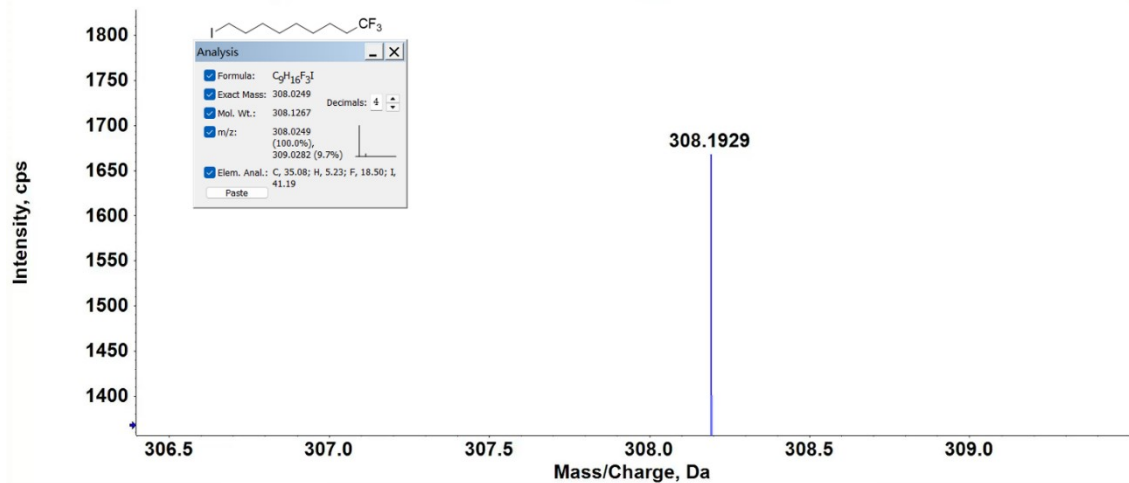
HRMS spectrum of **Compound 4**



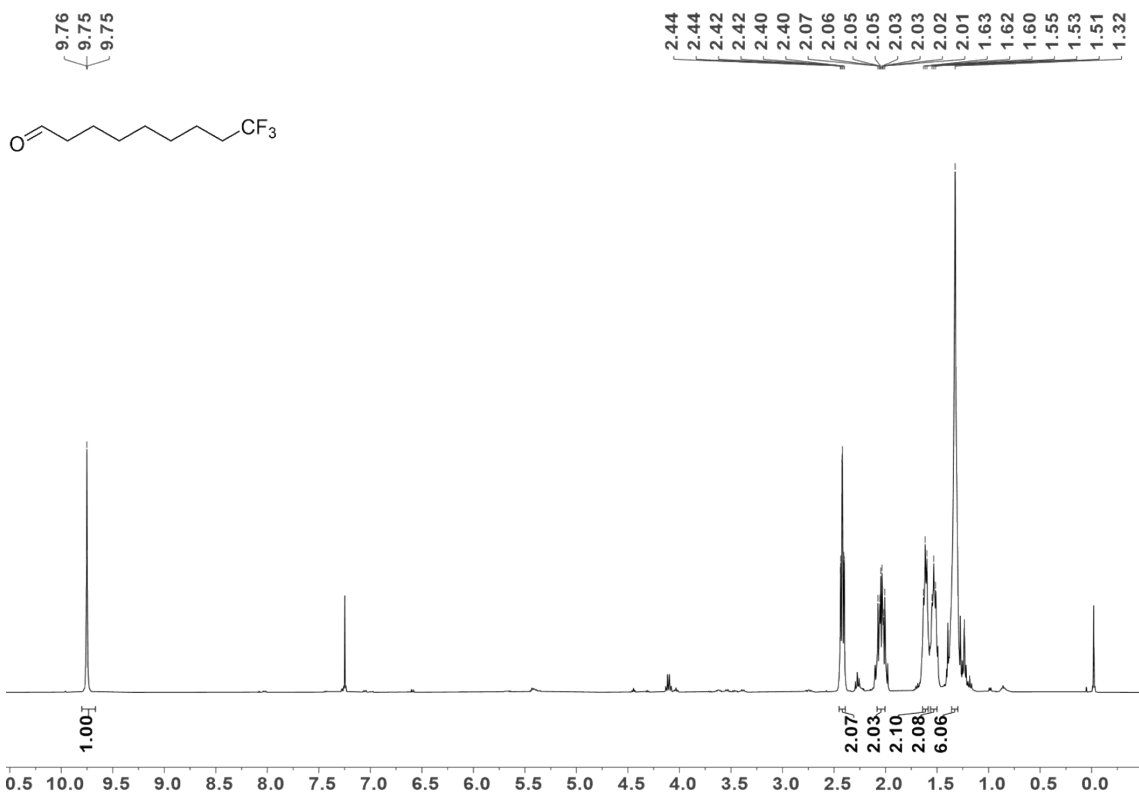
¹H NMR spectrum of **Compound 5**



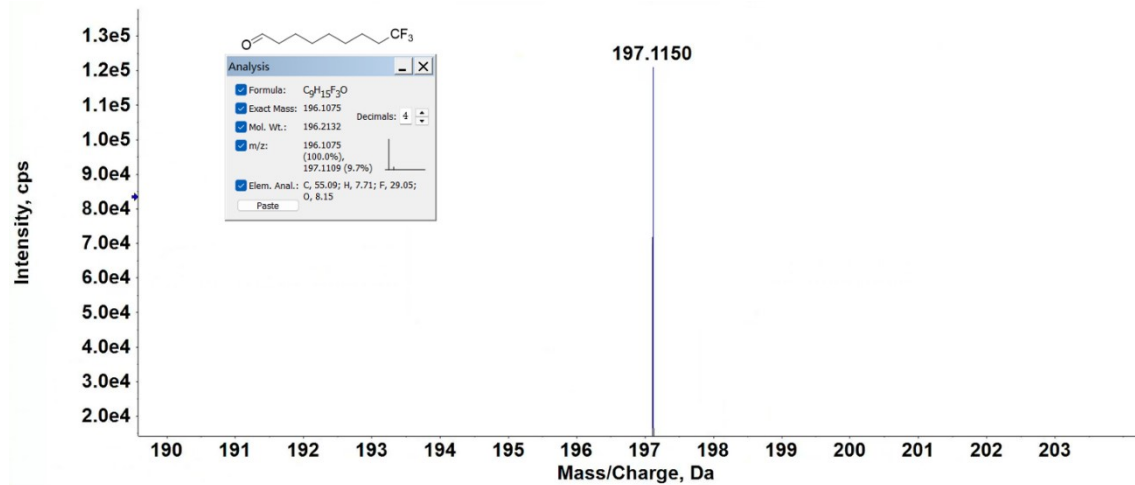
¹³C NMR spectrum of **Compound 5**



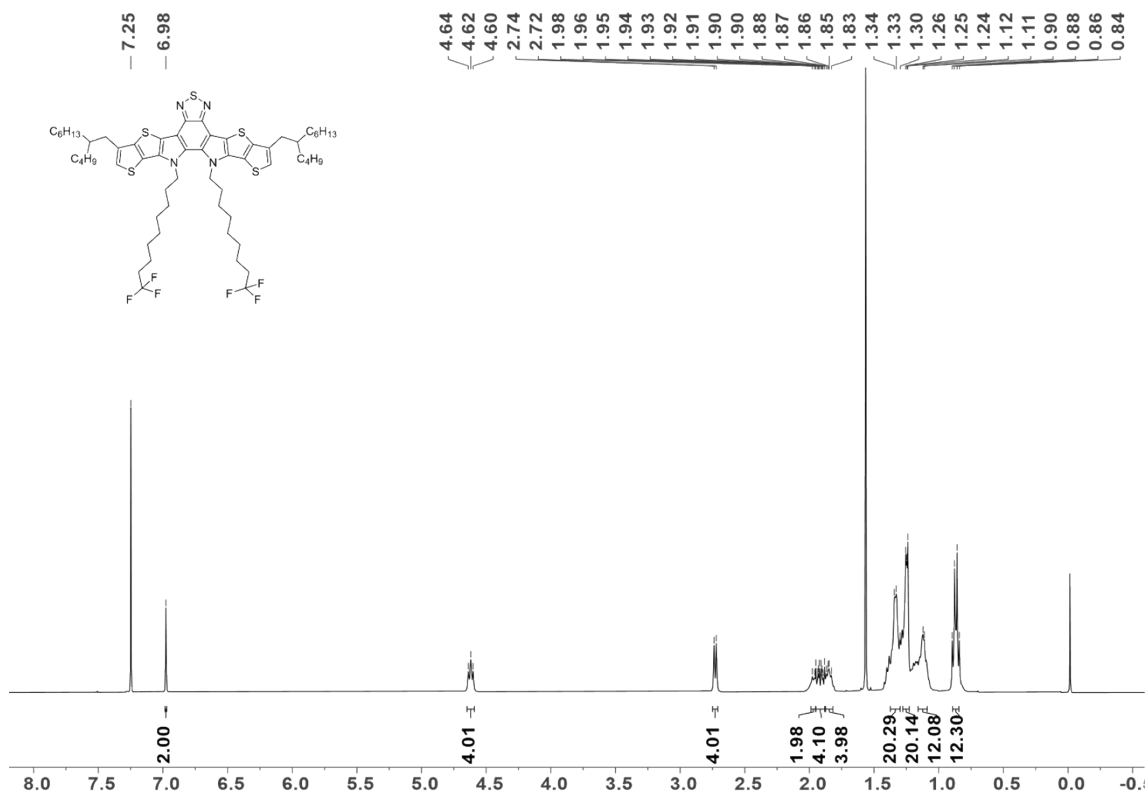
HRMS spectrum of **Compound 5**



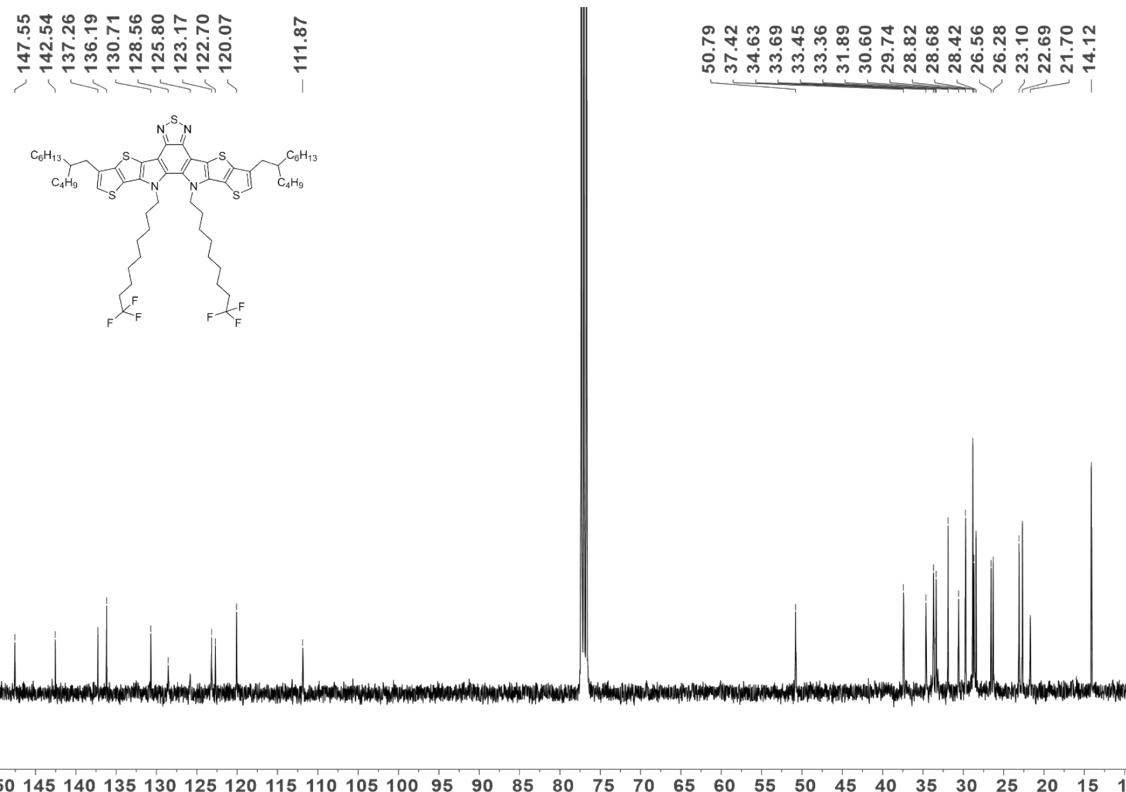
^1H NMR spectrum of **Compound 6**



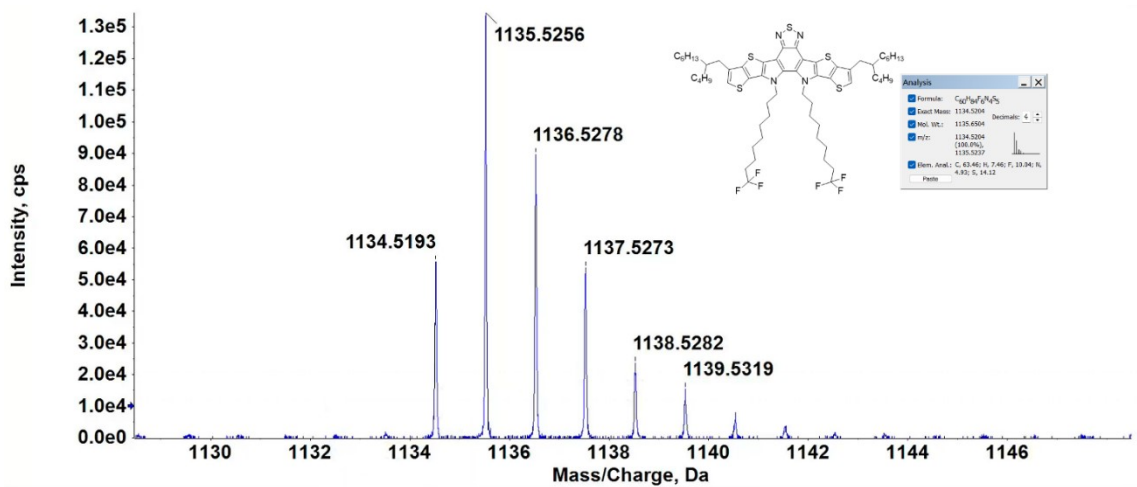
HRMS spectrum of **Compound 6**



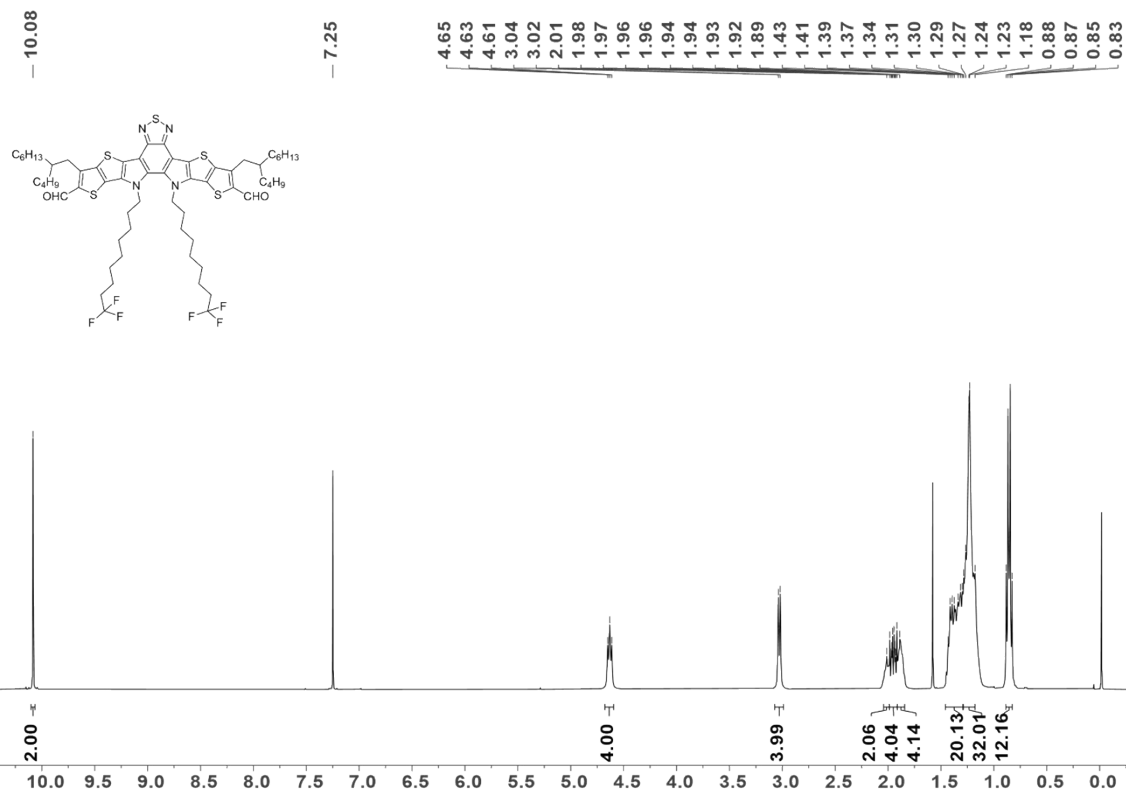
¹H NMR spectrum of **Compound 8**



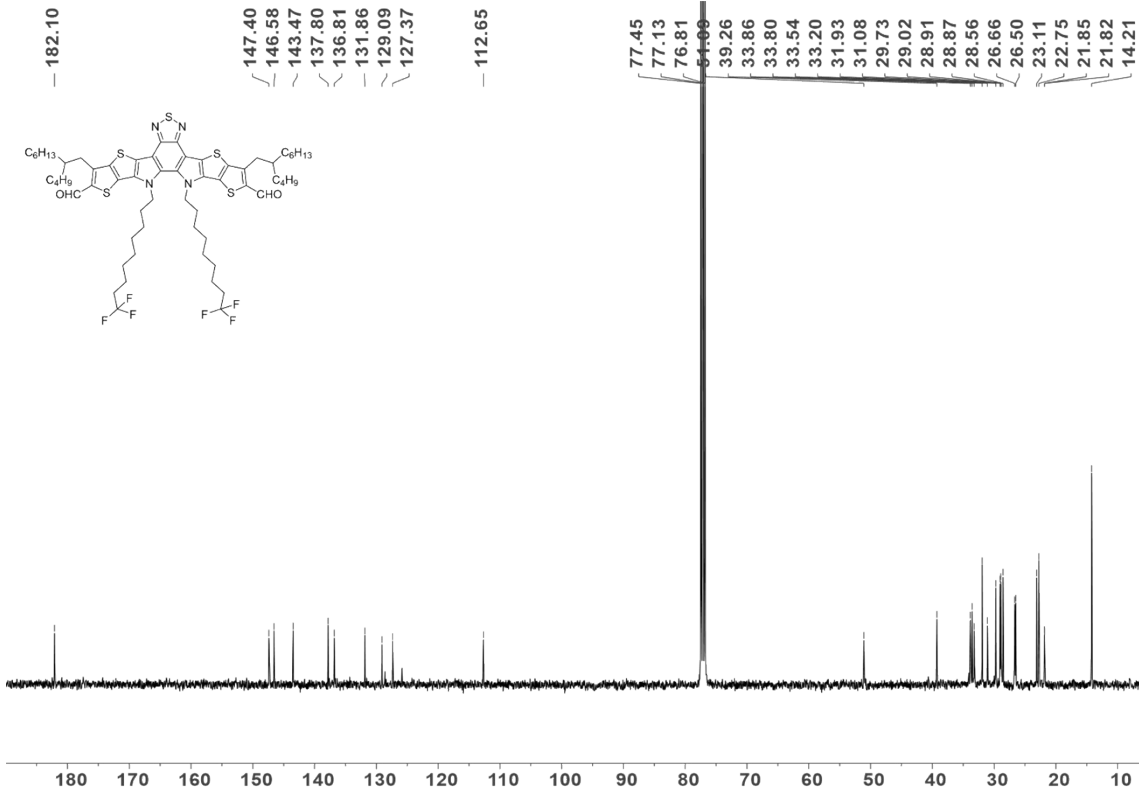
^{13}C NMR spectrum of **Compound 8**



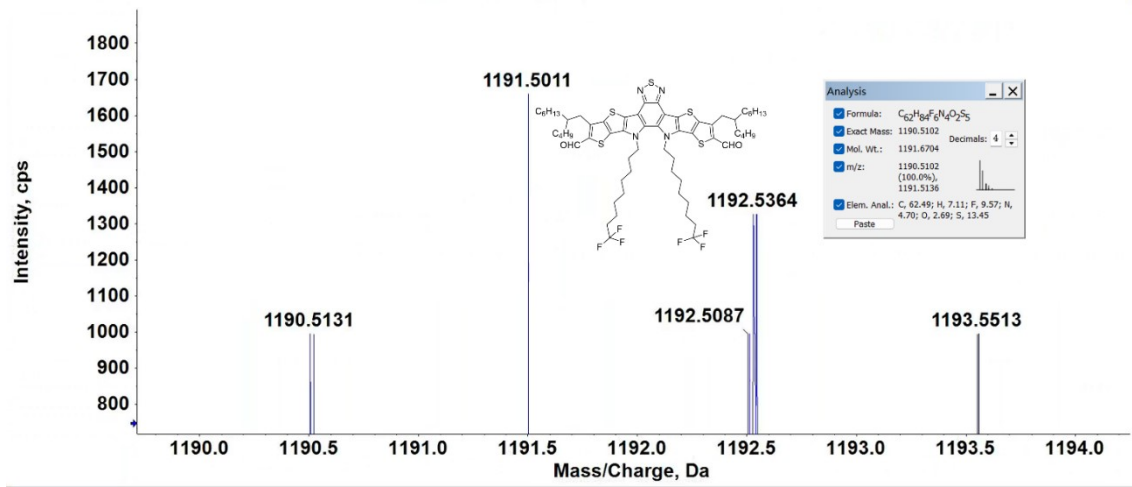
HRMS spectrum of **Compound 8**



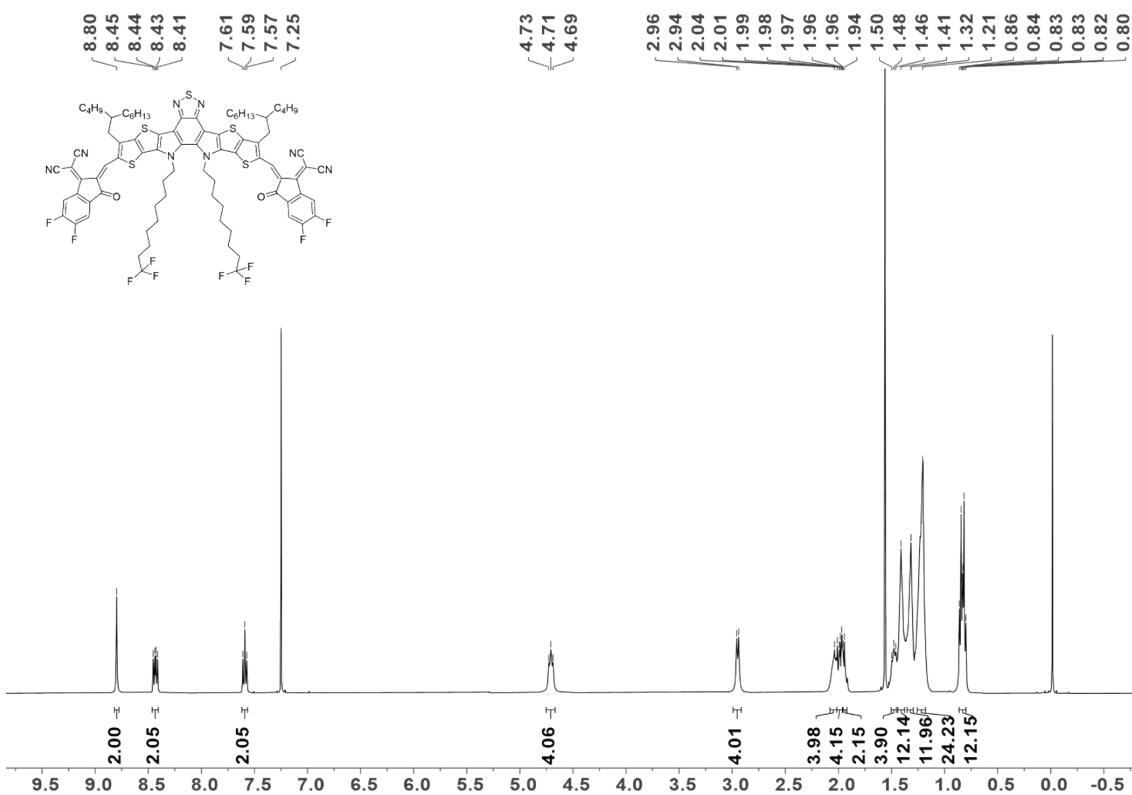
^1H NMR spectrum of **Compound 9**



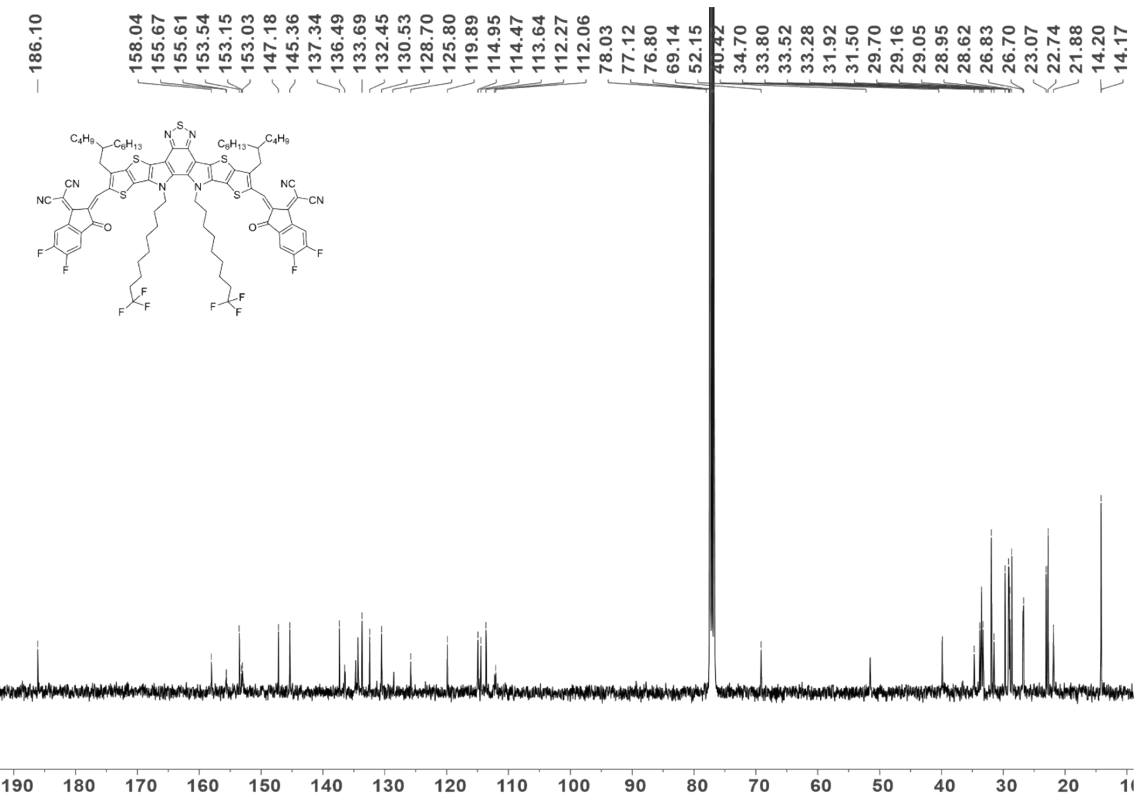
^{13}C NMR spectrum of **Compound 9**



HRMS spectrum of **Compound 9**



¹H NMR spectrum of **BTP-N3F**



¹³C NMR spectrum of **BTP-N3F**

MALDI,2,20250228

Analysis Info

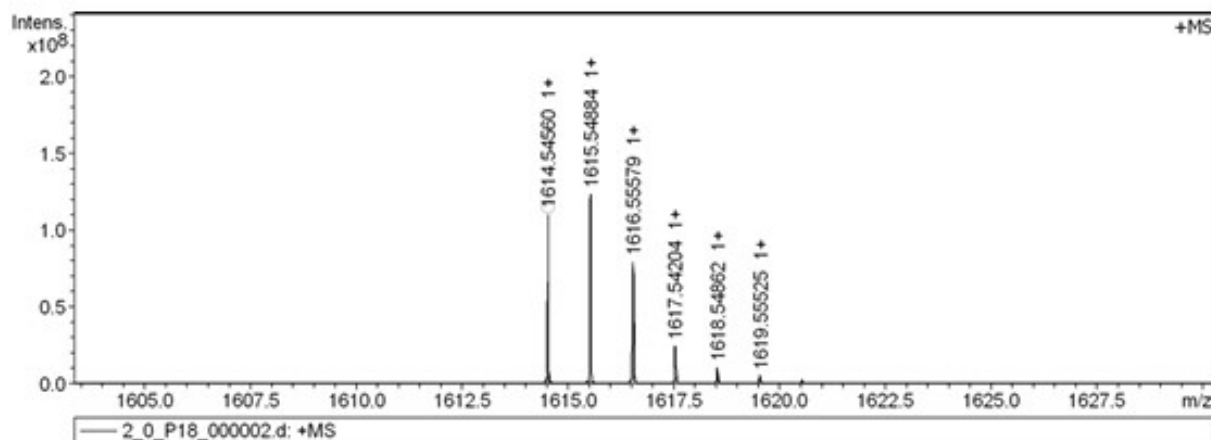
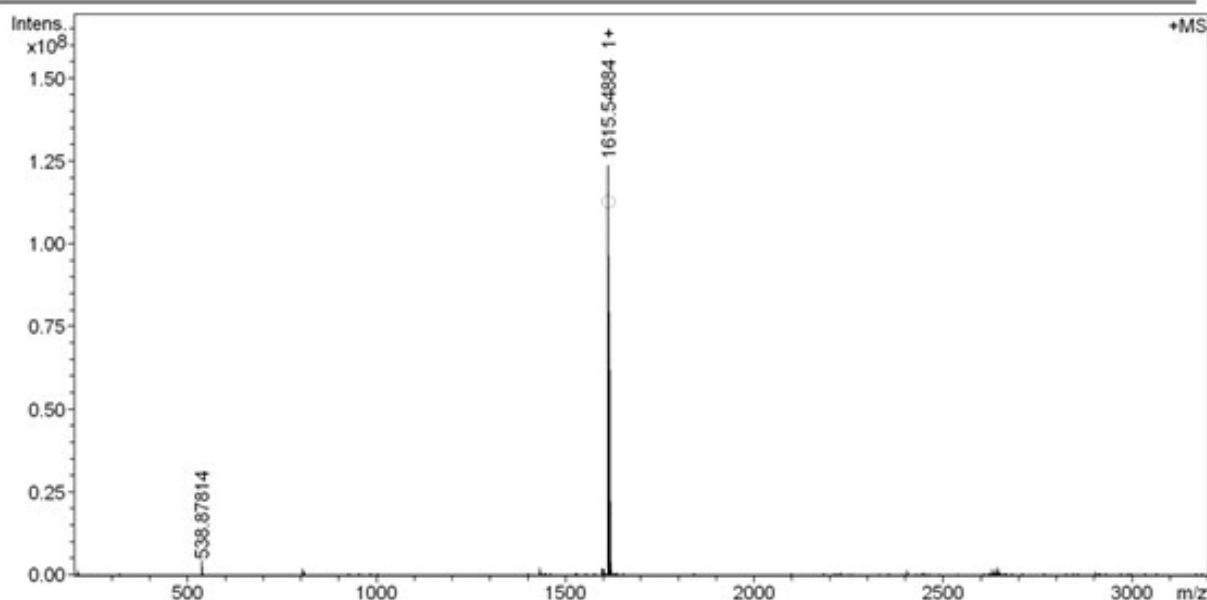
Analysis Name D:\Data\MALDI\2025\0228\dongjunwei\2_0_P18_000002.d
Method P20240925
Sample Name MURU-N-ESI
Comment

Acquisition Date 2/28/2025 4:02:43 PM

Operator
Instrument solariX

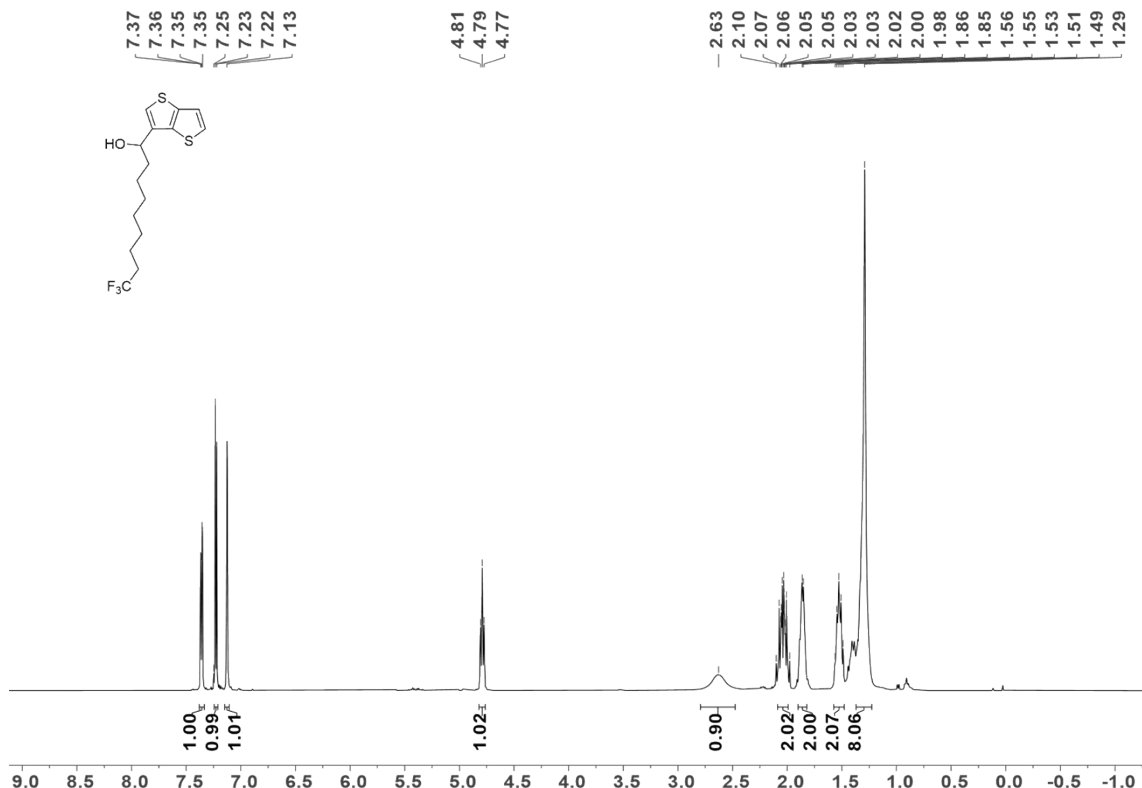
Acquisition Parameter

Acquisition Mode	Single MS	Acquired Scans	3	Calibration Date	Thu Oct 31 03:34:59
Polarity	Positive	No. of Cell Fills	1	Data Acquisition Size	2091152
Broadband Low Mass	202.1 m/z	No. of Laser Shots	23	Data Processing Size	4194304
Broadband High Mass	3200.0 m/z	Laser Power	21.6 lp	Apodization	Sine-Bell Multiplication
Source Accumulation	0.001 sec	Laser Shot Frequency	0.020 sec		
Ion Accumulation Time	0.010 sec				

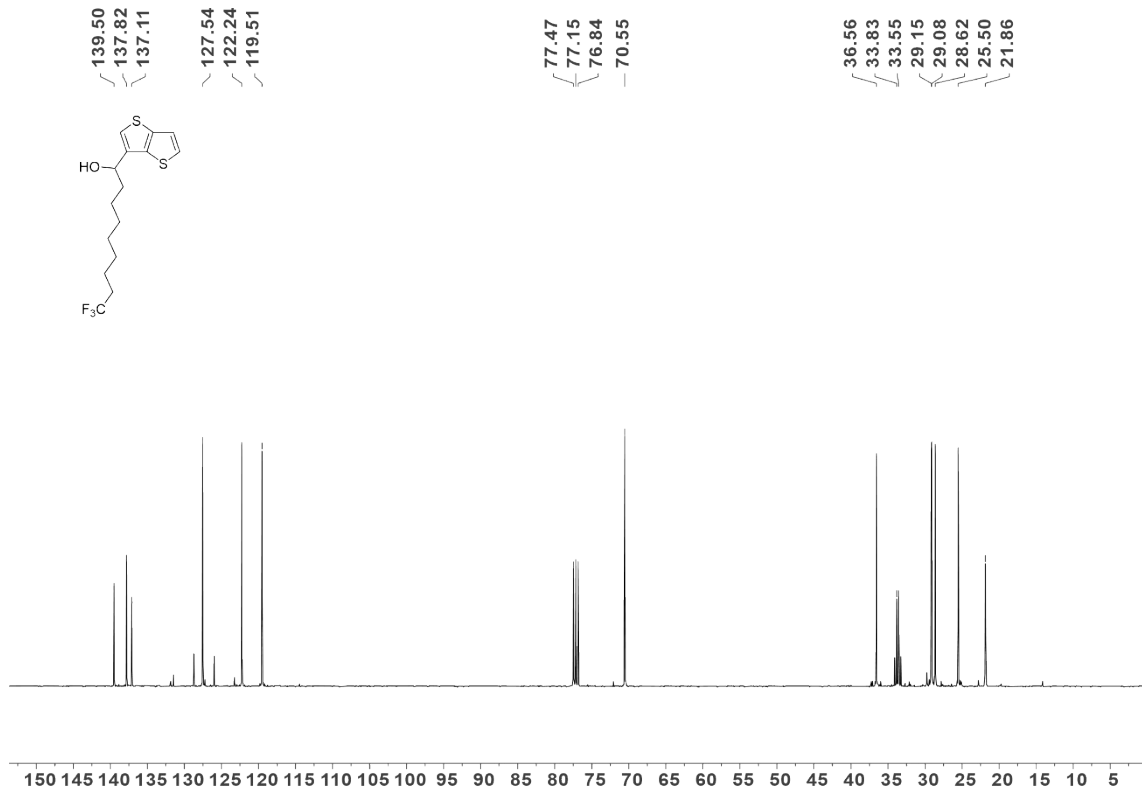


Meas. m/z	#	Ion Formula	Score	m/z	err [ppm]	Mean err [ppm]	mSigma	rdb	e ⁻ Conf	N-Rule
1614.545599	1	C86H8BF10N8O2S5	100.00	1614.546863	-0.8	-0.0	87.1	42.0	odd	ok

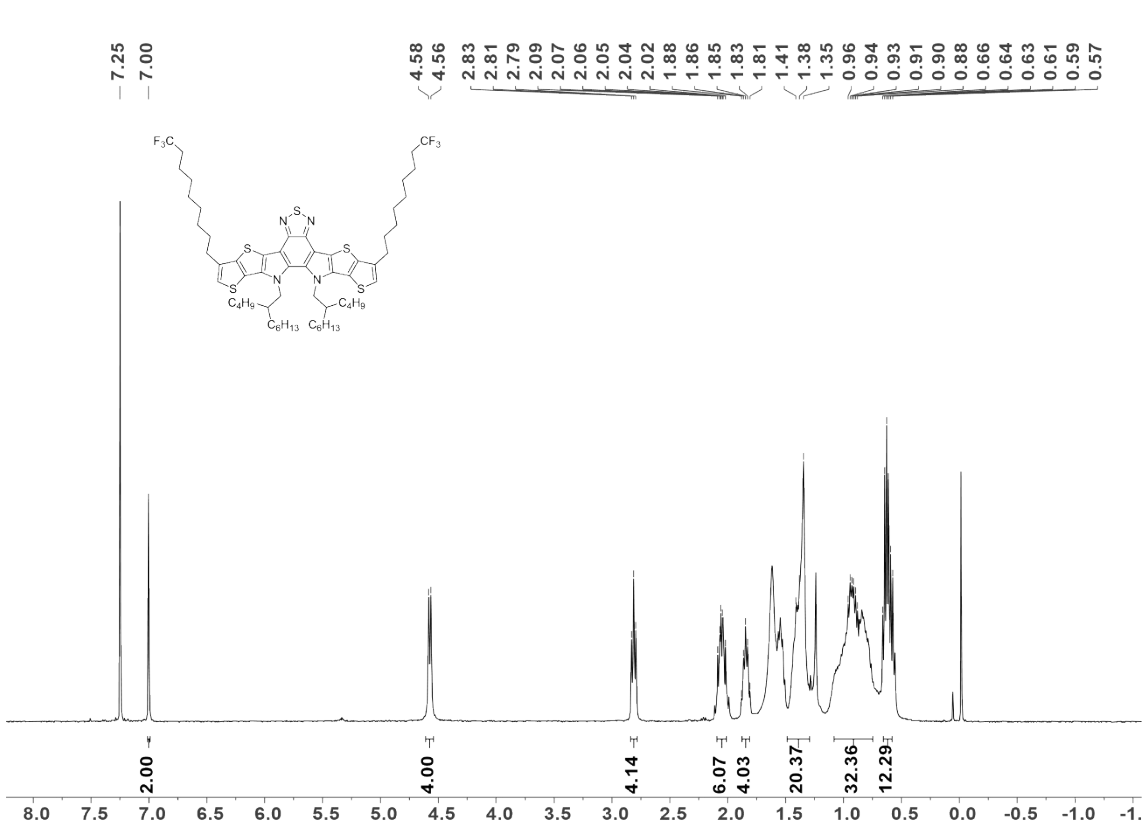
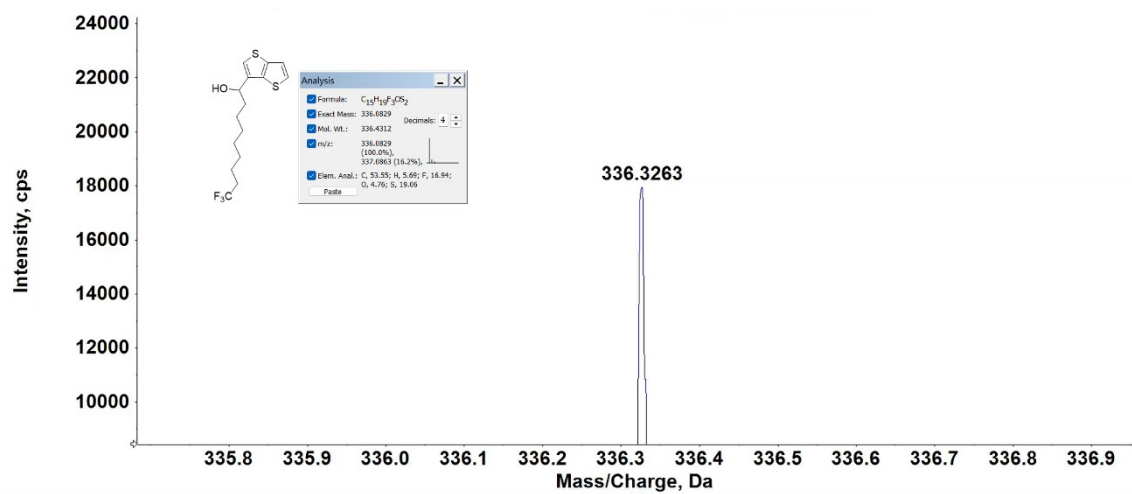
MALDI-TOF-MS spectrum of BTP-N3F

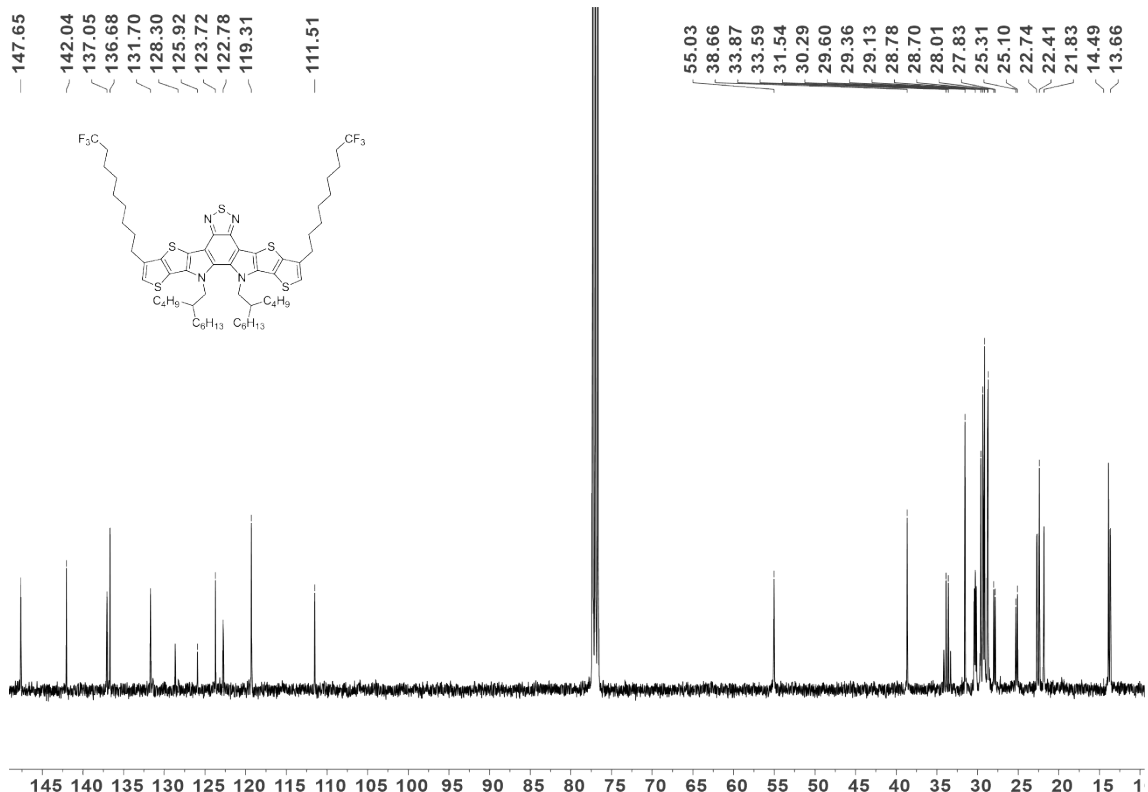


¹H NMR spectrum of **Compound 11**

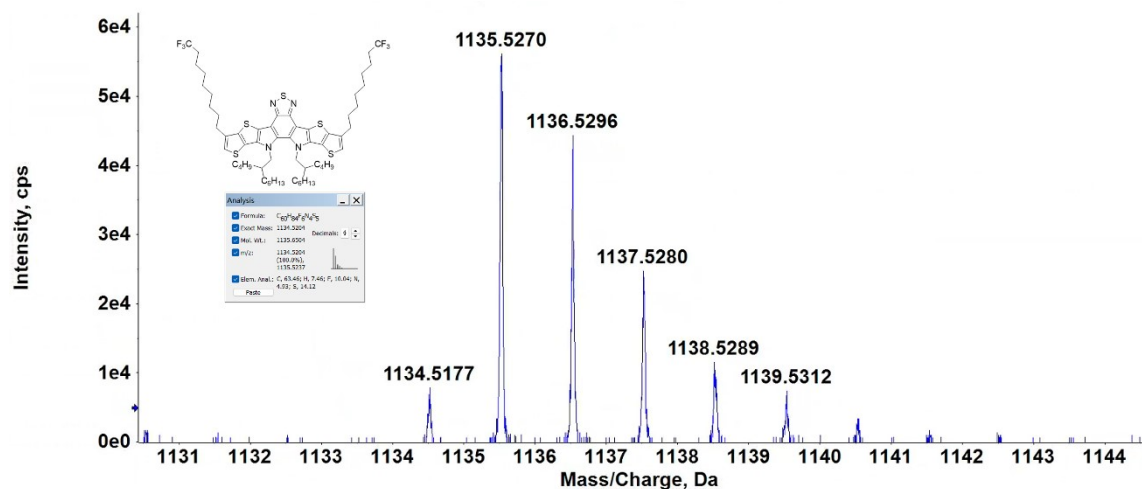


¹³C NMR spectrum of **Compound 11**

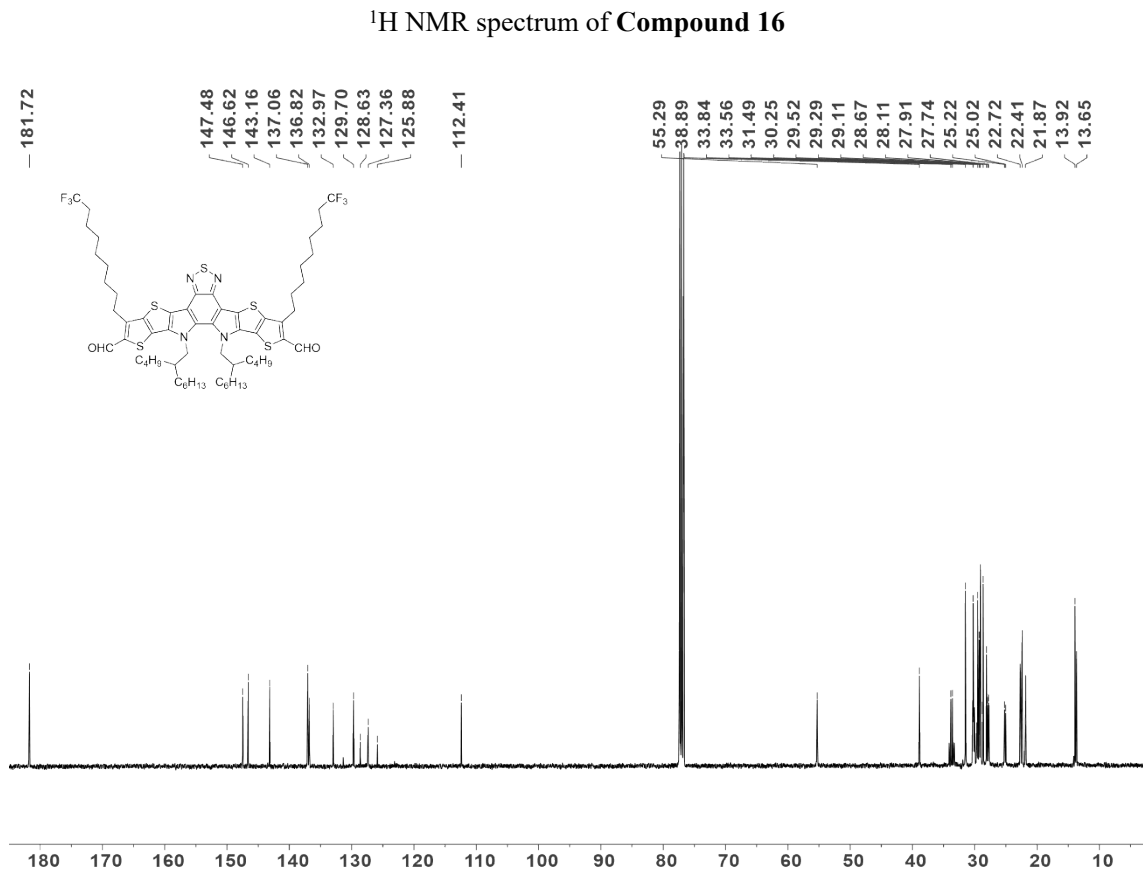
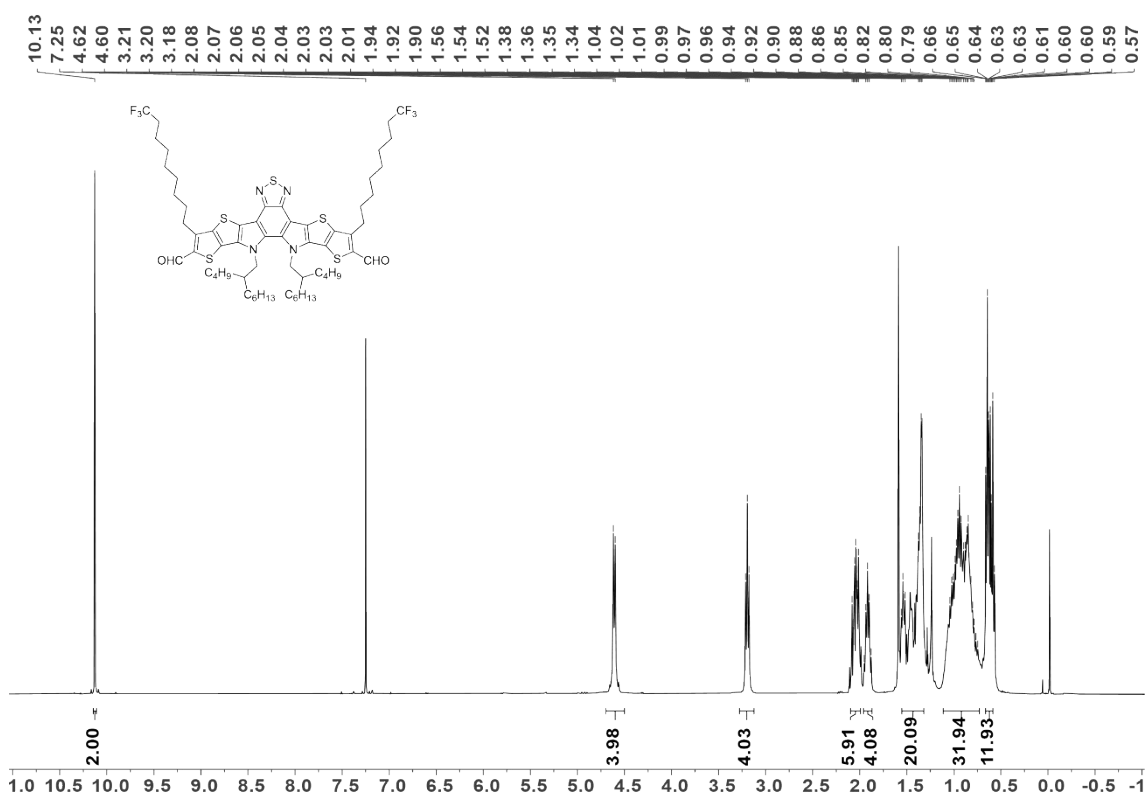


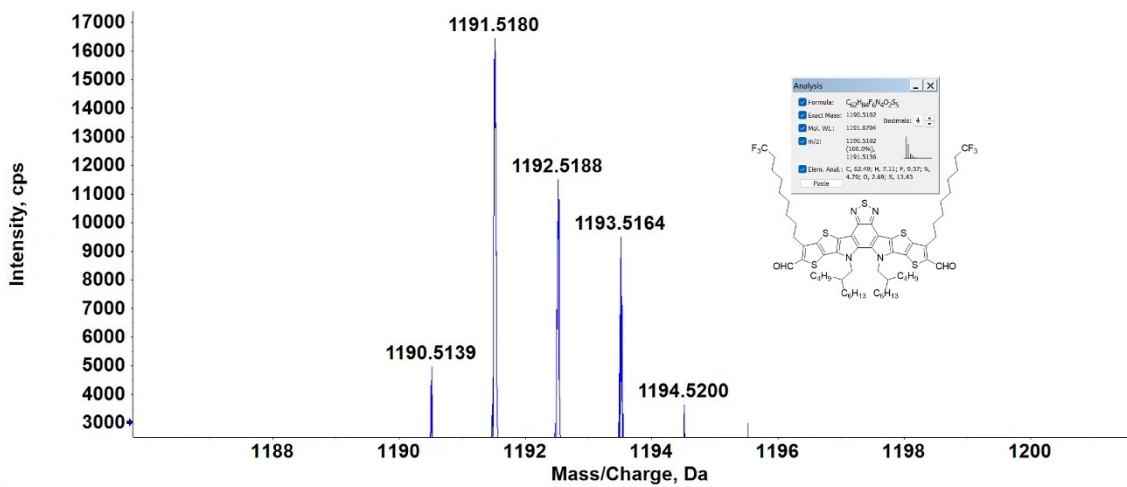


¹³C NMR spectrum of **Compound 15**

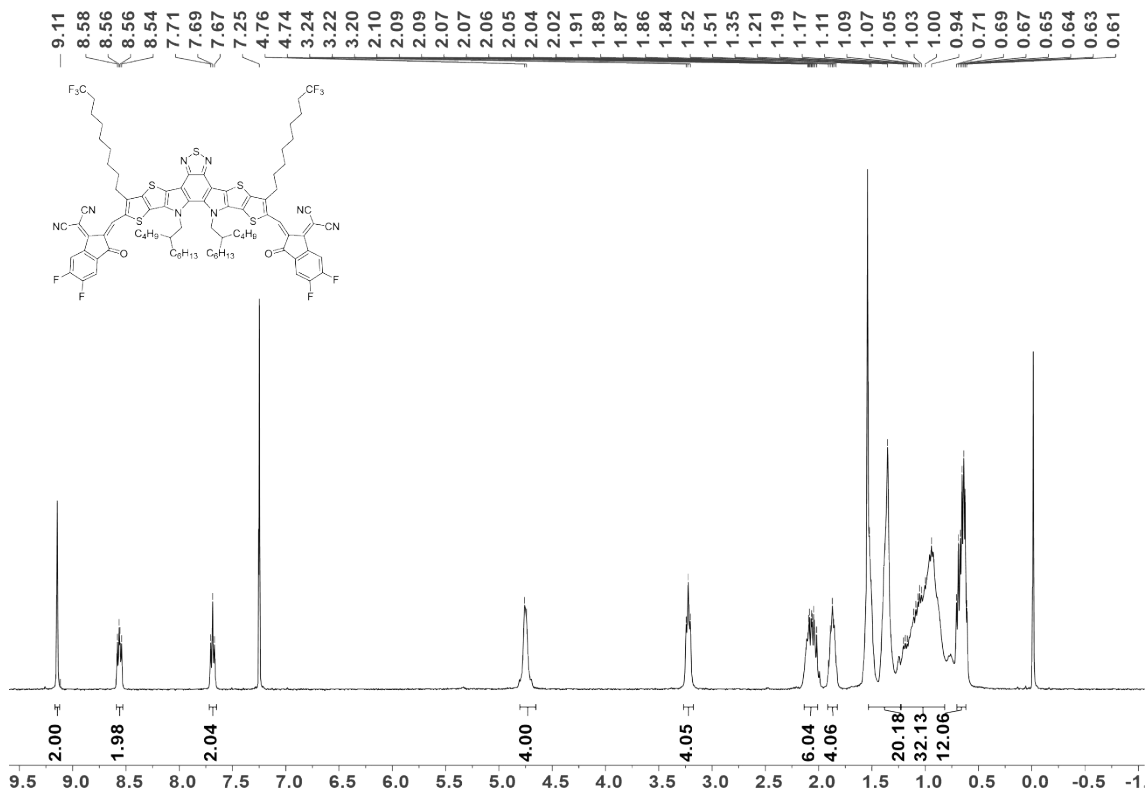


HRMS spectrum of **Compound 15**

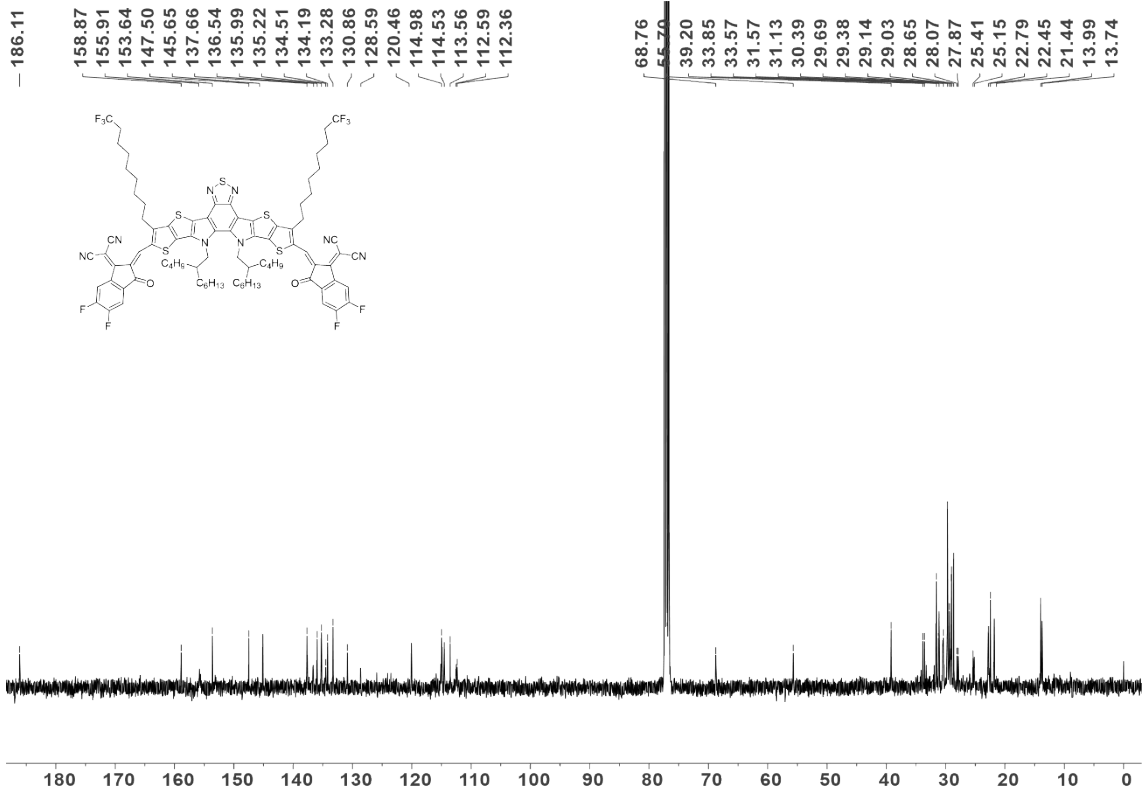




HRMS spectrum of **Compound 16**



¹H NMR spectrum of **BTP-C3F**



¹³C NMR spectrum of **BTP-C3F**

MALDI,1,20250228

Analysis Info

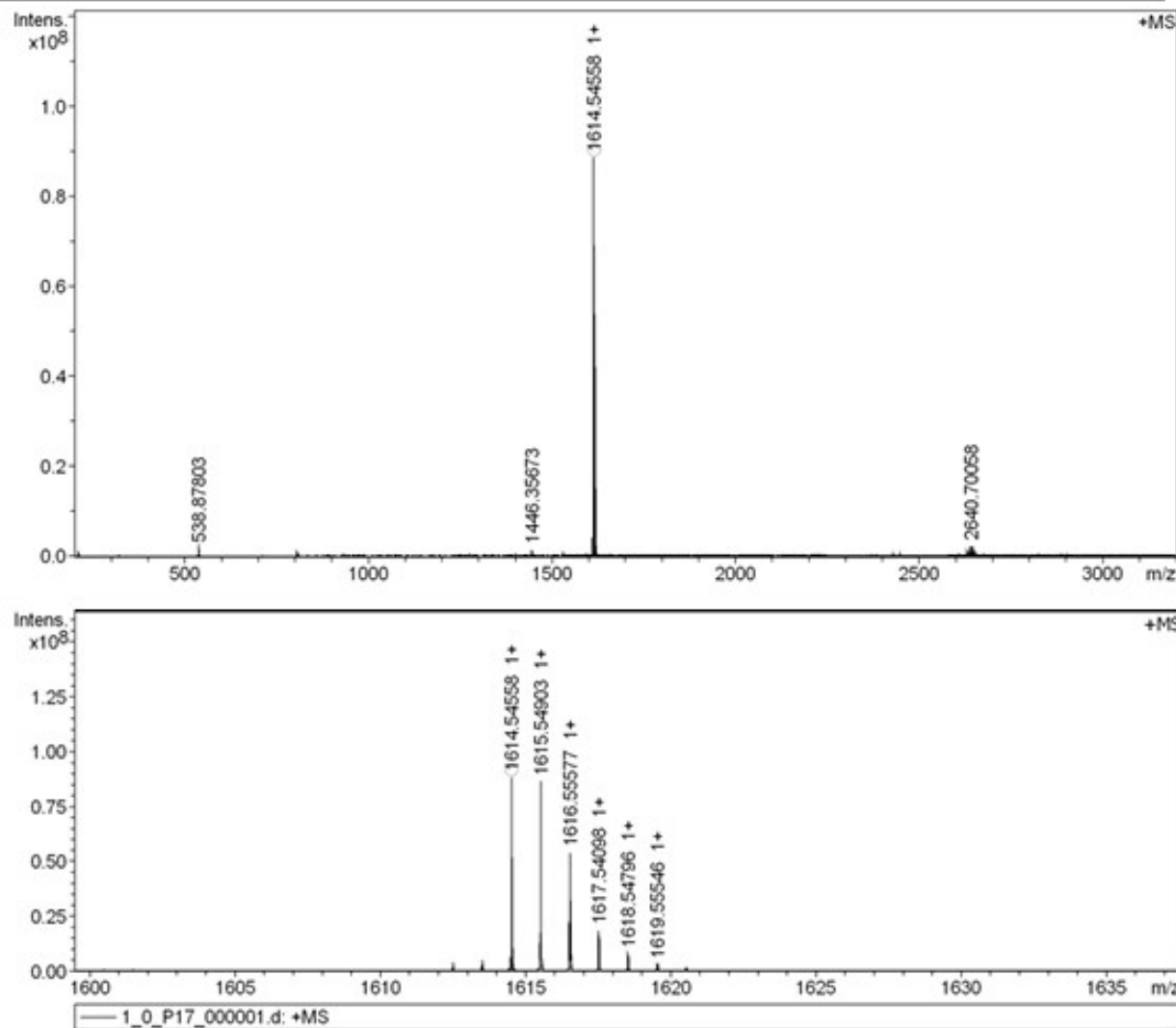
Analysis Name D:\Data\MALDI\2025\0228\dongjunwei\1_0_P17_000001.d
Method P20240925
Sample Name MURU-N-ESI
Comment

Acquisition Date 2/28/2025 4:01:07 PM

Operator
Instrument solariX

Acquisition Parameter

Acquisition Mode	Single MS	Acquired Scans	4	Calibration Date	Thu Oct 31 03:34:59
Polarity	Positive	No. of Cell Fills	1	Data Acquisition Size	2084152
Broadband Low Mass	202.1 m/z	No. of Laser Shots	18	Data Processing Size	4194304
Broadband High Mass	3200.0 m/z	Laser Power	21.6 lp	Apodization	Sine-Bell Multiplication
Source Accumulation	0.001 sec	Laser Shot Frequency	0.020 sec		
Ion Accumulation Time	0.010 sec				



Meas. m/z	#	Ion Formula	Score	m/z	err [ppm]	Mean err [ppm]	mSigma	rdb	e ⁻ Conf	N-Rule
1614.545575	1	C ₈₆ H ₈₈ F ₁₀ N ₈ O ₂ S ₅	100.00	1614.546863	-0.8	0.1	81.3	42.0	odd	ok

MALDI-TOF-MS spectrum of BTP-C3F

6. References

1. C. Li, J. Zhou, J. Song, J. Xu, H. Zhang, X. Zhang, J. Guo, L. Zhu, D. Wei, G. Han, J. Min, Y. Zhang, Z.

- Xie, Y. Yi, H. Yan, F. Gao, F. Liu and Y. Sun, *Nat. Energy*, 2021, **6**, 605-613.
- 2. N. Erdeljac, C. Thiehoff, R. P. Jumde, C. G. Daniliuc, S. Höppner, A. Faust, A. K. H. Hirsch and R. Gilmour, *J. Med. Chem.*, 2020, **63**, 6225-6237.
 - 3. L. L. Wu, C. L. Yang, F. C. Lo, C. H. Chiang, C. W. Chang, K. Y. Ng, H. H. Chou, H. Y. Hung, S. I. Chan and S. S. F. Yu, *Chem. Eur. J.*, 2011, **17**, 4774-4787.
 - 4. M. P. Hughes, K. D. Rosenthal, N. A. Ran, M. Seifrid, G. C. Bazan and T. Q. Nguyen, *Adv. Funct. Mater.*, 2018, **28**, 1801542.
 - 5. L. J. A. Koster, S. E. Shaheen and J. C. Hummelen, *Adv. Energy Mater.*, 2012, **2**, 1246-1253.
 - 6. H. Li, Y. Li, X. Dai, X. Xu and Q. Peng, *Angew. Chem. Int. Ed.*, 2024, **64**, e202416866.
 - 7. P. O. J. Scherer and S. F. Fischer, *Theoretical Molecular Biophysics*, Springer Nature, Berlin, Germany, 2017.
 - 8. R. B. Hall, *Thin Solid Films*, 1971, **8**, 263-271.
 - 9. I. Saini, J. Rozra, N. Chandak, S. Aggarwal, P. K. Sharma and A. Sharma, *Mater. Chem. Phys.*, 2013, **139**, 802-810.
 - 10. C. Y. Chang, W. C. Hsu, S. J. Wang and S. S. Hau, *J. Appl. Phys.*, 1986, **60**, 1042-1045.
 - 11. L. B. Schein and A. Tyutnev, *J. Phys. Chem. C*, 2008, **112**, 7295-7308.
 - 12. Y. Sun, L. Wang, C. Guo, J. Xiao, C. Liu, C. Chen, W. Xia, Z. Gan, J. Cheng, J. Zhou, Z. Chen, J. Zhou, D. Liu, T. Wang and W. Li, *J. Am. Chem. Soc.*, 2024, **146**, 12011-12019.
 - 13. T. Huang, Y. Zhang, J. Wang, Z. Cao, S. Geng, H. Guan, D. Wang, Z. Zhang, Q. Liao and J. Zhang, *Nano Energy*, 2024, **121**, 109226.
 - 14. L. Zhu, M. Zhang, G. Zhou, Z. Wang, W. Zhong, J. Zhuang, Z. Zhou, X. Gao, L. Kan, B. Hao, F. Han, R. Zeng, X. Xue, S. Xu, H. Jing, B. Xiao, H. Zhu, Y. Zhang and F. Liu, *Joule*, 2024, **8**, 3153-3168.
 - 15. H. Niu, C. Xiao, J. Xu, C. Xie, M. Duan, Z. Bu and W. Li, *Adv. Funct. Mater.*, 2024, **35**, 2413167.
 - 16. W. Su, X. Zhou, Q. Wu, Y. Wu, H. Qin, Z. Liang, H. Li, H. Bai, J. Guo, L. Jiang, Y. Liu, R. Ma, Y. Li, W. Zhu and Q. Fan, *Adv. Funct. Mater.*, 2024, **35**, 2415090.
 - 17. W. Su, X. Zhou, Z. F. Yao, H. Bai, Y. Duan, R. Sun, Y. Wu, Q. Wu, H. Qin, C. Zhao, W. Zhu, H. Y. Woo, J. Min, Y. Li, W. Ma and Q. Fan, *Adv. Funct. Mater.*, 2024, **34**, 2313744.
 - 18. X. Sun, C. Zhang, Y. Yao, J. Lv, J. Yao, X. Ding, M. Lu, L. Zhu, G. Zhang, H. Lin, Y. Shi, K. Wang, C. Yang, X. Ouyang, H. Hu, I. McCulloch and Y. Lin, *Adv. Funct. Mater.*, 2024, **34**, 2406060.
 - 19. Z. C. Suo, L. Y. Li, J. Liu, Z. Y. Yao, C. X. Li, X. J. Wan and Y. S. Chen, *Adv. Funct. Mater.*, 2024, **34**, 2409699.
 - 20. X. Cui, Y. Ji, Y. Liu, X. Ma, H. Li, P. Cheng, W. Huang and Z. Bo, *Adv. Energy Mater.*, 2024, **15**, 2403077.
 - 21. H. Gao, Q. Li, B. Fan, Z. Bi, W. Jiang, S. Zhang, Q. Fan, T. Chen, F. R. Lin, B. Kan, D. Lei, W. Ma and A. K. Y. Jen, *Adv. Energy Mater.*, 2024, DOI: 10.1002/aenm.202403121.
 - 22. D. He, J. Zhou, Y. Zhu, Y. Li, K. Wang, J. Li, J. Zhang, B. Li, Y. Lin, Y. He, C. Wang and F. Zhao, *Adv. Mater.*, 2023, **36**, 2308909.
 - 23. K. Liu, Y. Jiang, F. Liu, G. Ran, F. Huang, W. Wang, W. Zhang, C. Zhang, J. Hou and X. Zhu, *Adv. Mater.*, 2023, **35**, 2300363.
 - 24. H. Lu, W. Liu, G. Ran, J. Li, D. Li, Y. Liu, X. Xu, W. Zhang and Z. Bo, *Adv. Mater.*, 2023, **36**, 2307292.
 - 25. M. Lv, Q. Wang, J. Zhang, Y. Wang, Z. G. Zhang, T. Wang, H. Zhang, K. Lu, Z. Wei and D. Deng, *Adv. Mater.*, 2023, **36**, 2310046.
 - 26. L. Wen, H. Mao, L. Zhang, J. Zhang, Z. Qin, L. Tan and Y. Chen, *Adv. Mater.*, 2023, **36**, 2308159.
 - 27. Z. H. Chen, Y. Xiao, H. F. Yao, J. Z. Ren, T. Zhang, J. W. Qiao, S. Q. Zhu, R. C. Lin, X. T. Hao and J.

- H. Hou, *Adv. Mater.*, 2024, **36**, 2408858.
- 28. Y. Kan, Y. Sun, Y. Ren, Y. Xu, X. Jiang, H. Shen, L. Geng, J. Li, P. Cai, H. Xu, K. Gao and Y. Li, *Adv. Mater.*, 2024, **36**, 2312635.
 - 29. Y. Miao, Y. Sun, W. Zou, X. Zhang, Y. Kan, W. Zhang, X. Jiang, X. Wang, R. Yang, X. Hao, L. Geng, H. Xu and K. Gao, *Adv. Mater.*, 2024, **36**, 2406623.
 - 30. N. Wei, J. Chen, Y. Cheng, Z. Bian, W. Liu, H. Song, Y. Guo, W. Zhang, Y. Liu, H. Lu, J. Zhou and Z. Bo, *Adv. Mater.*, 2024, **36**, 2408934.
 - 31. Z. Yao, X. Cao, X. Bi, T. He, Y. Li, X. Jia, H. Liang, Y. Guo, G. Long, B. Kan, C. Li, X. Wan and Y. Chen, *Angew. Chem. Int. Ed.*, 2023, **62**, 202312630.
 - 32. T. Chen, Y. Zhong, T. Duan, X. Tang, W. Zhao, J. Wang, G. Lu, G. Long, J. Zhang, K. Han, X. Wan, B. Kan and Y. Chen, *Angew. Chem. Int. Ed.*, 2024, **64**, e202412983.
 - 33. H. Hu, S. Liu, J. Xu, R. Ma, Z. Peng, T. A. D. Peña, Y. Cui, W. Liang, X. Zhou, S. Luo, H. Yu, M. Li, J. Wu, S. Chen, G. Li and Y. Chen, *Angew. Chem. Int. Ed.*, 2024, **63**, e202400086.
 - 34. X. Wu, Y. Gong, X. Li, S. Qin, H. He, Z. Chen, T. Liang, C. Wang, D. Deng, Z. Bi, W. Ma, L. Meng and Y. Li, *Angew. Chem. Int. Ed.*, 2024, **64**, e202416016.
 - 35. Y. Li, Z. Ge, L. Mei, H. Ma, Y. Chen, X. Wang, J. Yu, G. Lu, R. Yang, X. K. Chen, S. Yin and Y. Sun, *Angew. Chem. Int. Ed.*, 2024, **63**, e202411044.
 - 36. K. Liu, Y. Jiang, G. Ran, F. Liu, W. Zhang and X. Zhu, *Joule*, 2024, **8**, 835-851.
 - 37. H. Liang, X. Bi, H. Chen, T. He, Y. Lin, Y. Zhang, K. Ma, W. Feng, Z. Ma, G. Long, C. Li, B. Kan, H. Zhang, O. A. Rakitin, X. Wan, Z. Yao and Y. Chen, *Nat. Commun.*, 2023, **14**, 4707.
 - 38. J. Fu, Q. Yang, P. Huang, S. Chung, K. Cho, Z. Kan, H. Liu, X. Lu, Y. Lang, H. Lai, F. He, P. W. K. Fong, S. Lu, Y. Yang, Z. Xiao and G. Li, *Nat. Commun.*, 2024, **15**, 1830.
 - 39. C. Chen, L. Wang, W. Xia, K. Qiu, C. Guo, Z. Gan, J. Zhou, Y. Sun, D. Liu, W. Li and T. Wang, *Nat. Commun.*, 2024, **15**, 6865.
 - 40. L. Wang, C. Chen, Y. Fu, C. Guo, D. Li, J. Cheng, W. Sun, Z. Gan, Y. Sun, B. Zhou, C. Liu, D. Liu, W. Li and T. Wang, *Nat. Energy*, 2024, **9**, 208-218.
 - 41. Z. Chen, J. Zhu, D. Yang, W. Song, J. Shi, J. Ge, Y. Guo, X. Tong, F. Chen and Z. Ge, *Energy Environ. Sci.*, 2023, **16**, 3119-3127.
 - 42. C. Guo, Y. Sun, L. Wang, C. Liu, C. Chen, J. Cheng, W. Xia, Z. Gan, J. Zhou, Z. Chen, J. Zhou, D. Liu, J. Guo, W. Li and T. Wang, *Energy Environ. Sci.*, 2024, **17**, 2492-2499.
 - 43. T. Jia, Y. Luo, Y. Hai, T. Lin, X. Qin, R. Ma, K. Fan, A. A. Sergeev, T. A. Dela Peña, Y. Li, M. Li, K. S. Wong, G. Li, J. Wu, S. Liu and F. Huang, *Energy Environ. Sci.*, 2024, **17**, 8593-8608.
 - 44. L. Xie, Z. Chen, D. Yang, X. Yu, X. Tong, J. Ge, W. Song, S. Yang, J. Zhu, P. Ding, G. Lu, X. Li, M. Long, J. Li, B. Zou, T. Liu, Q. Liu and Z. Ge, *Energy Environ. Sci.*, 2024, **17**, 7838-7849.
 - 45. W. Song, Z. Chen, C. Lin, P. Zhang, D. Sun, W. Zhang, J. Ge, L. Xie, R. Peng, D. Yang, Q. Liu, Y. Xu and Z. Ge, *Energy Environ. Sci.*, 2024, **17**, 7318-7329.
 - 46. Z. Zhang, W. Feng, Y. Zhang, S. Yuan, Y. Bai, P. Wang, Z. Yao, C. Li, T. Duan, X. Wan, B. Kan and Y. Chen, *Sci. China Chem.*, 2024, **67**, 1596-1604.
 - 47. X. Bi, X. Cao, T. He, H. Liang, Z. Yao, J. Yang, Y. Guo, G. Long, B. Kan, C. Li, X. Wan and Y. Chen, *Small*, 2024, **20**, 2401054.
 - 48. L. Zhang, Y. Wang, J. Wen, Y. Huang, J. Gao, Y. Duan, S. Park, W. Shin, Z. Ma, M. Liu, S. W. Cho, Y. Park, Y. M. Jung, H. Lee, W. Liu and Y. Liu, *Angew. Chem. Int. Ed.*, 2024, **63**, e202408960.
 - 49. W. Zhou, J. Liu, J. Xie, S. You, J. Deng, F. Yu, S. Y. Jeong, H. Y. Woo, F. Wu and L. Chen, *Angew. Chem. Int. Ed.*, 2024, **64**, e202415141.
 - 50. B. S. Zou, A. H. Liang, P. B. Ding, J. Yao, X. H. Zeng, H. X. Li, R. J. Ma, C. L. Li, W. W. Wu, D. Z.

- Chen, M. Qammar, H. Yu, J. C. Yi, L. Guo, S. H. Pun, J. E. Halpert, G. Li, Z. P. Kan and H. Yan, *Angew Chem Int Edit*, 2025, **64**, e202415332.
51. X. Liu, Z. Zhang, C. Wang, C. Zhang, S. Liang, H. Fang, B. Wang, Z. Tang, C. Xiao and W. Li, *Angew. Chem. Int. Ed.*, 2023, **63**, e202316039.
52. F. Liu, Y. Jiang, R. Xu, W. Su, S. Wang, Y. Zhang, K. Liu, S. Xu, W. Zhang, Y. Yi, W. Ma and X. Zhu, *Angew. Chem. Int. Ed.*, 2023, **63**, e202313791.
53. S. Chen, S. Zhu, L. Hong, W. Deng, Y. Zhang, Y. Fu, Z. Zhong, M. Dong, C. Liu, X. Lu, K. Zhang and F. Huang, *Angew. Chem. Int. Ed.*, 2024, **63**, e202318756.
54. X. Yu, P. Ding, D. Yang, P. Yan, H. Wang, S. Yang, J. Wu, Z. Wang, H. Sun, Z. Chen, L. Xie and Z. Ge, *Angew. Chem. Int. Ed.*, 2024, **63**, e202401518.
55. Y. He, W. Jing, C. Liao, X. Xu, Y. Duan, R. Li, L. Yu and Q. Peng, *Chem. Eng. J.*, 2024, **490**, 151920.
56. W. Y. Xia, B. J. Zhou, L. Wang, C. H. Guo, J. P. Zhou, J. C. Cheng, W. Sun, C. Chen, Z. R. Gan, W. Li, D. Liu and T. Wang, *Adv. Funct. Mater.*, 2024, **34**, 2408340.
57. M. Haris, Z. Ullah, S. Lee, D. H. Ryu, S. U. Ryu, B. J. Kang, N. J. Jeon, B. J. Kim, T. Park, W. S. Shin and C. E. Song, *Adv. Energy Mater.*, 2024, **14**, 2401597.
58. L. Kong, X. Wang, M. Li, Z. Zhang, M. Chen, L. Zhang, L. Ying, D. Ma and J. Chen, *Adv. Energy Mater.*, 2024, **14**, 2402517.
59. M. Zhou, C. Liao, Y. Duan, X. Xu, L. Yu, R. Li and Q. Peng, *Adv. Mater.*, 2022, **35**, 2208279.
60. M. Deng, X. Xu, Y. Duan, W. Qiu, L. Yu, R. Li and Q. Peng, *Adv. Mater.*, 2023, **36**, 2308216.
61. M. Deng, X. Xu, Y. Duan, L. Yu, R. Li and Q. Peng, *Adv. Mater.*, 2023, **35**, 2210760.
62. S. Hao, X. Xu, L. Yu, S. Peng, J. Xia, Y. Xie, C. Duan, H. Wu, R. Li and Q. Peng, *Adv. Mater.*, 2023, **35**, 2301732.
63. B. Pang, C. Liao, X. Xu, S. Peng, J. Xia, Y. Guo, Y. Xie, Y. Chen, C. Duan, H. Wu, R. Li and Q. Peng, *Adv. Mater.*, 2023, **35**, 2211871.
64. B. Pang, C. Liao, X. Xu, L. Yu, R. Li and Q. Peng, *Adv. Mater.*, 2023, **35**, 2300631.
65. X. Xu, W. Jing, H. Meng, Y. Guo, L. Yu, R. Li and Q. Peng, *Adv. Mater.*, 2023, **35**, 2208997.
66. L. Hu, J. Quan, J. Li, Z. Li, S. Lan, M. Yu, X. Liao, Y. Jin, X. Yin, J. Song, D. Zhou, Z. Li and Y. Chen, *Adv. Mater.*, 2024, **36**, 2413232.
67. C. Liao, X. Xu, T. Yang, W. Qiu, Y. Duan, R. Li, L. Yu and Q. Peng, *Adv. Mater.*, 2024, **36**, 2411071.
68. Y. Wang, K. Sun, C. Li, C. Zhao, C. Gao, L. Zhu, Q. Bai, C. Xie, P. You, J. Lv, X. Sun, H. Hu, Z. Wang, H. Hu, Z. Tang, B. He, M. Qiu, S. Li and G. Zhang, *Adv. Mater.*, 2024, **36**, 2411957.
69. M. Zhang, Z. Y. Wang, L. Zhu, R. Zeng, X. N. Xue, S. Liu, J. Yan, Z. Y. Yang, W. K. Zhong, G. Q. Zhou, L. X. Kan, J. Q. Xu, A. Y. Zhang, J. W. Deng, Z. C. Zhou, J. N. Song, H. Jing, S. J. Xu, Y. M. Zhang and F. Liu, *Adv. Mater.*, 2024, **36**, 2407297.
70. J. Qin, L. Wu, S. Huang, Z. Ou, X. Wang, Y. Yang, Y. Zheng, K. Sun, Z. Zhang, Z. Hu, Z. Liu, Y. Leng and J. Du, *Adv. Sci.*, 2024, **11**, 2409867.
71. T. Zhou, W. Jin, Y. Li, X. Xu, Y. Duan, R. Li, L. Yu and Q. Peng, *Adv. Sci.*, 2024, **11**, 2401405.
72. H. Meng, W. Jing, X. Xu, L. Yu and Q. Peng, *Angew. Chem. Int. Ed.*, 2023, **62**, 202301958.
73. M. An, Q. Liu, S. Y. Jeong, B. Liu, E. Huang, Q. Liang, H. Li, G. Zhang, H. Y. Woo, L. Niu, X. Guo and H. Sun, *Angew. Chem. Int. Ed.*, 2024, **63**, e202410498.
74. X. Chen, Y. Li, W. Jing, T. Zhou, X. Xu, Y. Duan, L. Yu, R. Li and Q. Peng, *Angew. Chem. Int. Ed.*, 2024, **63**, e202402831.
75. W. Liu, J. Wen, H. Yu, X. Zhan, Y. Wang, L. Zhang, Y. Fan, Z. You and Y. Liu, *Angew. Chem. Int. Ed.*, 2024, **64**, e202413135.
76. X. Zhang, H. Gao, Y. Kan, X. Wang, W. Zhang, K. Zhou, H. Xu, L. Ye, R. Yang, Y. Yang, X. Hao, Y.

- Sun and K. Gao, *Angew. Chem. Int. Ed.*, 2024, **64**, e202415583.
77. Y. T. Wang, W. J. Sun, Y. Zhang, B. Y. Zhang, Y. T. Ding, Z. Q. Zhang, L. Meng, K. Huang, W. Ma and H. L. Zhang, *Angew. Chem. Int. Ed.*, 2024, **64**, e202417643.
78. J. Y. Shi, P. F. Ding, J. T. Zhu, Z. Y. Chen, S. J. Gao, X. L. Yu, X. C. Liao, Q. Liu and Z. Y. Ge, *Energy Environ. Sci.*, 2024, **17**, 9144-9153.
79. C. Li, G. Yao, X. Gu, J. Lv, Y. Hou, Q. Lin, N. Yu, M. S. Abbasi, X. Zhang, J. Zhang, Z. Tang, Q. Peng, C. Zhang, Y. Cai and H. Huang, *Nat. Commun.*, 2024, **15**, 8872.
80. G. Wu, X. Xu, C. Liao, L. Yu, R. Li and Q. Peng, *Small*, 2023, **19**, 2302127.
81. X. Sun, X. Ding, F. Wang, J. Lv, C. Gao, G. Zhang, X. Ouyang, G. Li and H. Hu, *ACS Energy Lett.*, 2024, **9**, 4209-4217.
82. Q. Wang, S. Zhao, H. Ding, P. Zhu, Y. Fu, Y. Lv, X. Lu, H. Zhu, X. Liao and Y. Chen, *Sci. China Mater.*, 2024, DOI: 10.1007/s40843-024-3146-4.
83. C. Chen, L. Wang, Y. Sun, Y. Fu, C. Guo, B. Zhou, Z. Gan, D. Liu, W. Li and T. Wang, *Adv. Funct. Mater.*, 2023, **33**, 2305765.
84. L. Zhu, M. Zhang, J. Xu, C. Li, J. Yan, G. Zhou, W. Zhong, T. Hao, J. Song, X. Xue, Z. Zhou, R. Zeng, H. Zhu, C.-C. Chen, R. C. I. MacKenzie, Y. Zou, J. Nelson, Y. Zhang, Y. Sun and F. Liu, *Nat. Mater.*, 2022, **21**, 656-663.
85. L. Tu, H. Wang, W. Duan, R. Ma, T. Jia, T. A. Dela Peña, Y. Luo, J. Wu, M. Li, X. Xia, S. Wu, K. Chen, Y. Wu, Y. Huang, K. Yang, G. Li and Y. Shi, *Energy Environ. Sci.*, 2024, **17**, 3365-3374.
86. X. Ma, T. Li, G. Song, Z. He and Y. Cao, *Nano Lett.*, 2024, **24**, 3051-3058.
87. Y. Jiang, S. Sun, R. Xu, F. Liu, X. Miao, G. Ran, K. Liu, Y. Yi, W. Zhang and X. Zhu, *Nat. Energy*, 2024, **9**, 975-986.
88. H. Lu, D. Li, W. Liu, G. Ran, H. Wu, N. Wei, Z. Tang, Y. Liu, W. Zhang and Z. Bo, *Angewandte Chemie International Edition*, 2024, **63**, e202407007.
89. S. Guan, Y. Li, C. Xu, N. Yin, C. Xu, C. Wang, M. Wang, Y. Xu, Q. Chen, D. Wang, L. Zuo and H. Chen, *Adv. Mater.*, 2024, **36**, 2400342.
90. Z. Ge, J. Qiao, J. Song, X. Li, J. Fu, Z. Fu, J. Gao, X. Tang, L. Jiang, Z. Tang, G. Lu, X. Hao and Y. Sun, *Adv. Energy Mater.*, 2024, **14**, 2400203.
91. J. Song, C. Zhang, C. Li, J. Qiao, J. Yu, J. Gao, X. Wang, X. Hao, Z. Tang, G. Lu, R. Yang, H. Yan and Y. Sun, *Angew. Chem. Int. Ed.*, 2024, **63**, e202404297.
92. L. Kong, Z. Zhang, N. Zhao, Z. Cai, J. Zhang, M. Luo, X. Wang, M. Chen, W. Zhang, L. Zhang, Z. Wei and J. Chen, *Adv. Energy Mater.*, 2023, **13**, 2300763.
93. Z. Chen, S. Zhang, T. Zhang, J. Dai, Y. Yu, H. Li, X. Hao and J. Hou, *Joule*, 2024, **8**, 1723-1734.
94. Y. Cui, Y. Xu, H. Yao, P. Bi, L. Hong, J. Zhang, Y. Zu, T. Zhang, J. Qin, J. Ren, Z. Chen, C. He, X. Hao, Z. Wei and J. Hou, *Adv. Mater.*, 2021, **33**, 2102420.
95. Z. Wang, H. Wang, M. Du, X. Lai, F. He, Q. Guo, Q. Guo, A. Tang, X. Sun and E. Zhou, *Adv. Funct. Mater.*, 2023, **34**, 2313240.
96. Y. Wang, S. Zhang, J. Wang, J. Ren, J. Qiao, Z. Chen, Y. Yu, X.-T. Hao and J. Hou, *ACS Energy Lett.*, 2024, **9**, 2420-2427.
97. C. Guo, Y. Fu, D. Li, L. Wang, B. Zhou, C. Chen, J. Zhou, Y. Sun, Z. Gan, D. Liu, W. Li and T. Wang, *Adv. Mater.*, 2023, **35**, 2304921.
98. J. Liu, X. Duan, J. Song, C. Liu, J. Gao, M. H. Jee, Z. Tang, H. Y. Woo and Y. Sun, *Energy Environ. Sci.*, 2024, **17**, 3641-3650.
99. H. Lu, W. Liu, G. Ran, Z. Liang, H. Li, N. Wei, H. Wu, Z. Ma, Y. Liu, W. Zhang, X. Xu and Z. Bo, *Angew. Chem. Int. Ed.*, 2023, **62**, e202314420

100. M. Zhang, B. Chang, R. Zhang, S. Li, X. Liu, L. Zeng, Q. Chen, L. Wang, L. Yang, H. Wang, J. Liu, F. Gao and Z. G. Zhang, *Adv. Mater.*, 2023, **36**, 2308606.
101. K. Chong, X. Xu, H. Meng, J. Xue, L. Yu, W. Ma and Q. Peng, *Adv. Mater.*, 2022, **34**, 2109516.
102. G. Ding, T. Chen, M. Wang, X. Xia, C. He, X. Zheng, Y. Li, D. Zhou, X. Lu, L. Zuo, Z. Xu and H. Chen, *Nano Micro Lett.*, 2023, **15**, 92.
103. H. Liu, Y. Xin, Z. Suo, L. Yang, Y. Zou, X. Cao, Z. Hu, B. Kan, X. Wan, Y. Liu and Y. Chen, *J. Am. Chem. Soc.*, 2024, **146**, 14287-14296.
104. J. Fu, P. W. K. Fong, H. Liu, C.-S. Huang, X. Lu, S. Lu, M. Abdelsamie, T. Kodalle, C. M. Sutter-Fella, Y. Yang and G. Li, *Nat. Commun.*, 2023, **14**, 1760.
105. S. Luo, C. Li, J. Zhang, X. Zou, H. Zhao, K. Ding, H. Huang, J. Song, J. Yi, H. Yu, K. S. Wong, G. Zhang, H. Ade, W. Ma, H. Hu, Y. Sun and H. Yan, *Nat. Commun.*, 2023, **14**, 6964.
106. R. Zeng, M. Zhang, X. Wang, L. Zhu, B. Hao, W. Zhong, G. Zhou, J. Deng, S. Tan, J. Zhuang, F. Han, A. Zhang, Z. Zhou, X. Xue, S. Xu, J. Xu, Y. Liu, H. Lu, X. Wu, C. Wang, Z. Fink, T. P. Russell, H. Jing, Y. Zhang, Z. Bo and F. Liu, *Nat. Energy*, 2024, **9**, 1117-1128.
107. R. Zeng, L. Zhu, M. Zhang, W. Zhong, G. Zhou, J. Zhuang, T. Hao, Z. Zhou, L. Zhou, N. Hartmann, X. Xue, H. Jing, F. Han, Y. Bai, H. Wu, Z. Tang, Y. Zou, H. Zhu, C.-C. Chen, Y. Zhang and F. Liu, *Nat. Commun.*, 2023, **14**, 4148.
108. J. Wang, Y. Wang, P. Bi, Z. Chen, J. Qiao, J. Li, W. Wang, Z. Zheng, S. Zhang, X. Hao and J. Hou, *Adv. Mater.*, 2023, **35**, 2301583.
109. C. Zhang, Y. Shi, J. Tao, J. Zhang, H. Zhang, D. Qiu, C. Wang, C. Tian, Z. Wei and K. Lu, *Adv. Energy Mater.*, 2024, DOI: 10.1002/aenm.202403806.
110. H. Fang, Q. Chen, Y. Lin, X. Xu, J. Wang, M. Li, C. Xiao, C. R. McNeill, Z. Tang, Z. Lu and W. Li, *Angew. Chem. Int. Ed.*, 2024, **64**, e202417951.
111. H. Ma, J. Song, J. Qiao, B. Han, Q. Wang, M. H. Jee, L. Bu, D. Wei, H. Y. Woo, X. Hao and Y. Sun, *Energy Environ. Sci.*, 2025, **18**, 397-405.
112. X. Kong, N. Yang, X. Zhang, J. Zhang, Z. Li, X. Li, Y. Wu, R. Sun, J. Li, A. Li, J. Min, G. Yang and C. Sun, *Energy Environ. Sci.*, 2025, **18**, 386-396.
113. H. Wang, Z. Zhong, S. Gámez-Valenzuela, J. W. Lee, B. Li, C. Xu, J. Yang, H. Sun, B. J. Kim, B. Liu and X. Guo, *Adv. Funct. Mater.*, 2024, DOI: 10.1002/adfm.202418805.
114. Y. Li, Z. Jia, P. Huang, C. Gao, Y. Wang, S. Xue, S. Lu and Y. Yang, *Energy Environ. Sci.*, 2025, **18**, 256-263.
115. C. Sun, J. Wang, F. Bi, H. Jiang, C. Yang, Y. Li, J. Chu and X. Bao, *Energy Environ. Sci.*, 2025, **18**, 862-873.
116. H. Tian, Y. Luo, Z. Chen, T. Xu, R. Ma, J. Wu, G. Li, C. Yang and Z. Luo, *Adv. Energy Mater.*, 2024, DOI: 10.1002/aenm.202404537.
117. X. Gu, Y. Wei, R. Zeng, J. Lv, Y. Hou, N. Yu, S. Tan, Z. Wang, C. Li, Z. Tang, Q. Peng, F. Liu, Y. Cai, X. Zhang and H. Huang, *Angew. Chem. Int. Ed.*, 2024, **64**, e202418926.
118. J. Zhou, L. Wang, C. Liu, C. Guo, C. Chen, Y. Sun, Y. Yang, J. Cheng, Z. Gan, Z. Chen, W. Sun, J. Zhou, W. Xia, D. Liu, W. Li and T. Wang, *J. Am. Chem. Soc.*, 2024, **146**, 34998-35006.
119. Q. Zhang, H. Gao, L. Li, Y. Shen, M. Zuo, G. Lu, X. Wu and Y. Han, *Adv. Energy Mater.*, 2024, DOI: 10.1002/aenm.202404507.
120. J. Wang, P. Wang, T. Chen, W. Zhao, J. Wang, B. Lan, W. Feng, H. Liu, Y. Liu, X. Wan, G. Long, B. Kan and Y. Chen, *Angew. Chem. Int. Ed.*, 2025, DOI: 10.1002/anie.202423562.
121. L. Liu, F. Yu, D. Hu, X. Jiang, P. Huang, Y. Li, G. Tian, H. Lei, S. Wu, K. Tu, C. Chen, T. Gu, Y. Chen, T. Duan and Z. Xiao, *Energy Environ. Sci.*, 2025, **18**, 1722-1731.

122. K. Liu, Y. Jiang, F. Liu, G. Ran, M. Wang, W. Wang, W. Zhang, Z. Wei, J. Hou and X. Zhu, *Adv. Mater.*, 2024, **37**, 2413376.
123. J. Deng, J. Liu, C. Jin, S. Huang, S. Zhang, Z. Qin, J. Xie, L. Liu, L. Chen and Y. Chen, *Angew. Chem. Int. Ed.*, 2025, **64**, e202420385
124. R. Zeng, J. Deng, X. Xue, S. Tan, L. Kan, Y. Lin, W. Zhong, L. Zhu, F. Han, Y. Zhou, X. Gao, M. Zhang, Y. Zhang, S. Xu and F. Liu, *Angew. Chem. Int. Ed.*, 2025, **64**, e202420453.
125. S. Wang, S. Wang, J. Wang, N. Yu, J. Qiao, X. Xie, C. Li, M. S. Abbasi, R. Ding, X. Zhang, Y. Han, G. Lu, J. Zhang, X. Hao, Z. Tang, Y. Cai and H. Huang, *Adv. Energy Mater.*, 2025, DOI: 10.1002/aenm.202405205.
126. W. Zou, Y. Sun, L. Sun, X. Wang, C. Gao, D. Jiang, J. Yu, G. Zhang, H. Yin, R. Yang, H. Zhu, H. Chen and K. Gao, *Adv. Mater.*, 2025, **37**, 2413125.
127. H. He, X. Li, J. Zhang, Z. Chen, Y. Gong, H. Zhuo, X. Wu, Y. Li, S. Wang, Z. Bi, B. Song, K. Zhou, T. Liang, W. Ma, G. Lu, L. Ye, L. Meng, B. Zhang, Y. Li and Y. Li, *Nat. Commun.*, 2025, **16**, 787.
128. H. Chen, Y. Huang, R. Zhang, H. Mou, J. Ding, J. Zhou, Z. Wang, H. Li, W. Chen, J. Zhu, Q. Cheng, H. Gu, X. Wu, T. Zhang, Y. Wang, H. Zhu, Z. Xie, F. Gao, Y. Li and Y. Li, *Nat. Mater.*, 2025, **24**, 444-453.
129. J. Ren, J. Wang, J. Qiao, Z. Chen, X. Hao, S. Zhang and J. Hou, *Adv. Mater.*, 2025, DOI: 10.1002/adma.202418353.
130. C. Li, J. Song, H. Lai, H. Zhang, R. Zhou, J. Xu, H. Huang, L. Liu, J. Gao, Y. Li, M. H. Jee, Z. Zheng, S. Liu, J. Yan, X.-K. Chen, Z. Tang, C. Zhang, H. Y. Woo, F. He, F. Gao, H. Yan and Y. Sun, *Nat. Mater.*, 2025, **24**, 433-443.
131. T. Dai, Y. Meng, Z. Wang, J. Lu, Z. Zheng, M. Du, Q. Guo and E. Zhou, *J. Am. Chem. Soc.*, 2025, **147**, 4631-4642.
132. N. Wei, H. Lu, Y. Wei, Y. Guo, H. Song, J. Chen, Z. Yang, Y. Cheng, Z. Bian, W. Zhang, Q. Chen, Y. Liu, W. Zhao, X. Xu and Z. Bo, *Energy Environ. Sci.*, 2025, **18**, 2298-2307.
133. T. Jia, T. Lin, Y. Yang, L. Wu, H. Cai, Z. Zhang, K. Lin, Y. Hai, Y. Luo, R. Ma, Y. Li, T. A. Dela Peña, S. Liu, J. Zhang, C. Liu, J. Chen, J. Wu, S. Liu and F. Huang, *Nat. Commun.*, 2025, **16**, 871.
134. J. Wang, C. Sun, Y. Li, F. Bi, H. Jiang, C. Yang, X. Bao and J. Chu, *Nat. Commun.*, 2025, **16**, 1784.
135. L. Wang, C. Chen, Z. Gan, J. Cheng, Y. Sun, J. Zhou, W. Xia, D. Liu, W. Li and T. Wang, *Adv. Mater.*, 2025, DOI: 10.1002/adma.202419923.
136. Y. Li, H. Li, X. Xu, L. Yu, R. Li and Q. Peng, *Adv. Funct. Mater.*, 2025, DOI: 10.1002/adfm.202424327.
137. J. Guo, S. Qin, J. Zhang, C. Zhu, X. Xia, Y. Gong, T. Liang, Y. Zeng, G. Han, H. Zhuo, Y. Li, L. Meng, Y. Yi, J. Chen, X. Li, B. Qiu and Y. Li, *Nat. Commun.*, 2025, **16**, 1503.
138. X. Song, B. Zhang, X. Liu, L. Mei, H. Li, S. Yin, X. Zhou, H. Chen, Y. Lin, W. Zhu and X. K. Chen, *Adv. Mater.*, 2025, DOI: 10.1002/adma.202418393.
139. J. Zhou, X. Zhou, H. Jia, L. Tu, S. Wu, X. Xia, X. Song and Y. Shi, *Energy Environ. Sci.*, 2025, DOI: 10.1039/d4ee05848h.
140. Y. Jiang, K. Liu, F. Liu, G. Ran, M. Wang, T. Zhang, R. Xu, H. Liu, W. Zhang, Z. Wei, Y. Cui, X. Lu, J. Hou and X. Zhu, *Adv. Mater.*, 2025, DOI: 10.1002/adma.202500282.
141. M. Zhang, L. Zhu, J. Yan, X. Xue, Z. Wang, F. Eisner, G. Zhou, R. Zeng, L. Kan, L. Wu, W. Zhong, A. Zhang, F. Han, J. Song, N. Hartmann, Z. Zhou, H. Jing, H. Zhu, S. Xu, J. Nelson, Y. Zhang and F. Liu, *Joule*, 2025, DOI: 10.1016/j.joule.2025.101851.